1-1-2008

3-D modeling and simulation of crystal growth of $GE_{0.98}$ $Si_{0.02}$ under the influence of various gravity levels, G-jitter and rotating magnetic field using traveling solvent method

Mehdi Mohammadi Shemirani
Ryerson University

3-D MODELING AND SIMULATION OF CRYSTAL GROWTH OF $Ge_{0.98}$ $Si_{0.02}$ UNDER THE INFLUENCE OF VARIOUS GRAVITY LEVELS, G-JITTER AND ROTATING MAGNETIC FIELD USING TRAVELING SOLVENT METHOD

By

Mehdi Mohammadi Shemirani
Bachelor of Science
Tehran University
Bachelor of Technology
McMaster University

A Thesis

Presented to Ryerson University

In partial fulfillment of the requirement for the degree of

Master of Applied Science

In the Program of

Mechanical Engineering

Toronto, Ontario, Canada, 2008

AUTHOR'S DECLARATION

I hereby declare that I am the sole author of this thesis.

I authorize Ryerson University to lend this thesis to other institutions or individuals for the purpose of scholarly research.

I further authorize Ryerson University to reproduce this thesis by photocopying or by other means, in total or in part, at the request of their institutions or individuals for the purpose of scholarly research.

BORROWER'S PAGE

Ryerson University requires the signatures of all persons using or photocopying this thesis. Please sign below, and give address and sate.

.....

.....

.....

.....

.....

.....

.....

.....

.....

.....

.....

.....

.....

ABSTRACT

3-D Modeling and Simulation of Crystal Growth of $Ge_{0.98}$ $Si_{0.02}$ under the influence of Various Gravity Levels, G-jitter and Rotating Magnetic Field (RMF) using Traveling Solvent Method (TSM)

Master of Applied Science in Mechanical Engineering, 2008

Mehdi M. Shemirani

School of graduate Studies, Ryerson University

A three-dimensional numerical simulation was conducted to study the effect of a rotating magnetic (RMF) field on the fluid flow, heat transfer and mass transfer in the presence of various gravity levels by utilizing the traveling solvent method (TSM). The presence of the RMF suppressed the buoyancy convection in the $Ge_{0.98}Si_{0.02}$ solution zone in order to get homogeneity with a flat growth interface. It was found that the intensity of the flow at the centre of the crucible decreased at a faster rate compared to the flow near the walls when increasing magnetic field intensity is combined with a certain rotational speed. This behavior created a stable and uniform silicon distribution in the horizontal plane near the growth interface in the terrestrial condition. Different magnetic field intensities for different rotational speeds were examined in both terrestrial and micro-gravity conditions. The effects of residual acceleration, known as G-jitter, on board the International Space Station and European Space Orbiter were also investigated.

ACKNOWLEDGEMENTS

I have been fortunate to have the honor to work with Professor Dr. Ziad Saghir, the head of the research team in the Micro-gravity Laboratory of Ryerson University. The author would like to thank Dr. Ziad Saghir for his unconditional and invaluable support and guidance throughout the completion of this thesis.

The author also acknowledges the financial support of the Natural Sciences and Engineering Research Council of Canada (NSERC).

The author would also like to thank Dr.Greg Kawall, director of the Mechanical Engineering Graduate Program of Ryerson University for encouraging and guiding him to pursue this line of research.

I would also acknowledge and appreciate the support and useful suggestions of my colleagues, Dr. Yu (Claire) Yan and Tawfiq Jaber (PhD candidate).

DEDICATION

The author hereby would like to dedicate this thesis to his immediate family members, especially to his wife Soudie and his son Pedrum, as a token of humble and sincere appreciation, for their invaluable dedications and gracious support.

TABLE OF CONTENTS

LIST OF FIGURES

LIST OF TABLES

NOMENCLATURE

a	Amplitude (For Sine Term)
b	Amplitude (For Cosine Term)
B^*	Dimensionless magnetic field induction
B	Magnetic field induction (Tesla)
B_o	Reference magnetic field induction (Tesla)
B_r	Radial component of magnetic field induction (Tesla)
B_φ	Circumferential component of magnetic field induction (Tesla)
B_z	Axial component of magnetic field induction (Tesla)
C	Dimensionless concentration (atomic %)
c	Solute concentration (atomic %)
c_o	Reference solute concentration (atomic %)
Δc	Change in concentration (atomic %)
c_p	Specific heat at constant pressure (cal/g.K)
f	Frequency (Hz)
F	Dimensionless Frequency
F	External body (Magnetic) force
Gr	Grashof number
g	Gravity (cm/s^2)
g_o	Earth gravity (cm/s^2)
g_{st}	Static gravity (cm/s^2)
g_{vib}	Vibrational gravity (cm/s^2)
Ha	Hartmann number
L	Reference Length (cm)
p	Pressure ($g/cm^2.s^2$)
P	Dimensionless Pressure
Pr	Prandtl number
r	Radial direction(cm)
R	Dimensionless radial direction
Re	Reynolds number
Sc	Schmidt number
T	Temperature (^oC)
T_o	Reference temperature (^oC)
ΔT	Change in temperature (^oC)
U	Dimensionless radial velocity
u	Radial velocity (cm/s)
u_o	Reference velocity $=\sqrt{g\beta_T \Delta T L}$
U	Speed: $\sqrt{u^2+v^2+w^2}$ (cm/s)
v	Circumferential velocity (cm/s)
V	Dimensionless circumferential velocity
w	Axial velocity (cm/s)
W	Dimensionless axial velocity
z	Axial direction (cm)
Z	Dimensionless axial direction

Greek Symbols

α_T	Thermal diffusivity of the species (cm^2/s)
α_c	Solutal (mass) diffusivity of the species (cm^2/s)
β_c	Solutal expansion coefficient (1/at %Si))
β_T	Thermal expansion coefficient ($1/^oC$)
θ	Dimensionless temperature
κ	Thermalconductivity(cal/s.cm.K)
μ	Dynamic viscosity (g/cm.s)
ν	Kinematic viscosity (cm^2/s)
ρ	Density (g/cm^3)
σ	Electric conductivity (S/cm)
φ	Circumferential direction
ω	Angular velocity (rad/s)
Ω	Rotational speed (rpm)

Subscripts

o	Reference
i	i^{th} index
j	j^{th} index
m	Melt

Superscripts

M	Magnetic Field

CHAPTER 1
Introduction and Definitions

1.0 INTRODUCTION

In today's world with the rapid increase in demand for electronic devices which incorporate semiconductors, it is clear to expect a perfect and flawless product. A semiconductor by some definition is a material whose ability to conduct current is between that of a conductor (metals) and that of an insulator (most non-metals) [1]. Semiconductors therefore play an important role in today's technology. Electronic components which utilize semiconductors can be found in every subgroup such as computers, life saving medical devices, game consoles, cellular phones, graphic displays, and digital audio and video players to name a few. Although there are many types and varieties of materials to be used for semiconductors, silicon (Si) is still a widespread and most used among the others. It is understood and experimented that the addition of other semiconductors such as germanium (Ge) can noticeably enhance the performance of silicon transistors and circuitry; this in turn helps to make several new applications in the market that continuously seek new low cost, light weight and more reliable personal communication wireless devices. The reliability of the aforementioned products is highly dependent on the performance of the semiconductors being used in them. This reliance is based on the consistency of the internal arrangement of atoms in a three dimensional crystal structure and characteristics such as uniformity and purity of a bulk single crystal. These crystals, of course, should be produced under specific circumstances in order to

ensure high quality and satisfy the ever growing demand. The ultimate goal is to achieve a high level of purity, uniformity, homogeneity and a perfect crystalline structure.

1.1 Thesis Organization

This thesis is presented in six chapters and organized as follow:

> Introduction, brief information about crystals and physical properties of the materials used in this study are in chapter one.

> Literature review and information about growth techniques are discussed in the chapter two.

> In chapter three, theory and set up along with dimensional and non-dimensionalized forms of the continuity, energy, solute and Navier-Stokes equations are discussed. The boundary conditions are also presented in this chapter. The mesh sensitivity analysis for the solvent region is presented.

> Results for the steady state condition in both terrestrial and micro gravity can be found in chapter four.

> In chapter five, the transient (unsteady state) condition in the micro gravity condition is discussed. Also, in this chapter, the effects of both rotating magnetic field and residual acceleration (G-jitter) are analyzed.

> In the final chapter (chapter six) concluding remarks are presented.

1.2 Single Crystal and Crystal Structure

A crystal is referred to a solid material which has a unique arrangement of atoms in it and is referred as the crystal structure, as per mineralogists and cryptologists [2]. Every crystal structure consists of a single unit cell which can be classified as the smallest configuration of arranged atoms which makes each material's distinguishable characteristics. The specific arrangement of these unit cells in an array format creates the crystal lattice, as shown in Figure 1.

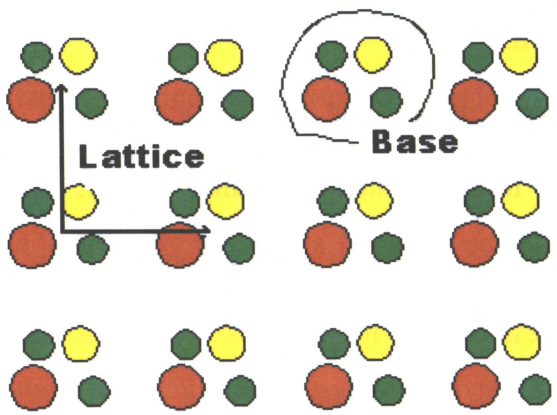

Figure 1 Crystal lattice [3]

There are several ways to have the atoms to be arranged in a volume. The difference in the gaps between the atoms will form a lattice. The lattice occupies a space which is called a unit cell; Figure 2 depicts the major types of the unit cells. It can be noted that if millions and millions of one of the type of crystals (Figure 2) be arranged uniformly in a three dimensional array then the crystal can be conceptualized.

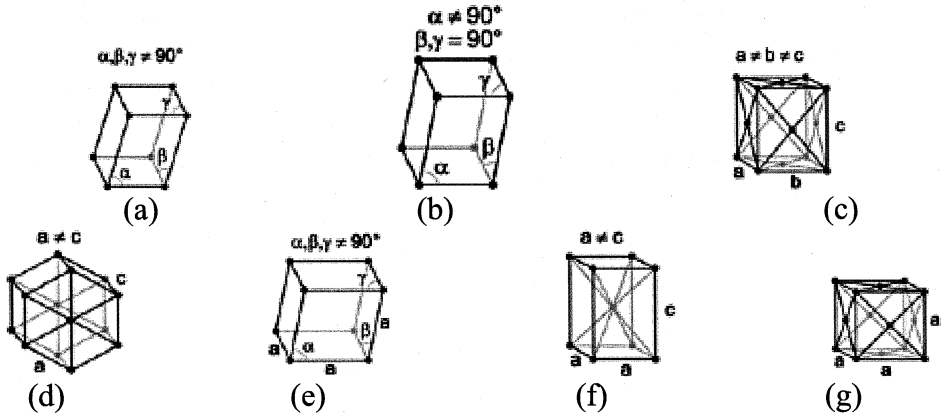

Figure 2 Types of unit cell [**4**]
a) Triclinic, **b**) Monoclinic, **c**) Orthorhombic,
d) Hexagonal, **e**) Trigonal, **f**) Tetragonal, **g**) Cubic

Single crystals attain specific arrays of atoms in which for example the long-range patterns exist in the entire material. It should be noted that not all the solids have crystal format Figure 3. Those which have no periodic structure are called amorphous solids and those which are built of many small segregated regions of single crystal are called polycrystalline solids.

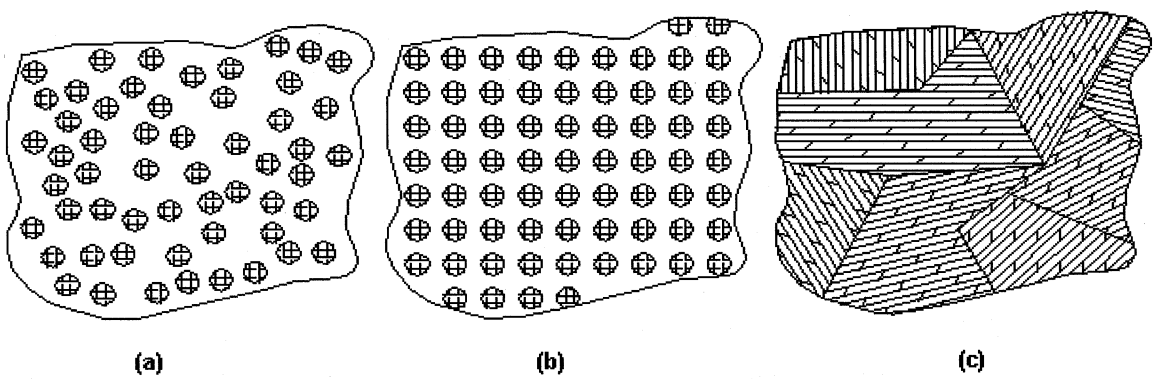

Figure 3 Types of solids [5]
a) Amorphous, **b**) Crystalline, **c**) Polycrystalline,

Ever growing demands for semiconductors now a days in electronic devices increase the need for the best crystalline with the least impurity in order to have the ultimate performance. Single crystals are being utilized in many electronic, optical, industrial and

medical equipments and applications. Both silicon and germanium crystals are playing a vital role in the aforementioned devices, therefore the impurities, defects and the methods of achieving a good single crystal would be discussed hereafter.

1.3 Crystal Defects

There are many different methods and techniques for crystal growth. Among those, the crystallization from the melt is the most practiced one. Inevitably, this way of crystal growth has some complications which baffle the process of obtaining a perfect arrangement of molecules or atoms of crystals as mentioned before. It should be noted that these complications are generally known as the growth defects [6]. Growth defects can be categorized as appeared in Figures 4 to 9 as follow;

- **Substitutions** which is a replacement of an atom with another atom in the crystal lattice.

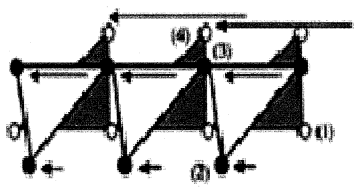

Figure 4 Substitutions [7]

- **Grain boundaries** which happens when two small grains of crystal have different crystallographic orientations.

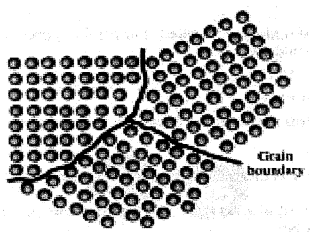

Figure 5 Grain boundaries [7]

- **Vacancies** which refer to the missing atom in the crystal lattice.

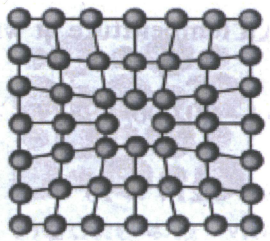

Figure 6 Vacancies [7]

- **Dislocations** which is referring to misalignment of the crystal lattice.

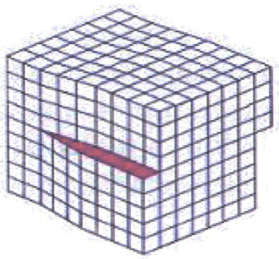

Figure 7 Crystal lattice dislocations [7]

- **Interstitials** which happen when an atom is being squeezed into the crystal lattice.

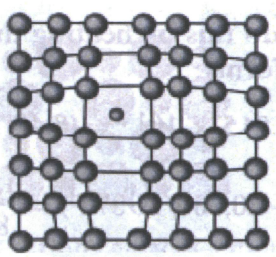

Figure 8 Interstitials [7]

- **Stacking** is referred to a disturbance in the regularity of the arrangement of the plane of atoms in a crystal lattice.

Figure 9 Stacking [7]

Each of the above defects individually or collectively contribute to the quality of the grown crystal; hence, all the researchers in crystal growth community are focusing on the finding of an explanation of relationships between the physical properties, crystal quality and the growth parameters, as well as a technique which suitably provides the path to achieve this objective.

1.4 Silicon (Si, Atomic Number 14) and its Physical Properties

On Earth, silicon is the second most abundant element (after oxygen) in the crust, making up 25.7% of the crust by mass [4]. Silicon crystal structure is cubic diamond.

(a) (b)

Figure 10, a) Silicon crystalline, a broken ingot, **b)** Silicon atom [8]

1.4.1 (Si) Physical Properties [9]

- **Density** (ρ) 2330 kg/m^3
- **Thermal Expansion Coefficient** (β_T) 2.8 x 10 $^{-6}$ / ^{0}K
- **Melting Temperature** (T_m) 1687.15 ^{0}K
- **Boiling Temperature** (T_b) 3538.15 ^{0}K
- **Thermal Conductivity** (k) 148 W/m - ^{0}K
- **Heat Capacity** (C_p) 705 J/kg - ^{0}K

1.5 Germanium (Ge, Atomic Number 32) and its Physical Properties

Germanium is a hard, grayish-white element that has a metallic luster and the same crystal structure as diamond. Germanium is a semiconductor. In its pure state, this metalloid is crystalline, brittle and retains its luster in air at room temperature [wikipedia]. Germanium crystal structure is also cubic diamond.

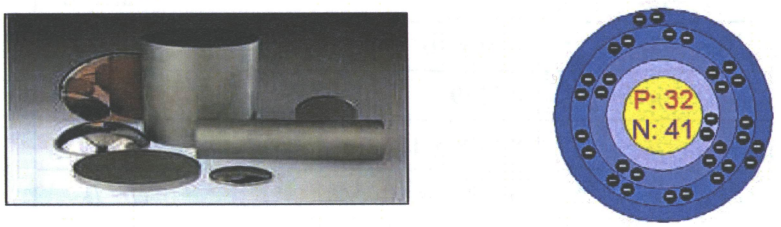

(a) (b)

Figure 11 a) Germanium crystalline, **b)** Germanium atom [8]

1.5.1 (Ge) Physical Properties [9]

- **Density** (ρ) 5320 kg/m^3
- **Thermal Expansion Coefficient** (β_T) 5.75 x 10 $^{-6}$ / ^{0}K

- **Melting Temperature** (T_m) 1214.4 ^{0}K
- **Boiling Temperature** (T_b) 3106.15 ^{0}K
- **Thermal Conductivity** (k) 59.9 W/m - ^{0}K
- **Heat Capacity** (C_p) 320 J/kg - ^{0}K

Table 1 presents the physical properties of the GeSi mixtures used in this study and also incorporated in all the input files which are used in the FIDAP (CFD software) for computational purposes.

Table 1 Physical properties of the GeSi in the Solvent Region [10]

Physical Properties of $Ge_{0.98}$ $Si_{0.02}$		
Symbol	**Values**	**Units**
c_p	0.04008	*J/g*.K
T_m	971	°C
α_c	0.52 x 10^{-4}	cm^2 /s
σ	2.5 x 10^4	S/cm
β_c	0.0051	/ at% Si
β_T	1.01 x 10^{-4}	1/ °C
κ	0.2559	W/cm/K
μ	8.3496 x 10^{-3}	*g/cm*.s
ν	1.53192 x 10^{-3}	cm^2 /s
ρ	5.4504	g /cm^3

1.6 Crystal Growth

As mentioned earlier, almost the entire semiconductor's single crystal has some sort of impurities and defects. Semiconductors in general and silicon and germanium in

particular, at first should be processed with an acceptable level of purity and then be used for growing the single crystal in a specific environment and condition. Since the properties of a material are highly affected by the aforementioned impurities, therefore the secondary stage of production of a single crystal has to be in a way to enhance the process and to achieve a much higher level of purity and homogeneity. It is a known fact that under the terrestrial (on the earth surface) condition, the hot fluid with less density in the crystal melt rises and the denser cool fluid falls down. This, obviously, is known as convective flow and causes the irregular distribution of the particles; also, to a larger extent, it affects on the perfection of the crystal growth. Gravity can also have a negative impact on the crystal growth process; it has effects on heat and mass transport. The convective fluid flow due to the buoyancy effect would also result in an uneven concentration distribution. There are several methods and techniques which have been employed to produce a single crystal, as well as methods to suppress the above convection. The following chapter discusses these methods.

CHAPTER 2

Literature Review on Methods and Techniques

2.0 Introduction

In this chapter, a review of the related published papers is presented and the methods and techniques which are common in crystal growth is discussed. Also the research goals are presented.

2.1 Methods and Techniques

There are many different methods and techniques which have been used from the early twentieth century, among which, the five most practiced ones for crystal growth purposes are: Czochralski technique (Cz), Bridgman method, Floating zone technique (FZ), Verneuil technique and traveling solvent method (TSM) also known as traveling heater method (THM). Each method or technique tries to achieve and fulfill a homogeneous purified single crystal growth.

2.1.1 Czochralski Technique (Cz)

In 1916, J. Czochralski developed this technique which incorporates a container mainly made of quartz (crucible) and a hanging seed over the molten material in the form of polycrystalline [11]. This molten material can be a metal (e.g., silver or gold …), a semiconductor (e.g., silicon or germanium…) or a manmade gemstone (only in Laboratories). Once the chunks of the base material are melted, the seed is dipped into the molten material Figure 12, and slowly being pulled up while the seed and the crucible

are rotating in an opposite direction (e.g., 2rpm for crucible and 8rpm for the seed), then crystal growth is finished and bulk crystal in the form of ingot is produced. Usually the large uniform diameter (approximately 200-300 mm and up to 1-2 meter in length) crystals are produced except in the starting and finishing stage of the growth. The pulling rate for growth is about few millimeters to a centimeter per hour [12].

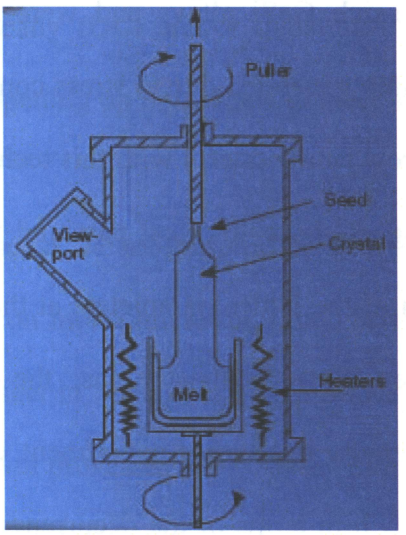

(a)

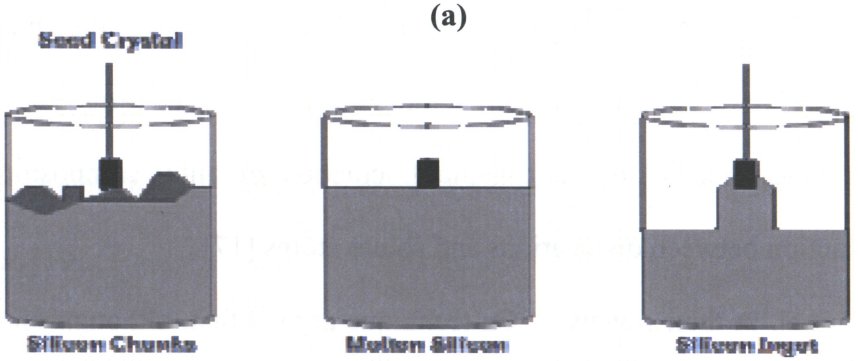

(b)

Figure 12 Cz technique.[13]
a) Schematic view of Cz furnace **b)** 3 stages of Cz technique.

There are some complications and imperfections associated with this technique as Yonenaga found defects in an experiment, utilizing this technique, such as straight dislocations with the Burgers vector parallel to the growth direction from the seed/crystal

interface even in Si-rich SiGe, $Si_{0.98}Ge_{0.02,}$ Such dislocations are so-called "misfit dislocations" which are generated due to the lattice parameter mismatch between seed and crystal [14]. Other defects found by Nonaka et al. in an experiment such as oxygen impurity with the presence of SiO as a result of the high temperature of the melt and interaction with the quartz (crucible). Also, some dislocations were generated from the four corners habits in the Si-rich GeSi alloys and were analyzed to be *Lomer-type* dislocations which were possibly generated due to stress concentrations [15]. Abrosimov et al, in their experiment to grow single crystal with this technique, define three stages as initial cone formation, pulling of the cylindrical part and the reverse cone formation. They also observed mismatch of the lattice parameters at the seed-melt interface, which results in mechanical stresses in the contact areas; the latter may exclude mono-crystalline growth [16]. Yonenaga in another experiment evaluated and discussed the velocity for single crystal growth in terms of the occurrence of the constitutional super-cooling. It was found that oxygen impurities (from the quartz crucible) make Si-O-Si quasi-molecules. The alloy becomes temperature insensitive. This may be due to the stress-built-in fields related to microscopic fluctuation of alloy composition and the dynamic interaction between dislocations and solute atoms [17].

Shcilz et al, in their review of Cz technique argued that, although this is one the most used technique to obtain Si-Ge single crystal due to the continuous loss of Si during the solidification process, the growing crystal shows a non-constant concentration profile. The simplest method for minimizing this macro-segregation is growing small crystal from a large batch of melt, which is not an economical method [12]. Kakimoto in an experiment focuses on an analytical approach for determining the effects of external

forces based on gravitational acceleration and of rotation of a crystal and crucible on convection. Also, the effect of electric, magnetic and electromagnetic forces on the melt convection was shown. Micro-voids are formed by agglomeration of vacancies that are introduced at a solid-liquid interface of silicon. One of the key points for controlling the vacancy flux in a crystal, especially that near the solid-liquid interface, is the control of the convection of melt. Steady (DC) and/or dynamic (AC) magnetic fields including electromagnetic fields are opening up new fields to meet an increasing demand for large-diameter crystals [18].

Rosenstein et al, discuss the axisymetric breaking instabilities in the CZ process of crystal growth from silicon melt (where the Prandtl number, $P_r = 0.01$). It was found that convective instability sets in through a Hopf bifurication displaying oscillations in time. CZ based crystal growth processes may display transitions from steady axisymetric flow into asymmetric time-dependent flows. This in turn may cause inhomogeneities in the grown crystal. No heat convection means that the Prandtl number is equal to zero. It has been shown that the electro-magnetic field has a stabilizing effect on the flow. It has also been shown that the mixed thermal flow and rotational speed is a destabilizing mechanism [19].

2.1.2 Float zone Technique (FZ)

This technique uses no crucible (container less) and the growth of single crystal is done in an inert atmosphere (Maximum 3 atm.) with three zones consists a feed rod of polycrystalline, a single crystal seed which are held in a vertical position with a gap in between to allow the melt zone to grow Figure 13.

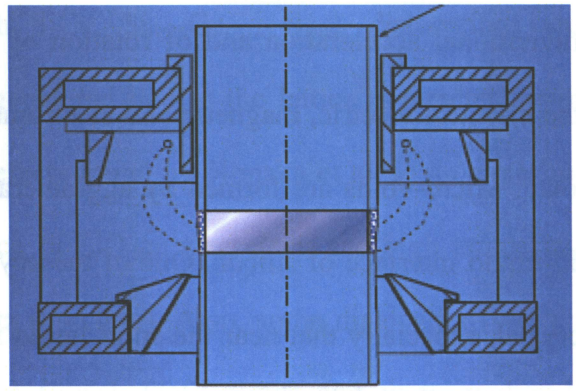

(a)

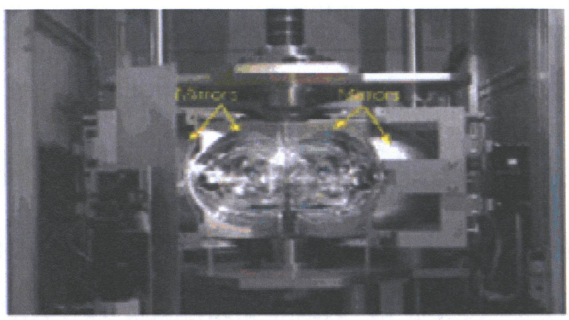

(b)

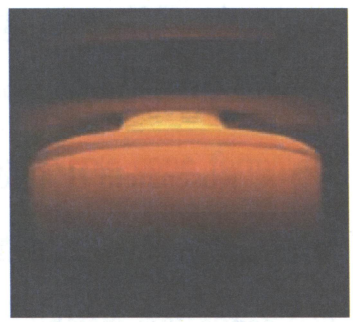

(c)

Figure 13 Floating Zone Technique.[20]
a) Schematic view, **b)** Fz Furnace, **c)** The actual melt area

Both feed rod and the seed rod are partially melted from the inner side by means of a high frequency inductive heating element. This molten area is then slowly moved upward while the seed rod is rotating until the whole polycrystalline is converted into a mono-crystal. The whole set up is contained in a mirror furnace. With this technique normally crystals up to 150mm in length and up to 8mm in diameter are produced at a rate of 0.25 to 10 mm per hour. There are some advantages and disadvantages associated with this technique. No crucible contamination, shape control, large growth rates and large grown crystals are among the advantages while the high melting compound, expensive technique, phase separation and stability and overflows are of disadvantages [20].

Noritake Usami et al, carried out an experiment using pre-synthesized SiGe feed rod with uniform composition and utilizing a high power semiconductor laser. The Ge composition of the grown SiGe crystal was smaller than that of the feed-rod especially during the initial stage of the growth. In their experiment, they found the polycrystallization took place, and the grown crystal does not follow the orientation of the seed [21]. Barz et al, experimented a floating zone technique but with a major difference and that is the use of a crucible, however, it was found that the formation of cracks in the crystals as a result of the sticking grown crystal to the crucible. With this method the growth of GeSi single crystals up to 50 at% has been performed. The use of wedge-shaped feed material allows the setting of a predefined concentration profile. Compared to crucible free float zoning, the preparation of the starting material is easier and the zone height is not limited [22].

Lin et al. discussed in an experiment that the thermal condition is one of the most important control parameters for crystal growth and developed an expert system-like algorithm which can be combined with commercial software such as FIDAP to investigate the thermal parameters for experimental growth of SiGe single crystal growth with the FZ technique. By evaluating two cases, one with the rotating magnetic field around the floating zone outside the furnace, it was found that the maximum pulling rate for GeSi crystal is limited by the maximum available temperature gradients at the liquid-solid interface. The second case was to control thermally induced stress in GeSi growth in a resistance furnace. It was observed that the number of thermally induced defects in a crystal is proportional to the magnitude of (∇^2 T) close to the liquid-melt interface [23]. Feonychev et al. studied the effect of a rotating magnetic field on convection stability and

crystal growth in zero gravity and on the ground by utilizing floating zone technique and stated that it is possible to effectively control the melt flow and impurity transfer. It was also found that the FZ method is the most promising for obtaining homogeneous mono-crystal with the use of a RMF in microgravity [24].

Saghir et al. performed a numerical simulation of float zone technique to grow a $Bi_{12}GeO_{20}$ crystal under terrestrial and microgravity conditions. It was found that the microgravity conditions results in a very stable float zone due to the less convection effect [25]. Dold et al. conducted an experiment to evaluate the growth rate of silicon crystal rate in the floating zone by utilizing the heat pulsation technique. It was shown that the instabilities in the melt can cause the dopant non-homogeneities, to overcome this problem, the heat pulses can produce a very fine gap in periodic time markers [26].

2.1.3 Bridgman Method

This method uses a tubular furnace which has three zones, Figure 14. Each heated at a different temperature. The "hot" zone is held at a temperature above the melting point of the material, while the "cold" zone is kept at a temperature below the melting point. The sample material is usually placed in a container made of an inert material (such as quartz).

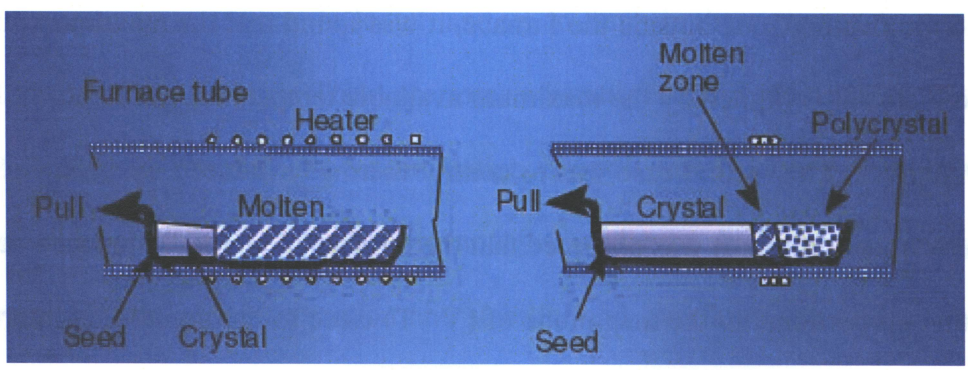

Figure 14 Schematic view of Bridgman Method [13]

Once a region of the sample is melted, the sample is slowly moved, and directional solidification takes place. The interface between the liquid and solid material, the solidification front, is particularly interesting to scientists. It is here that the flows in the molten material affect the final composition and structure of the solid and its properties. The ampoule contains the melt which moves through the axial temperature gradient in a furnace. This ampoule is necessary to support the melt, because in contrast to the float-zone method, the whole feed material is molten [27]. This method has its own advantages such as; simplicity, containers can be evacuated and sealed, control of shape and size of crystals and stabilized thermal gradients. Disadvantages are such as; Confinement, Thermal expansion of container versus the crystals, Can handle small melt volume and process is not visible [20].

Schilz et al. [12] in a review of this method state that in contrast to Czochralski technique, directional solidification, i.e. mostly the Bridgman process, can handle only a small melt volume, since heat flow should always be perpendicular to the phase boundary. Because of this problem and also due to the inevitability of the non-uniform composition profile after solidification, the Bridgman method has neither ever been applied for the growth of technically exploitable Si-Ge semiconductor material, nor has been a subject to intense research in this field. Experiment suggested that in bottom-seeded vertical Bridgman growth, the damping power of the solute field is predominant over the thermal influence. Also, observed segregation profiles exhibit a typical diffusion controlled shape.

Helmers st al. conducted a Bridgman growth of non-dilute Si_xGe_{1-x} mixed crystals and four samples of different composition reported. Fluctuations of growth rate and or

composition result in strong striation patterns. The spacing of the striae is found to be similar for all melt volumes, compositions and thermal environments used in this experiment. The crystal quality is generally poor. All samples show the grain structure. It was found that if the seed is of higher Si content than the first part of the grown crystal, formation of grain is considerably reduced. It was shown in the phase diagram that an increase of the Si content in the solid changes the equilibrium temperature at the phase boundary during solidification up to 10K per at%. Considering the fixed thermal field of a Bridgman facility, a changing Si concentration will move the position of the solid/liquid interface with respect to the furnace, and the growth rate differs from the velocity at which the cartridge passes through the heater. Thus, the monotonic decrease of Si concentration is accompanied by a slowing down of the growth velocity. The thermal environment can cause the striae only if the temperature accidentally fluctuates with the same frequency [28].

Dold et al. utilized the Bridgman method in a radiation heated mirror furnace. The growth velocity was 1.3mm/h. GeSi crystal in a range (Si<= at %) grown on a seed crystal with the diameter of 9mm and length from 30 to 40 mm. Si-concentration was restricted for the given set-up to about 10-15 at%. Axial and radial macro-segregation measured by X-ray (EDAX). The average Electro-phoretic deposition was in the range $6x10^4$ to $1x10^5$ and was enhanced at the seed/crystal interface and in the part grown in the vicinity of the container wall.

The full-width at half-maximum (FWHM) values of 20-40 arcsec obtained via Bartel's five crystal diffractometer of the (111) peak is best result reported up until this experiment. Although the quartz crucible is the best container for single crystal growth

but the interaction between the silicon and the ampoule wall leads to sticking of the crystal to the wall. During the cool down process, the grown crystal is subjected to heavy mechanical stress. Together with tension because of lattice mismatch due to concentration gradients, this might lead to cracking of the crystal or the ampoule wall. Constitutional super-cooling and a high silicon concentration increase at the growth beginning due to the use of Germanium seed-crystal cannot be avoided [29].

Walker et al. carried out an experiment utilizing the Bridgman method for crystal growth with a strong, low-frequency, rotating magnetic field. The study shows the motion of the melt driven by a low-frequency, spatially uniform, rotating magnetic field that is perpendicular to the axis of a cylindrical Bridgman ampoule. Since the magnetic force is so strong, the inertial effects are negligible and that viscous effects are confined to thin boundary layers which are adjacent to the ampoule surfaces and the crystal-melt interface. Outside the boundary layers, the melt nearly rotates as a rigid body with the angular velocity of the rotating magnetic field. Because of non-electrical conductivity, the static crystal acts as a generator in the rotating magnetic field and drives electric currents through the crystal-melt interface boundary layer, these currents from the slightly conducting crystal interact with the magnetic field to accelerate the azimuthally velocity. A strong, low frequency, rotating magnetic field would produce poor crystals with severe rotational striations. They conclude that a rotating magnetic field may produce beneficial mixing, but it may also produce potentially deleterious (harmful) deviations from axisymmetry in the melt motion. With a rotational magnetic field, it is not appropriate to treat the crystal as an electrical insulator because they can conduct the current [1]. The importance of the non-axisymmetric radial and axial velocities inside the

interface layer lies in their potential effects on the mass transport of dopants or species. Sometimes the dopant or one of the species in alloyed melts is rejected at the crystal-melt interface, producing a mass-diffusion boundary layer with an elevated concentration near the interface [30].

Feonychev et al. also studied the Bridgman method by showing that the flow arising in a conducting liquid under the effect of a rotating magnetic field as well as under its interaction with gravitational and thermo-capillary convection, region of mixed flows, in which the impurity in crystal growth were found [12].

2.1.4 Verneuil Method

The verneuil method is a commercial method for growing crystals such as gems. It was developed by Verneuil in 1902. Figure 15 shows a schematic view of the principle of the method. The apparatus is basically an oxyhydrogen torch through which powders of the material to be grown are passed. Then powders would melt in the flame and form a small pond on a seed crystal. The crystal is grown on the seed crystal which is being lowered down as the crystal builds up on top of it. The crystal being grown by this method has a cylindrical shape. Similar to float zone, Verneuil method is also a non crucible method which is an advantage since less contaminations come to play. By this method larger crystals are grown. A disadvantage of this method is that the growing crystal is exposed to a large temperature gradient therefore; some of the crystals grown this way have been broken in pieces [31].

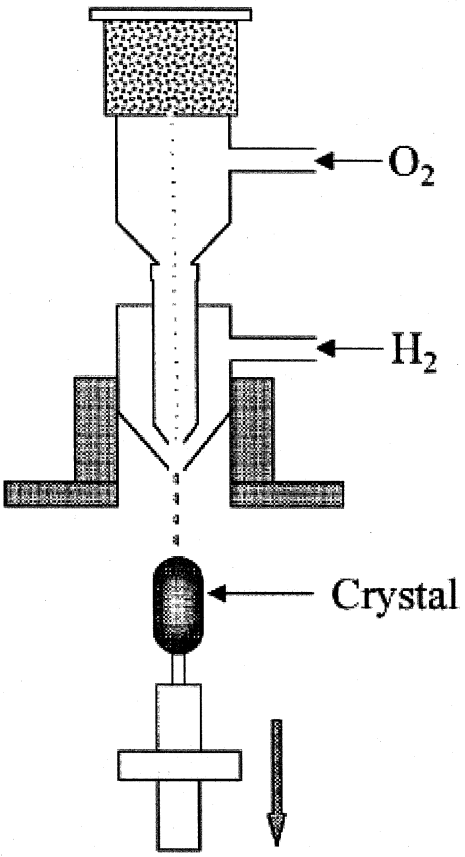

Figure 15 Schematic view of Verneuil apparatus [31]

2.1.5 Traveling Solvent Method (TSM)

The TSM also known as Traveling Heater Method (THM) is a solution growth technique for growing and synthesizing binary (is a compound that contains two different elements, such as NaCl (salt) and ternary compound (such as iron (III) carbonate, $Fe_2(CO_3)_3$) semiconductors. With this process, a constant, controlled, but slow growth is achieved, Figure 16. The quality of grown crystals in TSM is very sensitive to the relative movement of the temperature profile that determines the growth rate. THM has a number of advantages over melt techniques, namely less thermal stresses, growth of ternary alloys, and uniform crystal composition [32]. Another advantage of this method is that

since the process and experiment is being conducted in a relatively lower temperature environment compared to that of the zone melting, therefore, the parameters such as pressure and the oxygen contamination of the quartz as well as the possibility of the container (ampoule) fracture are being reduced which leads to the growth of a crystal with less thermal stresses and higher purity [33]. So far known disadvantages of this method can be mentioned as; the size of the bulk crystals (about 10 mm in diameter) [34] and the growth rate less than 5 mm per day, however, the growth of large diameter (> 5 cm) single crystal Si_xGe_{1-x} alloy for technological applications is limited to the fabrication of pre-synthesized homogeneous feed rods by using this approach [35].

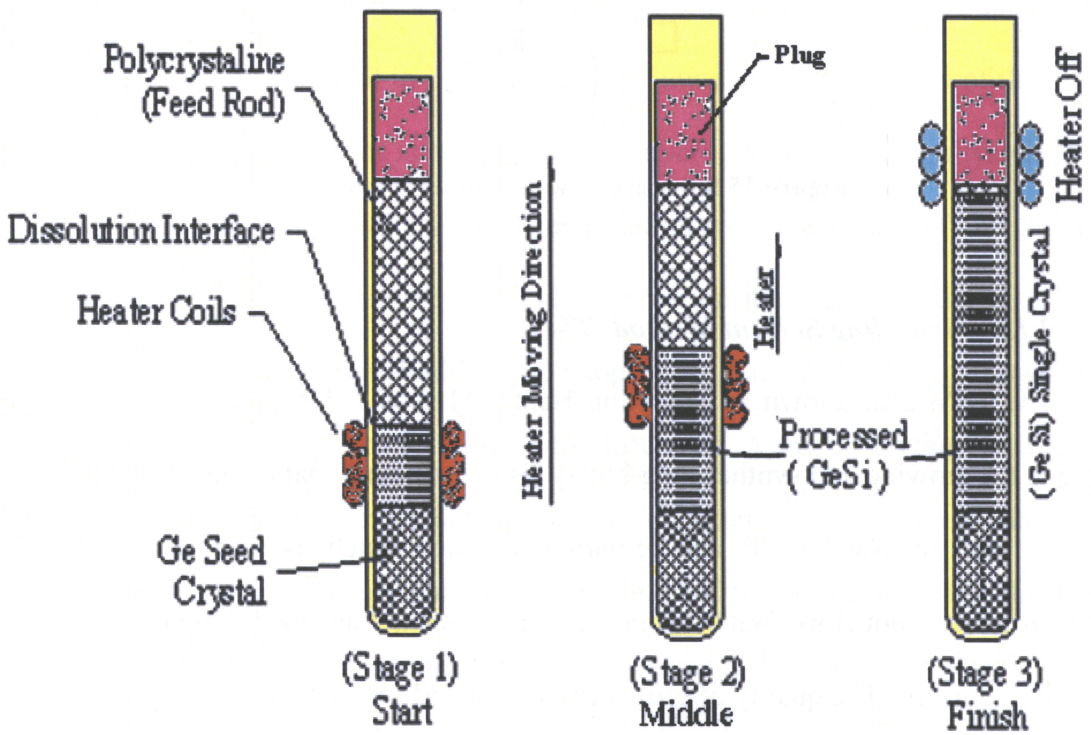

Figure 16 Schematic view of Traveling Solvent Method, Excerpted from [48]

Labrie et al, in another study by utilizing TSM with Ge seed, found that the fluctuations in chemical composition along axis and transverses to the Si_xGe_{1-x} samples

were typically less than (+ -) 0.4 and 0.3 at% respectively. Macroscopic composition non-homogeneities along the growth axis in the TSM grown samples correlate strongly with those within the Si_xGe_{1-x} feed-rods which in turn depend noticeably on the quenching rate of the molten alloy. It was noted that the microscopic striation along the growth axis, which is a problem observed in other crystal growth technique, TSM has the least amount of the aforementioned problem [35].

Labrie et al. carried out a single crystal growth of Ge-Si with composition ranging from 2-15 at% using TSM. Electron microprobe (EMP), Laue x-ray and Hall Effect techniques were used to characterize the quality of the materials. A change of conductivity from n-type to p-type in the TSM sample was observed as the Si composition is increased from 2 to 5 at % in the feed rods. TSM is suitable crystal growth technique since it has the least amount of segregation in the crystals [36].

Saghir et al, studied the coriolis and centrifugal forces in the SiGe bulk crystal growth and found that the application of rotation have a considerable effect on the buoyancy-induced flow in terrestrial condition. An optimal rotational speed (7 rpm) was found that lessened the convective flow, provided a uniform concentration along the growth interface, and gave symmetrical characteristics to the 3-D buoyancy-induced flow. However, in the microgravity condition where $g=10^{-4}g_0$ the rotation of the crucible had negative effect [37]. Saghir et al in another study investigated different heating conditions. Heat losses by radiation have been taken into the consideration. Numerical analysis results showed that the convective heat transfer significantly influences the solute distribution in the liquid zone and affects the growth rate significantly. It was also

observed that even though the fluid flow has a small effect on the heat transfer but it plays an important role in the concentration distribution within the melt. Results indicated that with the asymmetric heater profile, weak flow around the growth interface enables a uniform concentration boundary layer to be formed [38].

Lan et al, emphasized that THM is a powerful and versatile technique for growing a single crystal, especially for materials that cannot readily be grown due to phase transformation or decomposition. Due to the use of solvent, a low growth temperature is allowed, so that the temperature gradient and the corresponding thermal-stress-induced defects can be reduced. Similar to other crystal-growth processes, the interface control in the TSM is of prime importance. A flat or slightly convex interface shape toward the solution is most desirable for growing single crystal. When the convection induced by buoyancy force is neglected (zero gravity), mass transport is mainly occurs through diffusion. If the crystal growth speed is too high, constitutional super-cooling may occur and causes the breakdown of the growth front. The solvent volume is an important parameter in TSM [39].

Saghir et al, carried out another study and investigated the effect of an axial magnetic field combined with crucible rotation. By increasing the magnetic field intensity, the intensity of the flow at the centre of the crucible decreased at a faster rate compared to the flow near the walls. This phenomenon created a stable and uniform silicon distribution in the horizontal plane and became relatively homocentric. The addition of a crucible rotation showed an improvement in the suppression of the flow intensity. It was also found that the silicon distribution remained the same in both cases [40].Saghir et al in a study described the effect of the rotating magnetic field on the

growth of SiGe, utilizing traveling solvent method under both uniform and non-uniform heater profile conditions. Results showed that the RMF has a considerable effect on the silicon concentration near the growth interface, changing the shape of the concentration profile from convex to nearly flat when the magnetic field intensity has increased from 2 to 15mT. Also showed that a non-uniform heating profile has significant effect on the low magnetic filed intensity (i.e. 2mT) [41].

2.2 Research Goals

This study would thrive to model and simulate the growth of $Ge_{0.98}Si_{0.02}$, a high quality bulk single crystal with homogeneous, high purity and uniform composition on top of the growth interface, by employing the TSM technique. This, of course, can be achieved by taking the suppression of the convection due to the buoyancy effect, in the terrestrial condition, in the $Ge_{0.98}Si_{0.02}$ solvent region into the consideration. Applying different intensities of the rotating magnetic field in the terrestrial condition and also by applying micro gravity along with the residual acceleration known as G-jitter in the space condition, are methods utilized in this thesis to reach to the aforementioned goals.

CHAPTER 3

Theoretical Approach, Numerical Solution and Set up

3.0 Introduction

This chapter presents the numerical solution technique and the governing equations which will be used in the computer simulations. Since the model is a cylindrical shape, therefore all the equations are considered in cylindrical coordinates and introduced in a transient condition. Growth technique, model description, boundary conditions, mesh sensitivity analysis and finite element analysis will be discussed .

3.1 Numerical Solution Technique

Since this study focuses on the solution zone (solvent region), the full non-linear Navier-Stokes equations for laminar (Re = 690.5), transient condition incompressible Newtonian flows are solved, by taking the Boussinesq approximation equation 3.1 into consideration. Convective heat and mass transfer along with the external forces such as rotating magnetic field both in terrestrial and microgravity condition are also taken into the consideration. The effect of residual acceleration known as g-jitter on board of the spacecrafts will be discussed in the chapter five. The temperature is calculated by utilizing the experimental field temperature, done by Dalhousie University, for this model. There are some assumptions which were put forward into the input files for the computational simulations. The input files for several cases are presented in the Appendix E. The aforementioned assumptions are as follow:

1. The flow is laminar
2. The fluid is Newtonian
3. The flow is viscous
4. The solvent is electrically conductive
5. Except density, all other thermo-physical properties are constant
6. Ampoule's translational speed is very minimal
7. Non-slip condition for velocity on the boundaries

3.1.1 Bossinesq Approximation

The Bossinesq approximation states that the fluid density is a linear function of the temperature and concentration.

$$(\rho-\rho_0) = -\rho_0[\beta_T(T-T_0)-\beta_C(C-C_0)] \tag{3.1}$$

3.1.2 Finite Element Analysis

Solving the governing equation for the purpose of modeling and simulation can be carried out with several methods such as control volume and finite element methods. In this study, the finite element method (FEM) is utilized. It is very effective and accurate for solving all kinds of partial differential equations. By applying FEM, we try to minimize the infinite number of degrees of freedom (DoF) in a given problem to a manageable finite number of DoF by a system of algebraic equations. A model under study and analysis is then divided into smaller areas known as elements. Each element is defined by a finite number of points known as nodes by which all the variables in the analysis, such as speed, concentration, pressure and temperature to name a few, can be

evaluated and analyzed [42]. In the model under study for this thesis, which has over fourteen thousand nodes, the Glarkin finite element method approximation has been employed for silicon concentration and velocity in the solvent region along three axes (*u, v, w* and C) as well as the solvent temperature and pressure (*T* and *P*). This was done to reduce partial differential equations and boundary conditions to a set of algebraic equations, as mentioned above. This is completed by using the segregated algorithm to solve those equations [43].

GAMBIT, which is commercial software, has been used to make a three dimensional geometry of the model under this study. Once the eight-node hexahedron elements produced via meshing the model by GAMBIT, the geometry and the associated mesh are exported to another commercial software known as FIDAP [43]. FIDAP is computational fluid dynamics (CFD) software and is used to numerically model the crystal growth of $Ge_{0.98}$ $Si_{0.02}$ in this study. Figure 17 depicts the finite mesh of the solvent region in this study.

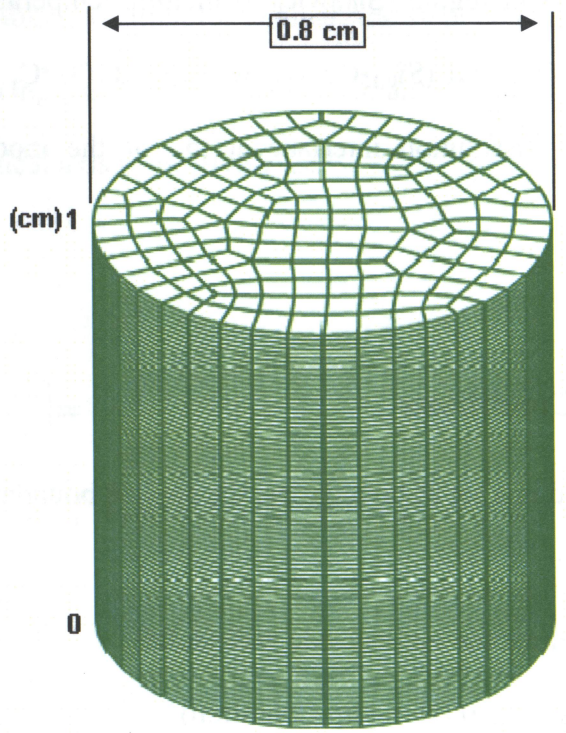

Figure 17 Finite Elements of the Model, solvent region

3.2 Model Description

The model in this study is the middle section of the entire set up which is the solvent region. The model has a cylindrical shape with 0.8 cm diameter and the height of 1 cm. The top of the model is considered as the dissolution interface which is attached to the feed rod, and the bottom of the model is attached to the substrate or the seed (Ge) and is defined as the growth interface. The model is held in a quartz ampoule with a wall thickness of 0.1 cm. A set of heating coil is used to heat up the model at the external surface of the quartz container. A uniform temperature profile, provided by Dalhousie University, is assumed along the circumferential direction. This profile is then converted to non-dimensional format in terms of length and temperature and later applied to the solvent region of the TSM process, by using a best fit polynomial curve to be read by the

FIDAP. Since the solvent region ($Si_{0.02}Ge_{0.98}$) melting temperature, which is 971 °C, is less than that of the feed rod ($Si_{0.15}Ge_{0.85}$), which is 1100 °C, therefore the Si will be segregating from the dissolution interface at top of the model towards the growth interface at the bottom.

3.3 Boundary Conditions

This model is confined in a set of boundaries; the applied boundary conditions are as follow;

1. At the quartz ampoule vertical side wall (solid):
   - $u = 0, v = 0, w = 0$ (Non-slip Condition)
   - $\frac{\partial c}{\partial r} = 0$
2. At the dissolution Interface, Horizontal plane at the top of the model
   - $c = c_1 = 0.15$
3. At the growth interface, Horizontal plane at the bottom of the model
   - $c = c_2 = 0.02$

Where c_2 and c_1 are the silicon (Si) concentration in the crystal growth process at growth and dissolution interfaces respectively. These values excerpted from [44].

3.4 Dimensional Governing Equations

3.4.1 Navier-Stokes Equations:

The full Navier-Stokes equation for laminar, transient condition incompressible Newtonian flows, by taking the Boussinesq approximation is defined for radial, circumferential and vertical axis respectively as:

r-component:

$$\rho\left(\frac{\partial u}{\partial t}+u\frac{\partial u}{\partial r}+\frac{v}{r}\frac{\partial u}{\partial \varphi}+w\frac{\partial u}{\partial z}-\frac{v^2}{r}\right)= -\frac{\partial p}{\partial r}+\mu\left(\nabla^2 u-\frac{u}{r^2}-\frac{2}{r^2}\frac{\partial v}{\partial \varphi}\right)+F_r^M+\rho g_r\left[\beta_T(T-T_0)-\beta_C(c-c_0)\right] \tag{3.2}$$

φ-component:

$$\rho\left(\frac{\partial v}{\partial t}+u\frac{\partial v}{\partial r}+\frac{v}{r}\frac{\partial v}{\partial \varphi}+w\frac{\partial v}{\partial z}+\frac{uv}{r}\right)= -\frac{1}{r}\frac{\partial p}{\partial \varphi}+\mu\left(\nabla^2 v+\frac{2}{r^2}\frac{\partial v}{\partial \varphi}-\frac{v}{r^2}\right)+F_\varphi^M+\rho g_\varphi\left[\beta_T(T-T_0)-\beta_C(c-c_0)\right] \tag{3.3}$$

z-component:

$$\rho\left(\frac{\partial w}{\partial t}+u\frac{\partial w}{\partial r}+\frac{v}{r}\frac{\partial w}{\partial \varphi}+w\frac{\partial w}{\partial z}\right)= -\frac{\partial p}{\partial z}+\mu\left(\nabla^2 w\right)+F_z^M+\rho g_z\left[\beta_T(T-T_0)-\beta_C(c-c_o)\right] \tag{3.4}$$

Where the Laplacian (del) operator is defined as;

$$\nabla^2=\left(\frac{1}{r}\frac{\partial}{\partial r}\left(r\frac{\partial}{\partial r}\right)+\frac{1}{r^2}\frac{\partial^2}{\partial \varphi^2}+\frac{\partial^2}{\partial z^2}\right) \tag{3.5}$$

The melt temperature (T_0) of Germanium (Ge) and the Silicon (Si) concentration (c_0) are used as the reference temperature and concentration respectively. Equations (3.2), (3.3)

and (3.4) satisfy the momentum equations (Navier-Stokes) in the solvent region in all three directions of radial (r), angular (φ) and axial (z) respectively. Three external forces F_r^M, F_φ^M and F_z^M represent the magnetic body force components along the r, φ and z direction respectively and are defined as;

$F_r^M = -\sigma B_r^2 u$, $F_\varphi^M = -\sigma B_\varphi^2 v$ and $F_z^M = 0$ [45]. It is clear that the magnetic body force components, acting on the solvent region, are only in the radial and angular directions respectively.

3.4.2 Energy Equation:

Energy equation for the solvent region (liquid phase) is presented as:

$$\rho c_p \left(\frac{\partial T}{\partial t} + u\frac{\partial T}{\partial r} + \frac{v}{r}\frac{\partial T}{\partial \varphi} + w\frac{\partial T}{\partial z} \right) = \kappa \left(\frac{1}{r}\frac{\partial}{\partial r}\left(r\frac{\partial T}{\partial r} \right) + \frac{1}{r^2}\frac{\partial^2 T}{\partial \varphi^2} + \frac{\partial^2 T}{\partial z^2} \right) \tag{3.6}$$

Where c_p and κ are specific heat and thermal conductivity of the solvent respectively.

3.4.3 Continuity (mass conservation) Equation:

The continuity equation is expressed as:

$$\frac{\partial \rho}{\partial t} + \frac{1}{r}\frac{\partial}{\partial r}(ru) + \frac{1}{r}\frac{\partial v}{\partial \varphi} + \frac{\partial w}{\partial z} = 0 \tag{3.7}$$

3.4.4 Mass Transport Equation:

$$\frac{\partial c}{\partial t} + u\frac{\partial c}{\partial r} + \frac{v}{r}\frac{\partial c}{\partial \varphi} + w\frac{\partial c}{\partial z} = \alpha_c \left(\frac{1}{r}\frac{\partial}{\partial r}\left(r\frac{\partial c}{\partial r} \right) + \frac{1}{r^2}\frac{\partial^2 c}{\partial \varphi^2} + \frac{\partial^2 c}{\partial z^2} \right) \tag{3.8}$$

Where c and α_c are silicon concentration and solutal diffusivity respectively.

3.5 Dimensional Analysis

Dimensional analysis, simply put, is another useful tool of modern fluid mechanics. It is basically the mathematics of dimensions of quantities [46]. This method is used to reduce the number and complexity of experimental variables which affect a given physical phenomenon, by using a sort of compacting technique [47]. Reynolds number, Prandtl number and Grashof number are a few examples of dimensionless parameters which are used in this study, Table 1.

3.5.1 Dimensionless Variables

The dimensionless variables are used to achieve the aforementioned goals. They are used to help make all the governing equations such as Navier-Stokes equations to become non-dimensional which further on enhance and expedite the computation processes.

These variables can be defined as follow;

$$\mathrm{R}=\frac{r}{L}\ ,\ U=\frac{u}{u_0}\ ,\ V=\frac{v}{u_0}\ ,\ W=\frac{w}{u_0}\ ,\ Z=\frac{z}{L}\ ,\ \theta=\frac{T-T_0}{\Delta T}\ ,\ C=\frac{c-c_0}{\Delta c}\ ,$$

$$P=\frac{pL}{\mu u_0}\ ,\ B^*=\frac{B}{|B_0|}\ ,\ \omega^*=\frac{\omega L}{u_0}\ ,\ F=\frac{fL}{u_0}\ \text{and}\ \tau=\frac{tu_0}{L}.$$

Where R and Z are considered as non-dimensional radial and axial coordinates, respectively. U, V and W are dimensionless radial, angular and axial velocity, respectively. θ (theta) is the non-dimensional temperature, C is the dimensionless solute concentration, P is dimensionless hydrodynamic pressure, B^* is dimensionless variable of

magnetic field induction, ω^* is non-dimensional angular velocity, F is dimensionless frequency and τ is referred to the dimensionless variable of time (t). The reference velocity (u_0) is defined as; $u_0 = \sqrt{g\beta_T \Delta TL}$ where L is the characteristic (reference) length, T_0 is the reference temperature (melt temperature of Ge) and ΔT is set equal to one for simplicity.

Table 2 Some dimensionless parameters, excerpted from [47] and [4].

Parameter	**Definition**	**Qualitative Ratio**	**Application**
Reynolds Number	$\mathrm{Re} = \frac{\rho u_0 L}{\mu}$	$\frac{Inertia}{Vis\cos ity}$	Almost Always
Schmidt Number	$Sc = \frac{\nu}{\alpha_c}$	$\frac{Viscous}{Solutal\ diffusivity}$	Mass transfer
Prandtl Number	$\mathrm{Pr} = \frac{c_p \mu}{\kappa}$	$\frac{Dissipation}{Thermal\ Conductivity}$	Heat Convection
Peclet Number (Thermal)	$(\mathrm{P}e)_T = \frac{LV}{\alpha} = \mathrm{Re}\,.\,\mathrm{Pr}$	$\frac{Inertia}{Thermal\ Diffusivity}$	F.E.A Heat transfer
Peclet Number (Diffusion)	$(\mathrm{P}e)_m = \frac{LV}{D} = \mathrm{Re}\,.\,\mathrm{Sc}$	$\frac{Inertia}{Mass\ Diffusivity}$	F.E.A Fluid Flow
Hartmann Number	$Ha = \lvert B_0 \rvert L\sqrt{\frac{\sigma}{\mu}}$	$\frac{Magntic\ Force}{Viscous\ Force}$	Magnetic field effect
Grashof (Thermal)	$Gr_T = \frac{\beta_T \Delta T g L^3 \rho^2}{\mu^2}$	$\frac{Buoyancy}{Viscousity}$	Natural Convection
Grashof (Solutal)	$Gr_c = \frac{\beta_c \Delta C g L^3 \rho^2}{\mu^2}$	$\frac{Buoyancy}{Viscousity}$	Natural Convection

3.5.2 Dimensionless form of Governing Equations

The detailed and step by step non-dimensionalization of all the governing equations can be found in appendix "A".

3.5.2.1 Navier-Stokes Equations

The dimensionless transient Navier-Stokes equation for ***r***, ***φ*** and ***z*** directions are presented respectively as follow:

r-component:

$$\begin{aligned}&\mathrm{Re}\left(\frac{\partial U}{\partial \tau}+U\frac{\partial U}{\partial R}+\frac{V}{R}\frac{\partial U}{\partial \varphi}+W\frac{\partial U}{\partial Z}-\frac{V^2}{R}\right)=\\&-\frac{\partial P}{\partial R}+\left(\nabla^2 U-\frac{U}{R^2}-\frac{2}{R^2}\frac{\partial V}{\partial \varphi}\right)-\frac{1}{2}Ha^2\omega^* B_1^2+\frac{(Gr_T)_r}{\mathrm{Re}}\theta-\frac{(Gr_C)_r}{\mathrm{Re}}C\end{aligned} \tag{3.9}$$

φ-component:

$$\begin{aligned}&\mathrm{Re}\left(\frac{\partial V}{\partial \tau}+U\frac{\partial V}{\partial R}+\frac{V}{R}\frac{\partial V}{\partial \varphi}+W\frac{\partial V}{\partial Z}+\frac{UV}{R}\right)=\\&-\frac{1}{R}\frac{\partial P}{\partial \varphi}+\left(\nabla^2 V+\frac{2}{R^2}\frac{\partial V}{\partial \varphi}-\frac{V}{R^2}\right)+\frac{1}{2}Ha^2\omega^* B_2^2+\frac{(Gr_T)_\varphi}{\mathrm{Re}}\theta-\frac{(Gr_C)_\varphi}{\mathrm{Re}}C\end{aligned} \tag{3.10}$$

z-component:

$$\begin{aligned}&\mathrm{Re}\left(\frac{\partial W}{\partial \tau}+U\frac{\partial W}{\partial R}+\frac{V}{R}\frac{\partial W}{\partial \varphi}+W\frac{\partial W}{\partial Z}\right)=\\&-\frac{\partial P}{\partial Z}+\left(\nabla^2 w\right)+0+\frac{Gr_{T_z}}{\mathrm{Re}}\theta-\frac{Gr_{C_z}}{\mathrm{Re}}C\end{aligned} \tag{3.11}$$

3.5.2.2 Energy Equation

$$\left(\frac{\partial\theta}{\partial\tau}+U\frac{\partial\theta}{\partial R}+\frac{V}{R}\frac{\partial\theta}{\partial\varphi}+W\frac{\partial\theta}{\partial Z}\right)=\frac{1}{Re.Pr}\left(\frac{\partial^2\theta}{\partial R}+\frac{1}{R^2}\frac{\partial^2\theta}{\partial\varphi^2}+\frac{\partial^2\theta}{\partial Z^2}\right) \tag{3.12}$$

3.5.2.3 Continuity Equation

$$\frac{\partial\rho}{\partial\tau}+\frac{1}{R}\frac{\partial}{\partial R}(RU)+\frac{1}{R}\frac{\partial V}{\partial\varphi}+\frac{\partial W}{\partial Z}=0 \tag{3.13}$$

3.5.2.4 Mass Transport Equation

$$\frac{\partial C}{\partial\tau}+U\frac{\partial C}{\partial R}+\frac{V}{R}\frac{\partial C}{\partial\varphi}+W\frac{\partial C}{\partial Z}=\frac{1}{Re.Sc}\left(\frac{\partial^2 C}{\partial R^2}+\frac{1}{R^2}\frac{\partial^2 C}{\partial\varphi^2}+\frac{\partial^2 C}{\partial Z^2}\right) \tag{3.14}$$

3.6 Mesh Sensitivity Analysis

Since time and accuracy ultimately are the essence, therefore to achieve the best and most reliable results and saving computational time and storage capacity, an optimum number of nodes and elements should be defined. For this reason, mesh sensitivity analysis was carried out and ideal numbers of nodes on both circumferential and axial edges were selected based on the heat flux across the dissolution interface in solvent region. As it can be read from the Figure 18 and Table 3, a mesh with 40 circumferential nodes by 80 axial nodes is where the curve is becoming a straight line. A mesh is deemed to be acceptable when the value of the average heat flux changes from one tenth of watts per cm^2 from a coarse mesh to the range of thousandth watts per cm^2 to the next finer mesh. For this reason and the aforementioned reasons, the 40 x 80 mesh combination reasonably meets the computational need and simulation becomes satisfactory for the analysis in this study.

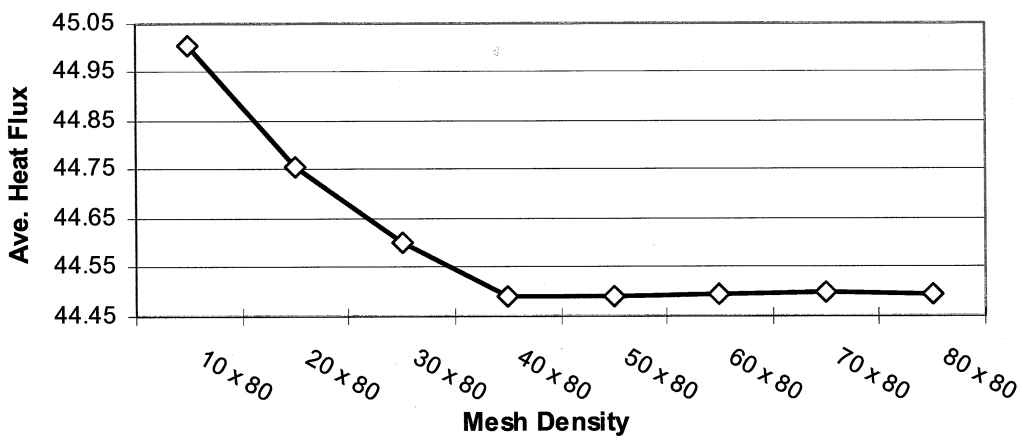

Figure 18 Mesh densities vs. Average heat flux at Dissolution Interface, excerpt from Table 3

Table 3 Mesh Sensitivity analysis

Item	Mesh Density (Grids) (circumferential x Axial)	Average Heat Flux Dimensionless Values From FIDAP
1	10 x 80	45.0061
2	20 x 80	44.7551
3	30 x 80	44.5999
4	40 x 80	44.4918
5	50 x 80	44.4909
6	60 x 80	44.4940
7	70 x 80	44.4978
8	80 x 80	44.4956

Figure 19 shows eight different settings of nodes for the mesh sensitivity study, numbers represent the circumferential by axial respectively.

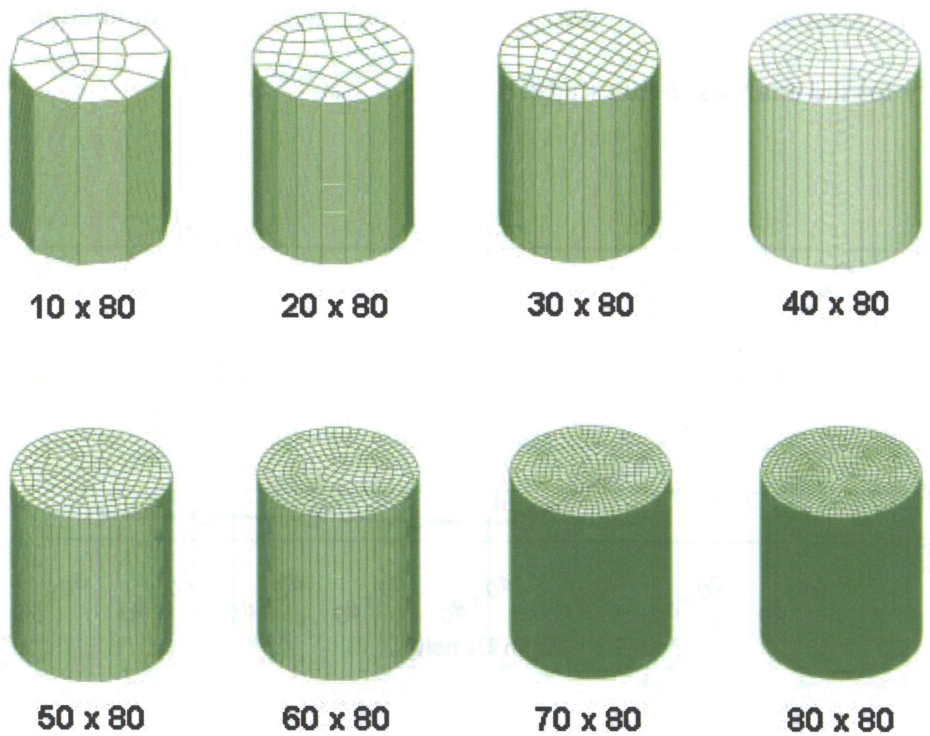

Figure 19 Different Mesh densities

3.7 The Applied Technique

The Traveling Solvent Method (TSM) is the technique being chosen for this study. In TSM which consists of three sections, the source or the feeding section is $Si_{0.15}Ge_{0.85}$ alloy which is a polycrystalline material and located on the top of the set up, the solvent region or molten part is the middle part and the substrate or the seed (Ge) lies at the bottom section. All the three sections are held in a quartz ampoule [48]. The ampoule is placed in a furnace and the solution (melt) zone would be heated by surrounding heating elements Figure 20. Since the melt temperature of the solvent region is much less than that of the quartz, therefore there would be no oxygen penetration from quartz into the melt and consequently no contamination or impurity occurs which is a great advantage of this technique.

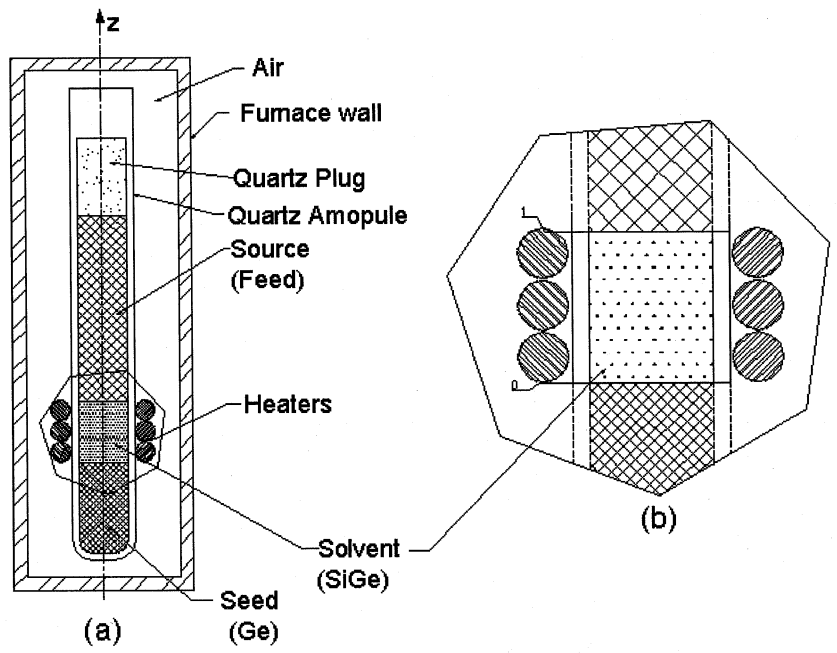

Figure 20 Schematic view of (TSM) procedure, employed to produce the Crystal of $Si_{0.02}Ge_{0.98}$ alloy [48]
a) - Complete set up
b) – Solvent region ($Si_{0.02}Ge_{0.98}$), magnified

CHAPTER 4
Terrestrial and Microgravity Conditions
Results and discussions in Steady State

4.0 INTRODUCTION

The results compiled through the simulation of the solvent region of the model for different gravitational conditions is discussed in this chapter. Two conditions which are taken into the consideration are the terrestrial condition and the microgravity condition. In each scenario, the silicon distribution, along with the speed of distribution, is examined. The effects of applied magnetic field with different intensities and also with several different rotations are discussed.

4.1 Temperature Conditions

Figure 21, depicts the uniform heating profile plotted based on the polynomial obtained from the Dalhousie University which is an experimented result applied on the model. This profile reveals a large temperature gradient in the melt zone (solvent region), the maximum dimensionless temperature is read as 58.4 (Appendix C, Table-c1) or 1029.4 °C in the solvent region, with this temperature profile, it is expected to observe the convection pattern where the hotter particle near the wall of the quartz container also known as crucible would rise to the top of the region and the cooler particles falling down in the middle of the solvent region to the bottom of the region.

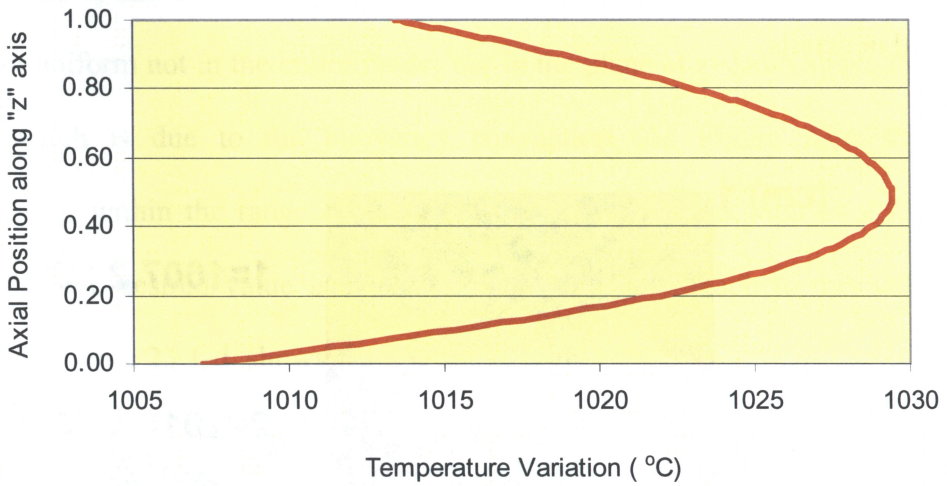

Figure 21 Uniform Temperature Heater Profile, applied to the solvent region of the model, (Based on an experimental study conducted by Dalhousie University)

4.2 Terrestrial Condition

The terrestrial condition refers to the earthbound condition where the acceleration due to the gravity where; $g = 9.81\ m/s^2$. As described in previous chapters, the attempt through out the studies conducted before [37], [40], [49] and in this study, is to suppress the buoyancy induced convection in the solvent region. Therefore, to see the conditions such as the temperature variation, silicon distribution (molecule) and the speed of the distribution, should be observed prior to any further action being taken. Since the condition close to the growth interface is of the interest to us because the more flat and uniform silicon distribution with the concentration as close as to 2 percent, the better the result is to be considered. Therefore, a plane is cut through the model at z=0.1 cm would be considered to be the defining level for this study. Figure 22, shows the temperature distribution along the vertical cross-sections of the model (solvent region). Further on, the

effects of suppressing this observed convection by using rotating magnetic field will be discussed in details.

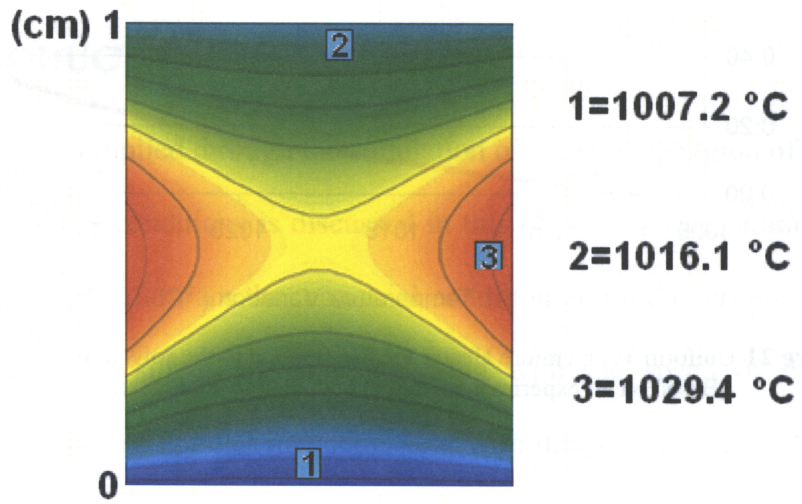

Figure 22 Temperature distributions in a vertical cross section passing through the center axis of the model in Terrestrial condition.

From Figure 22, it can be seen that the temperature distribution, in the vertical cross-section of the model, forms both concaves and convexes. This shows the variation of the radial temperature gradients but this is very minimal variation since the semiconductor materials' heat transfer is mainly governed by the conduction not the convection [50]. The solvent region has a relatively low Prandtl number in the order of 13×10^{-4} (since Dimensionless Prandtl number is defined as $P_r = c_p \mu / k$, there should either be less dynamic viscous force (μ) or higher thermal diffusivity (k) involved to make this number so small). Therefore the buoyant convection due to thermal effects is too weak to have noticeable impacts on the temperature distribution in the solvent region and hence can be neglected.

From Figure 23-a, and 23-b, one can see the distribution of the silicon (Si) content of the solute is not uniform not in the entire model nor in the plane at z=1mm above the growth interface, which is due to the buoyancy convection. As Figure 23-c shows, the concentration is within the range of as little as 4.9 percent to as high as 9.33 percent. Knowing that the desired value is 2 percent and attempt to reach to this value is the ultimate goal. Figure 23.1-d, shows that the speed of the

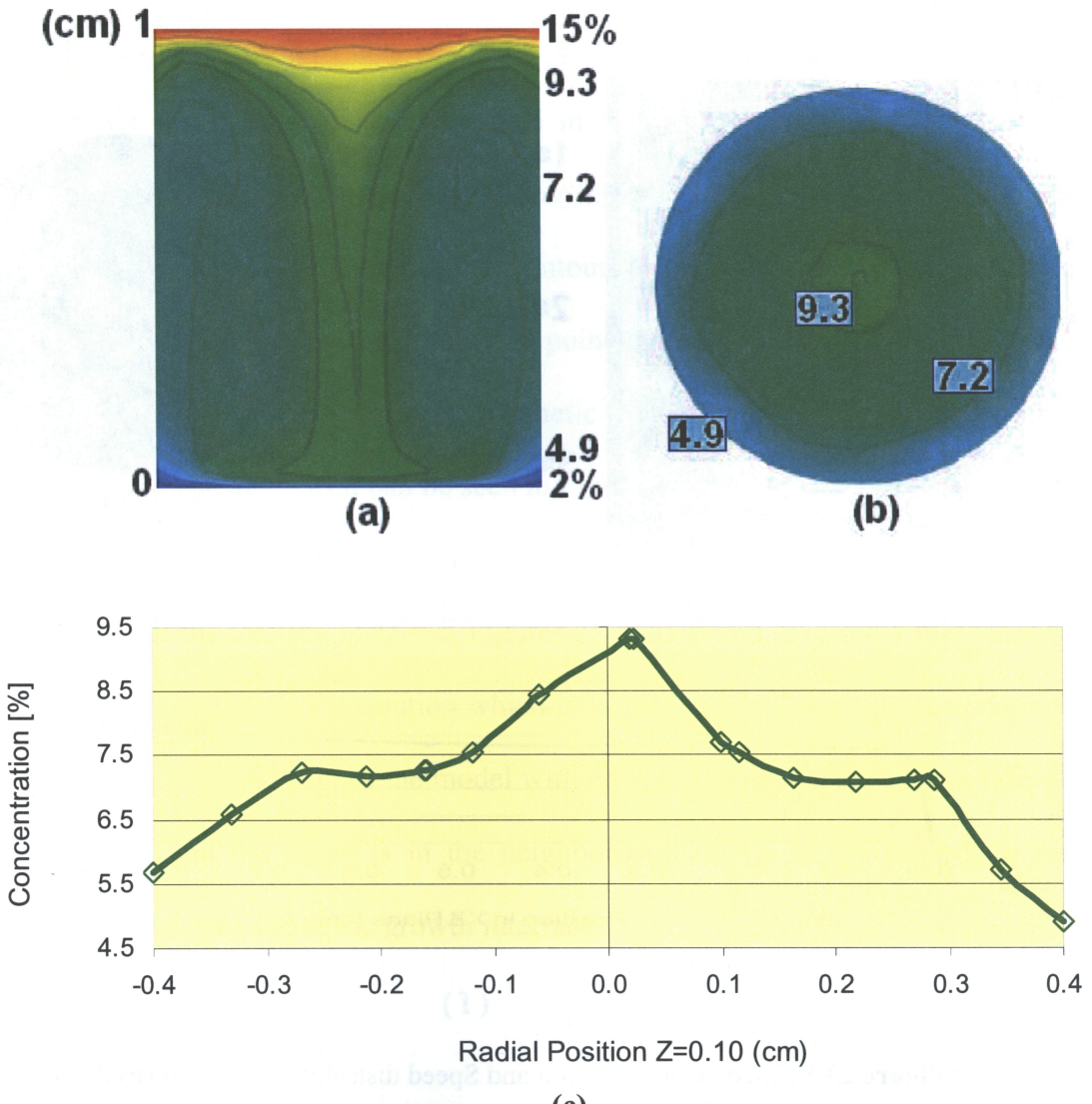

Figure 23 Silicon Concentration and Speed distribution, in Terrestrial Condition
a)- Concentration in Vertical cross section
b)- Concentration in Horizontal cross section
c)- Concentration plot at z=0.1cm above Growth Interface

distribution is somehow chaotic since there are three loops formed in the vertical cross section. In Figure 23.1-f which shows the silicon distribution of the entire model along the vertical axis, although there is a platform at about 9 percent, but from the growth interface or z=0 to the horizontal plane at z=1 mm above the interface, there is a huge variation in terms of concentration from 2 to 9 percent. Other means such as those aforementioned should be employed and the obtained result would then be analyzed and discussed.

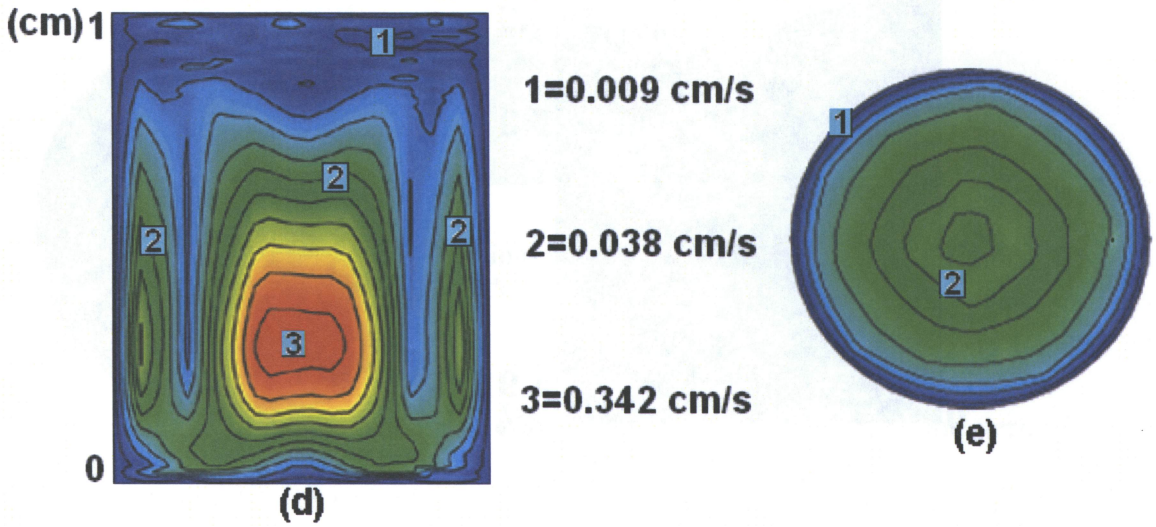

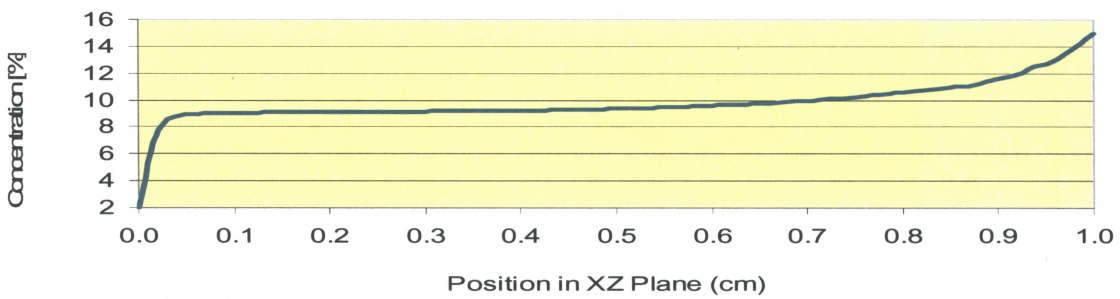

(f)

Figure 23.1 Silicon Concentration and Speed distribution, in Terrestrial Condition

d)- Speed in Vertical cross section
e)- Speed in Horizontal cross section
f)- Concentration along vertical axis of the entire model

4.2.1 Effects of Applied Rotating Magnetic field in Terrestrial Condition

In order to suppress or overcome the induced buoyancy convection in the solvent region, an external uniform magnetic field is applied which acts as a body force. This external force works in the opposite direction of the aforementioned convection in the solvent region. This magnetic filed suppress the sinking motion of the heavier particles in the melt in the central vertical axis of the solvent, therefore, there would be less segregation in the center and as a result of this, less radial concentration gradients would happen. To obtain a better result, several magnetic field intensities (**B** = 10, 15 and 20 mT) and rotations ($\boldsymbol{\Omega}$ = 2, 6 and 8 rpm) were taken into the consideration and carefully studied. Figures 24 a-b-c, reveal silicon distribution contours of the solvent, and it is quite obvious that it is not uniform and from the percentage point of view, it is ranged from as low as 5 percent to as high as 9.3 percent with magnetic field intensity of **B**=10 and with the rotation of $\boldsymbol{\Omega}$ = 2 and again as it can be seen in Figure 24-d the silicon concentration from z=0 to z=1mm above the growth interface is within 2 to 9.3 percent.

As in the case of the rotation of $\boldsymbol{\Omega}$ = 6, Figures 25-a, 25-b and 25-c show that there is no improvement in the silicon distribution which indicates that still there is more deposit in the middle, due to the gravity, of the model with compare to the areas near the side walls of the crucible, and the range is in the neighborhood of 4.8 to 8.4 percent in radial distribution at z=1 mm above the growth interface.

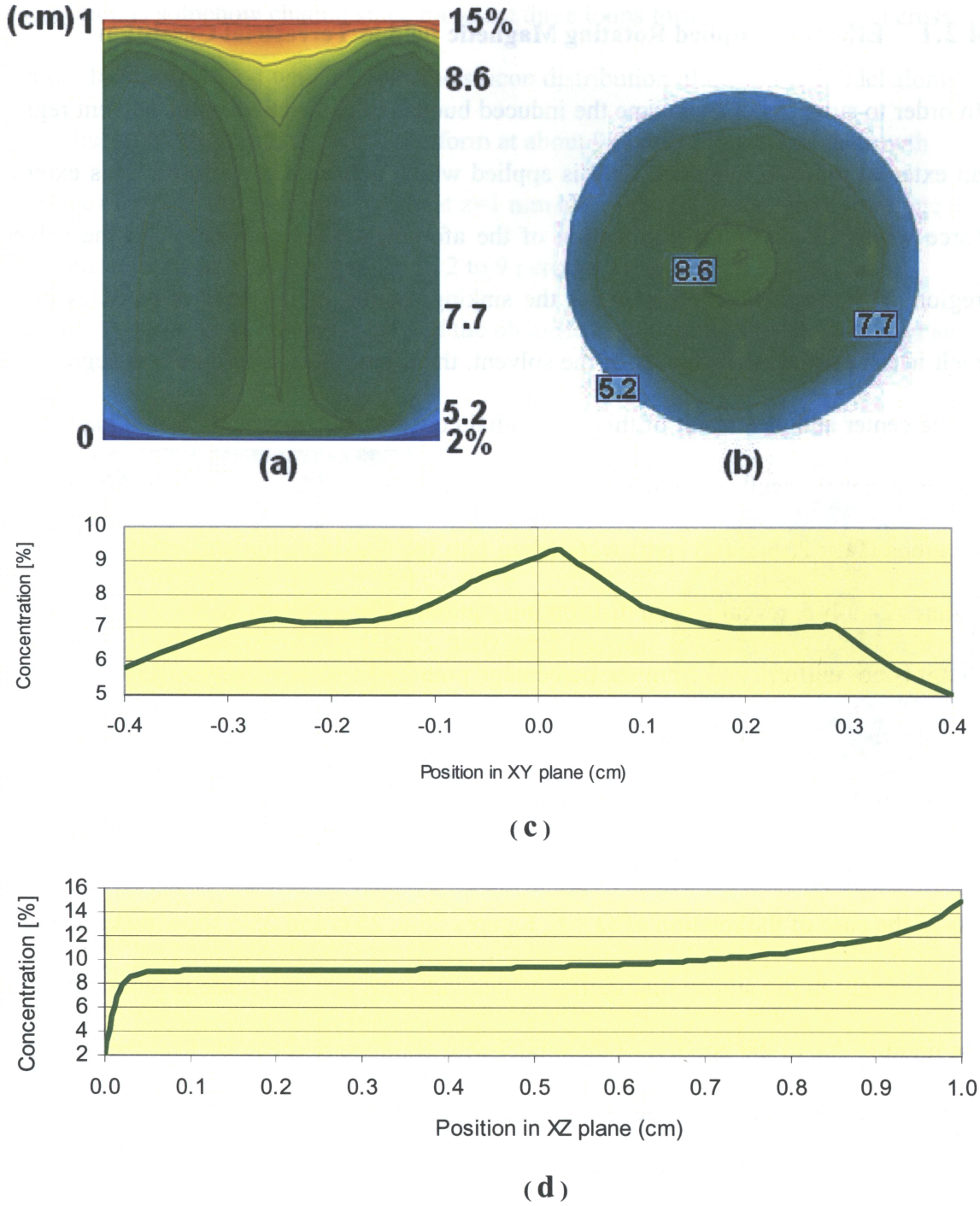

Figure 24 Silicon Concentration under magnetic force of **B**=10mT and rotation of **Ω** = 2 rpm, in Terrestrial Condition

a) - Concentration in Vertical cross section
b) - Concentration in Horizontal cross section
c) - Concentration plot at z=0.1cm above Growth Interface
d) - Concentration along the vertical axis of the entire model

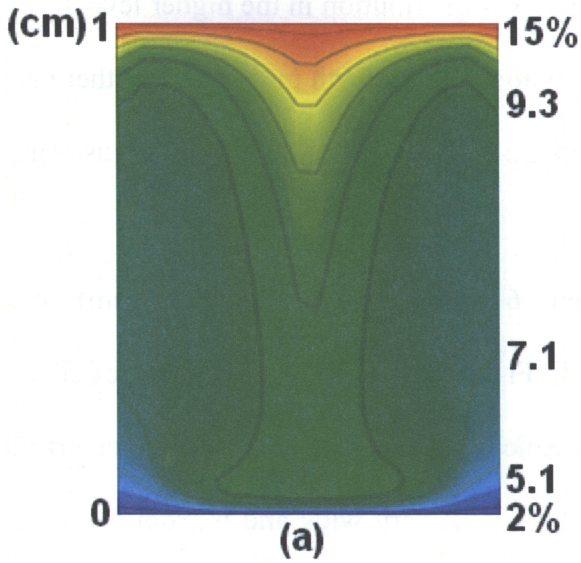

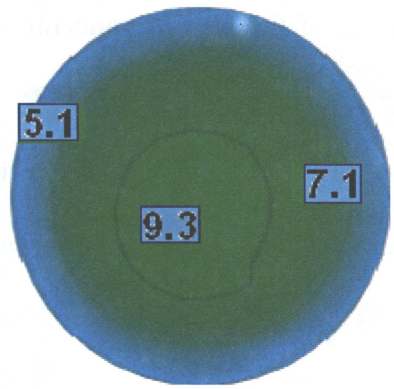

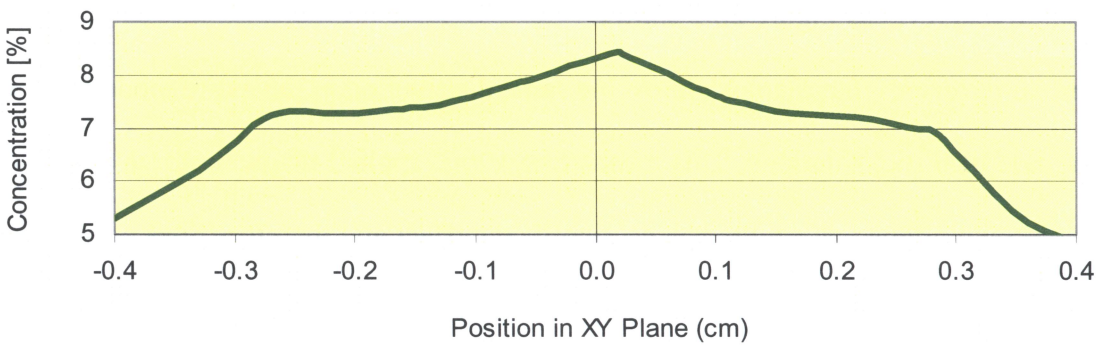

(c)

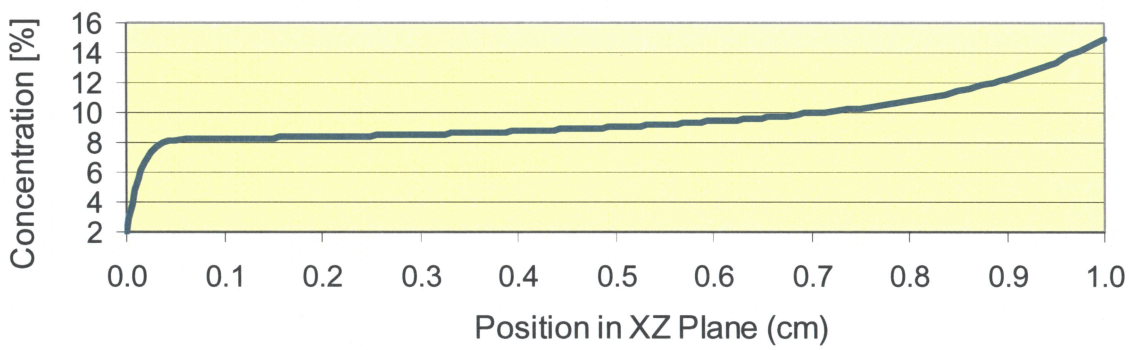

(d)

Figure 25 Silicon Concentration under magnetic force of **B**=10mT and rotation of **Ω** = 6 rpm, in Terrestrial Condition

a)- Concentration in Vertical cross section

b)- Concentration in Horizontal cross section

c)- Concentration plot at z=0.1cm above Growth Interface

d)- Concentration along the vertical axis of the entire model

Figure 25-d, shows that however there is a smoother distribution in the higher level of the model but in the area of our interest or z=1mm above the growth interface, still there is a sharp descending of the silicon concentration from about 8.4 to 2 percent in just 1mm height of the model.

By increasing the number of rotation from 6 revolutions per minute (rpm) to 8 revolutions per minute as it can be observed in Figures 26-a-b, the distribution of silicon concentration is becoming partially uniform since the contours are more concentric at z=1mm but as far as the range is concerned, it is still very wide and is from 5.1 to 8.6 percent in that level as Figure 26-c shows.

Figure 26-d, reveals that there is almost the same distribution in the entire model as it was in the case of 6 rpm rotations. This means that 10mT applied magnetic force along with the eight revolutions per minute has no significant effect and therefore does not suppress the buoyancy driven convection in the solvent region.

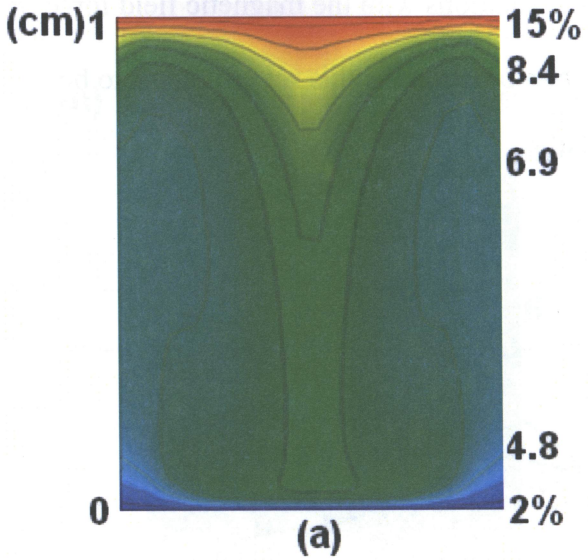

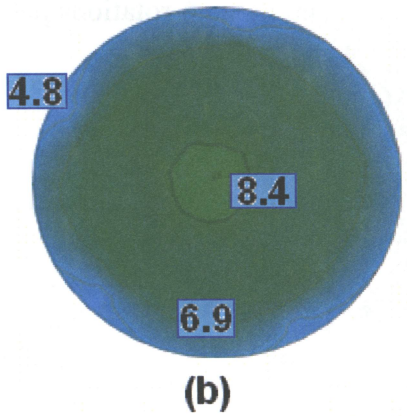

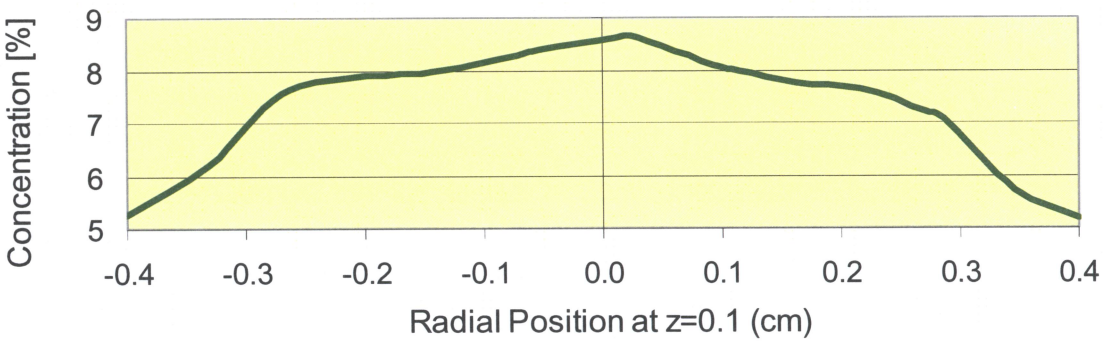

(c)

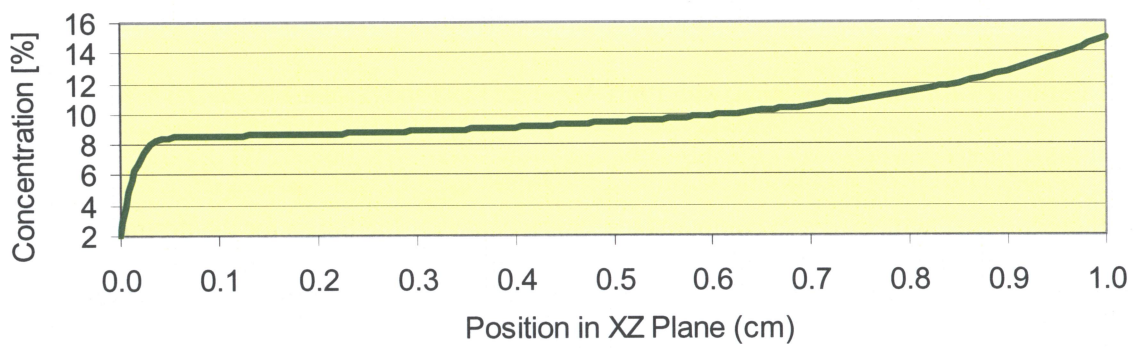

(d)

Figure 26 Silicon Concentration under magnetic force of **B**=10mT and rotation of **Ω** = 8 rpm, in Terrestrial Condition

a)- Concentration in Vertical cross section,

b)- Concentration in Horizontal cross section

c)- Concentration plot at z=0.1cm above Growth Interface

d)- Concentration along the vertical axis of the entire model

Figure 27, compares the three different applied rotations with the magnetic field force of B=10mT and it is quite obvious that the best combination for this set up, seems to be 10mT magnetic force with 6 rotations per minute.

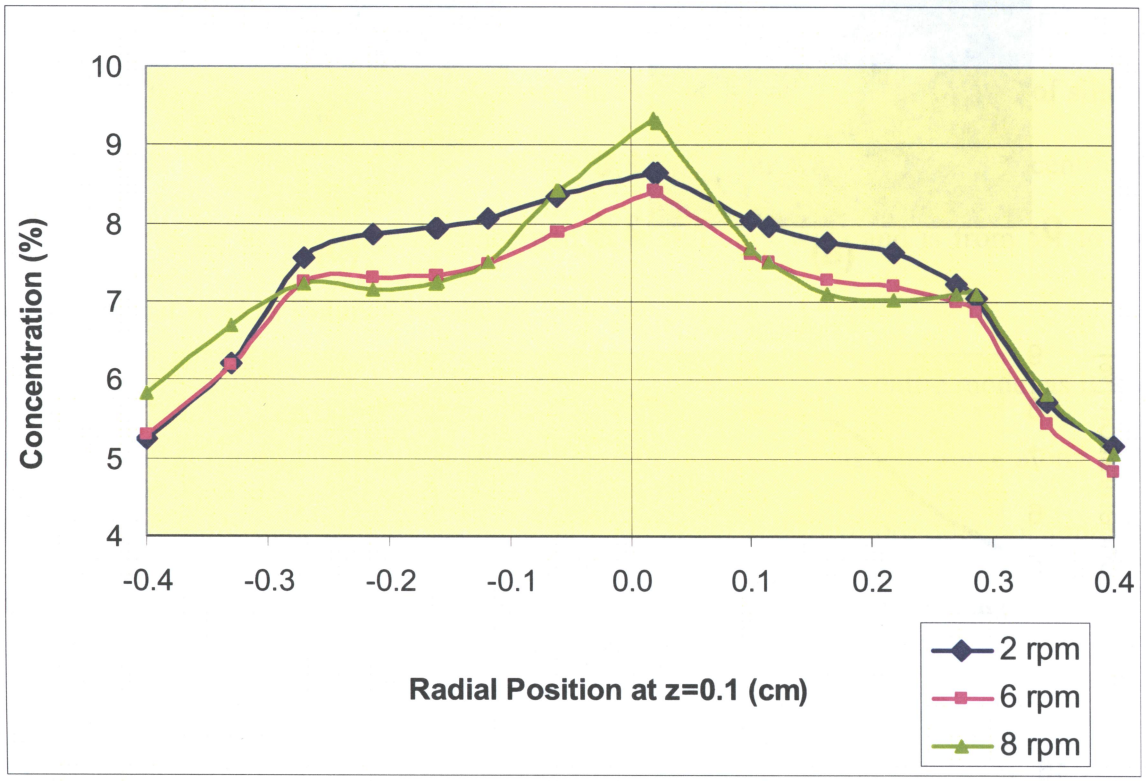

Figure 27 Terrestrial Condition, with 10mT Magnetic Field and rotation of 2, 6, and 8 rpm

Although, 10mT with 6 rpm in comparison seems a better setting but as for the desirable level of silicon concentration particularly near the growth interface, is far from the acceptable result.

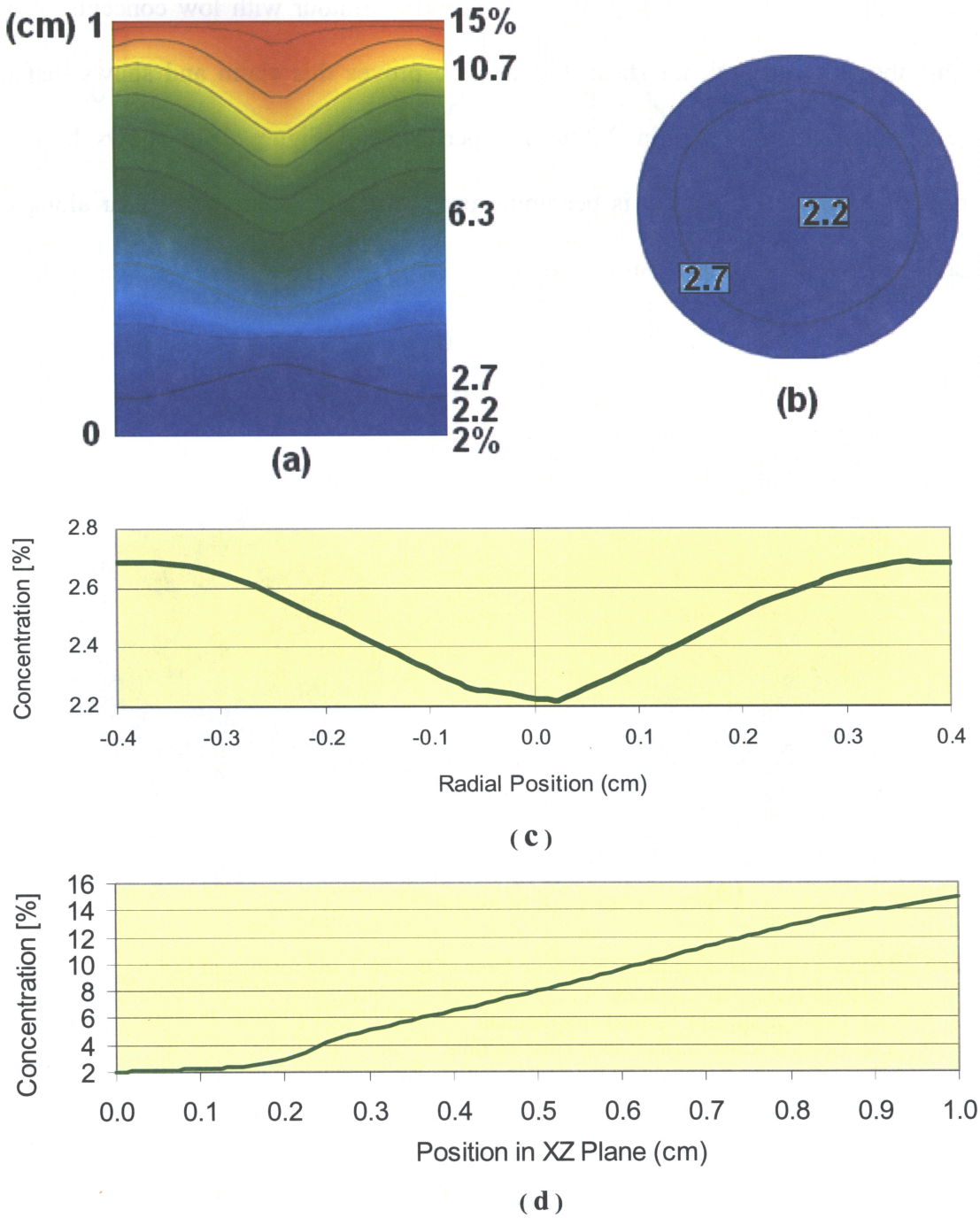

Figure 28 Silicon Concentration under magnetic force of **B**=15mT and rotation of **Ω** = 2 rpm, in Terrestrial Condition

a)- Concentration in Vertical cross section
b)- Concentration in Horizontal cross section
c)- Concentration plot at z=0.1cm above Growth Interface
d)- Concentration along the vertical axis of the entire model

Figure 28-a, depicts that contours are becoming flatter and horizontally more uniform and Figure 28-b shows that there is only one concentric contour with low concentration at z=1mm above the growth interface. Figure 28-c proves this claim and shows that the range of distribution is within 2.2 to 2.6 percent and Figure 28-d shows how the distribution in the entire model is becoming proportionally (relatively) linear along the "Z" axis and it is almost flat at around z=1mm.

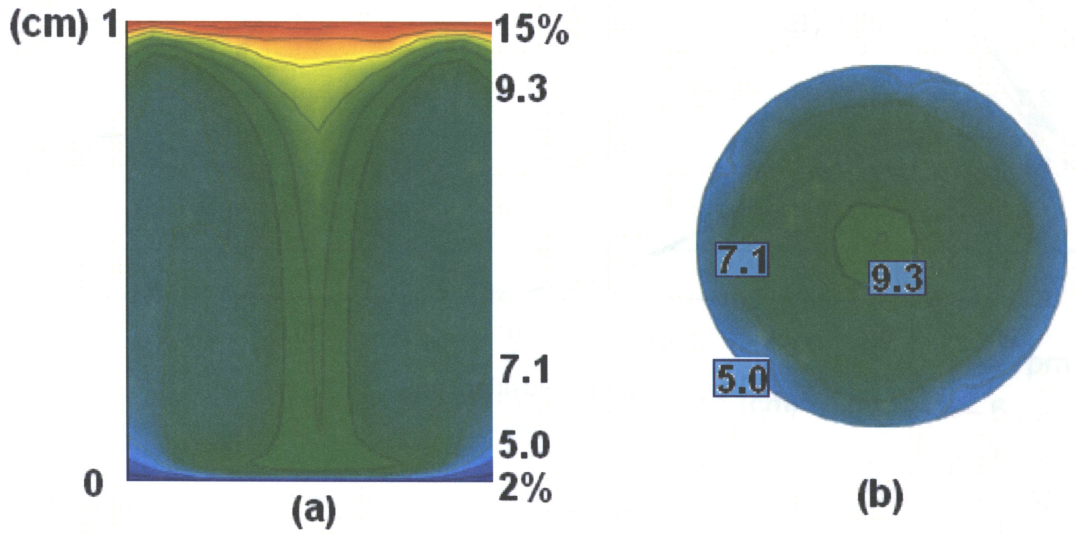

Figure 29 Silicon Concentration under magnetic force of **B**=15mT and rotation of **Ω** = 6 rpm, in Terrestrial Condition
a)- Concentration in Vertical cross section
b)- Concentration in Horizontal cross section

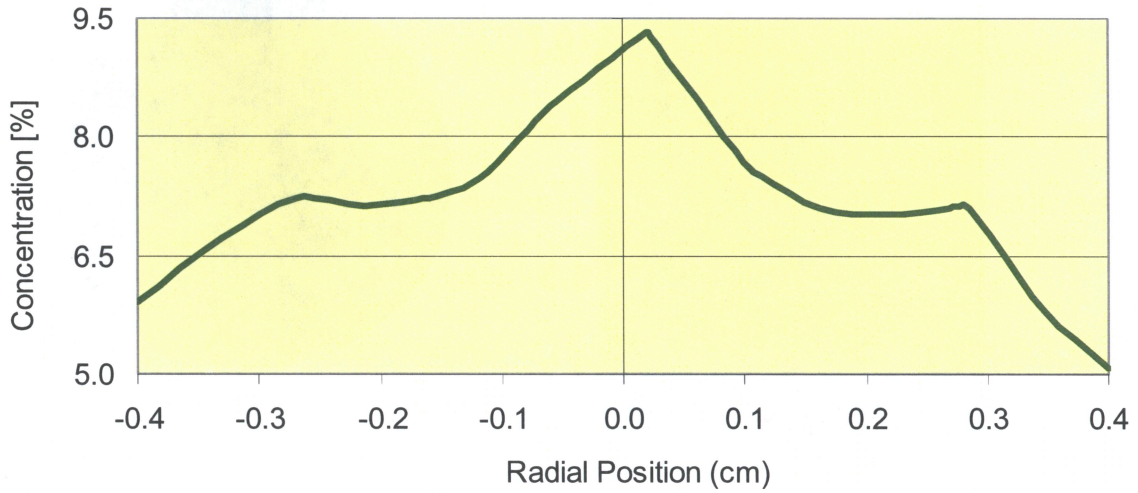

(c)

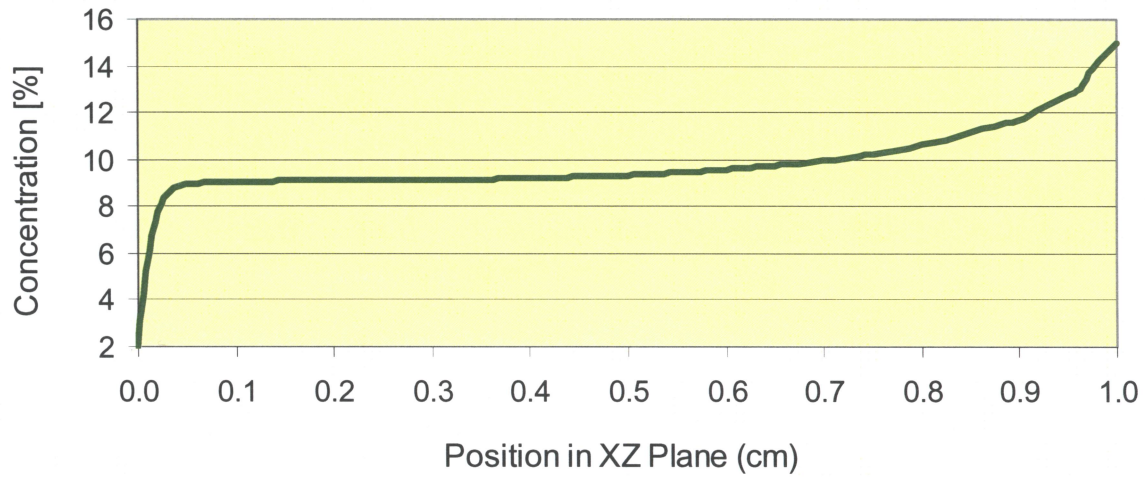

(d)

Figure 29.1 Silicon Concentration under magnetic force of **B**=15mT and rotation of **Ω** = 6 rpm, in Terrestrial Condition
c) - Concentration plot at z=0.1cm above Growth Interface
d) - Concentration along the vertical axis of the entire model

By applying the rotation of six revolution per minute, as it can be seen in Figure 29 a-b, the silicon concentration becomes unstable again and ranges from 5 percent near the wall of the crucible to 9.3 percent in the middle of the model at z=1mm above growth interface. As Figure 29.1-d shows, the almost flat platform of distribution moves to higher percentage and again a large variation of concentration between z=0 to z=1mm, from 2 to 9 percent respectively.

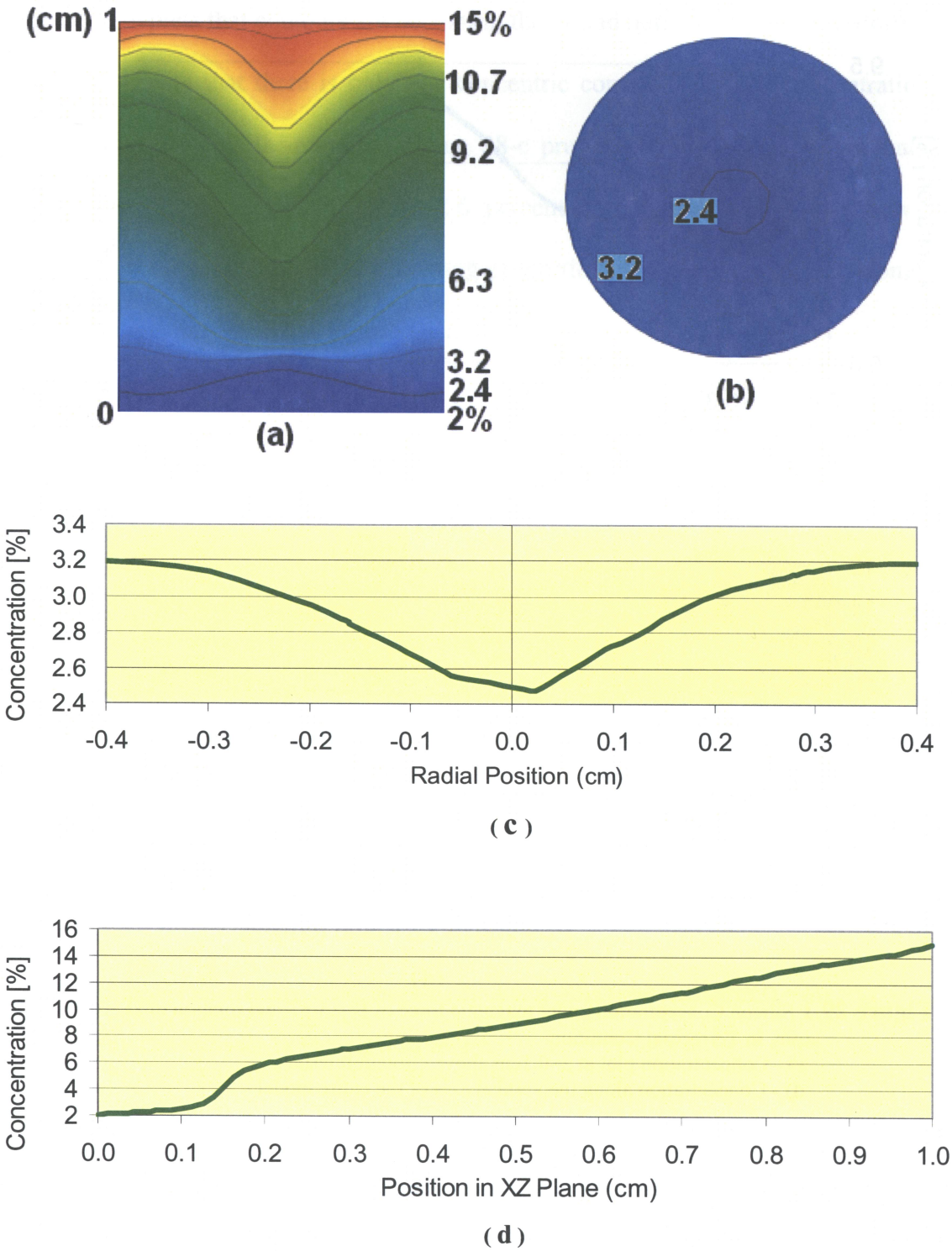

Figure 30 Silicon Concentration under magnetic force of **B**=15mT and rotation of **Ω** = 8 rpm, in Terrestrial Condition
a)- Concentration in Vertical cross section
b)- Concentration in Horizontal cross section
c)- Concentration plot at z=0.1cm above Growth Interface
d)- Concentration along the vertical axis of the entire model

Figure 30-a-b show the contours, once again, are becoming relatively parallel and flatter in the lower zone and Figure 30-c illustrates the concentration at z=1mm above growth interface is within 2.4 percent in the middle of the model to 4.2 percent near the crucible wall. For the entire model as it is shown in the Figure 30-d, the distribution is not as uniform as it was in the case of two rotations.

Figure 31 compares three combinations of 15mT of applied magnetic force with 2, 6, and 8 rpm of rotations. Since the silicon concentration is in the range of 2.2 percent to 2.6 percent, therefore, the best combination in this set up is, 15mT applied magnetic and the rotations of 2 rpm.

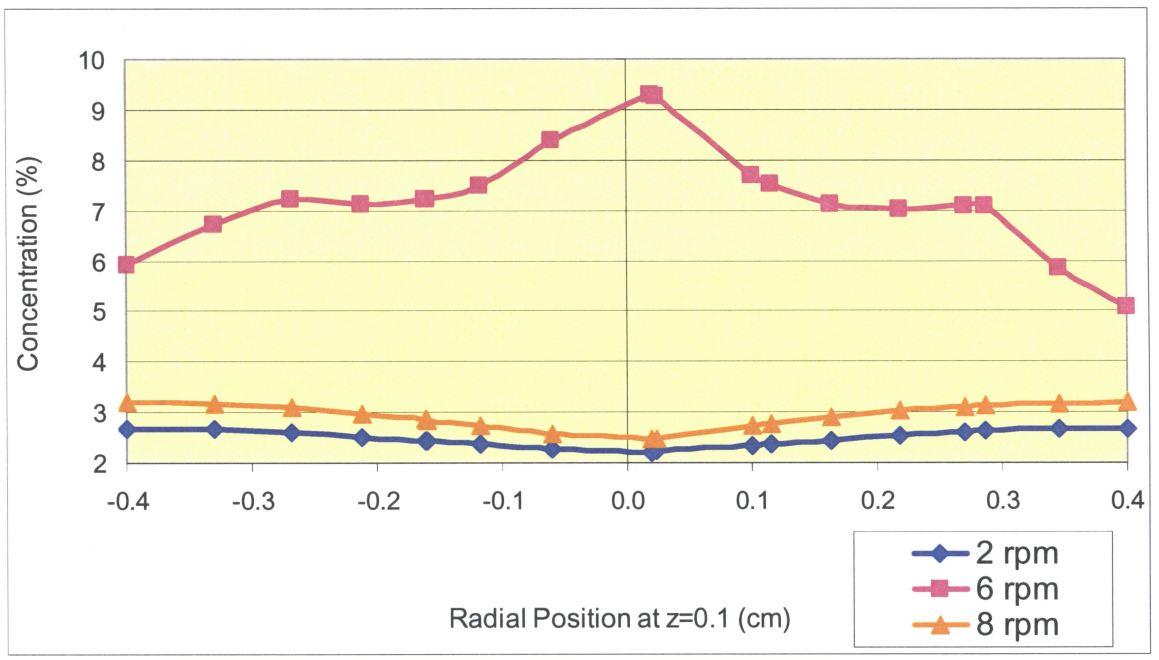

Figure 31 Terrestrial Condition, with 15mT Magnetic Field and rotation of 2, 6, and 8 rpm

Figures 32-a-b-c, show the silicon distribution in the solvent region when a 20mT magnetic field is applied. Although the range of concentration is limited from 3.7 to 4.4 percent but the plot of the horizontal plane at z=1mm above growth interface shows two humps and this is as a result of the convection imposed by additional magnetic field force being applied. Figure 32-d reveals that the concentration is not linear and has a large variation in the lower zone close to the growth interface and that is within 2 to 8.5 percent in just 1mm above the interface.

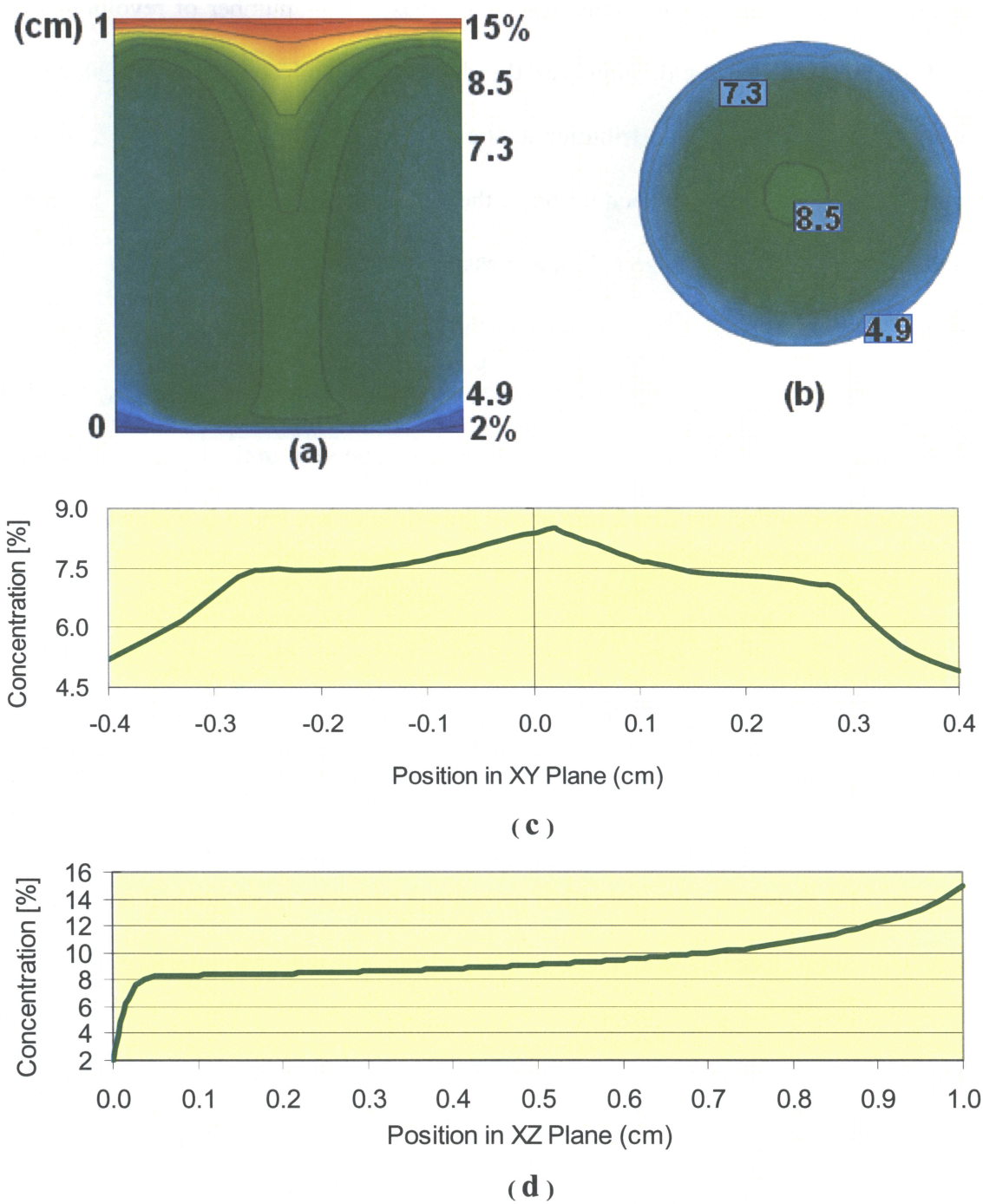

Figure 32 Silicon Concentration under magnetic force of **B**=20mT and rotation of **Ω** = 2 rpm, in Terrestrial Condition.

a)- Concentration in Vertical cross section

b)- Concentration in Horizontal cross section

c)- Concentration plot at z=0.1cm above Growth Interface

d)- Concentration along the vertical axis of the entire model

For the case of the Ω = 6, it seems that the increase in the number of revolutions with 20mT of the magnetic field, improves the distribution and concentration along with lowering down the range of distribution to about 4 percent.

Figures 33-a-b, shows the concentration in the vertical cross section passing through the middle of the model and horizontal plane passing at z=1mm above growth interface. The range of concentration as it can be seen in the Figure 33-c, is within 2.1 percent in the middle of the model to 2.6 percent near the wall of the crucible. But in terms of the concentration distribution in the entire model as it can be seen in the Figure 33-d, there is a large variation within the first 2 mm above growth interface and it is within 2 percent to about 7 percent.

As for the case of eight revolution per minute, Figures 34-a-b-c, depict a more flat and relatively horizontal contours along vertical cross section and again the distribution range of 2.1 to 2.6 percent at z=1mm above growth interface. However, as for the entire model as Figure 34-d shows, the concentration percentage becomes more gradual and relatively linear with almost a flat portion within z=0 to z=2mm above growth interface.

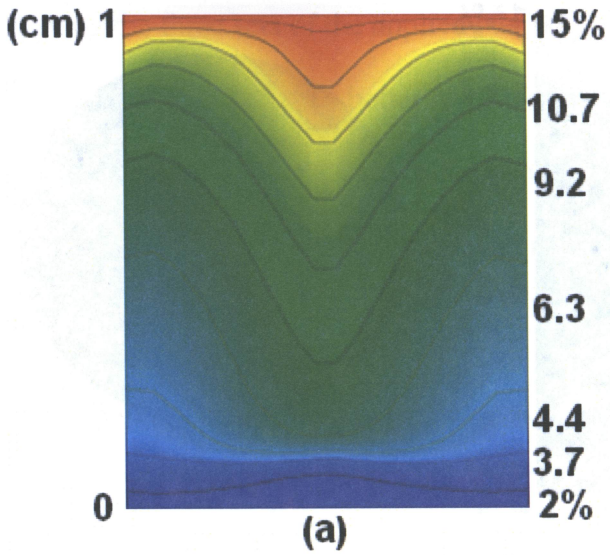

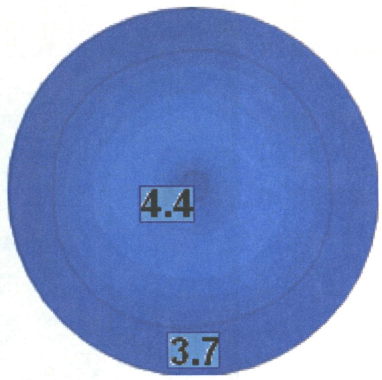

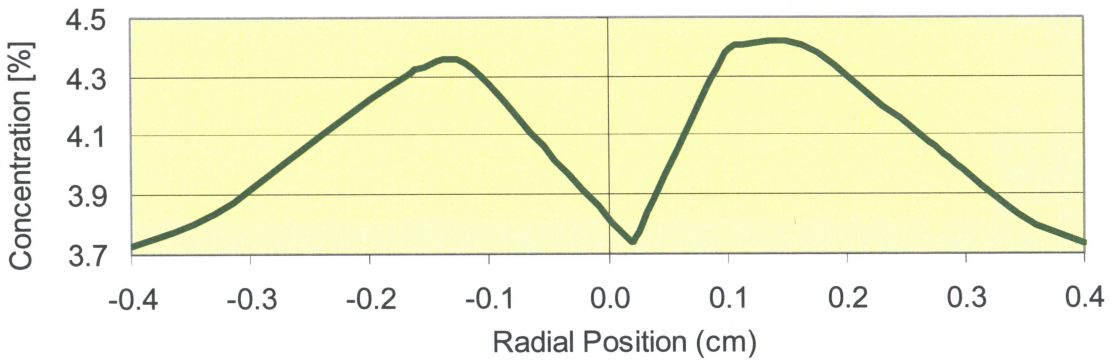

(c)

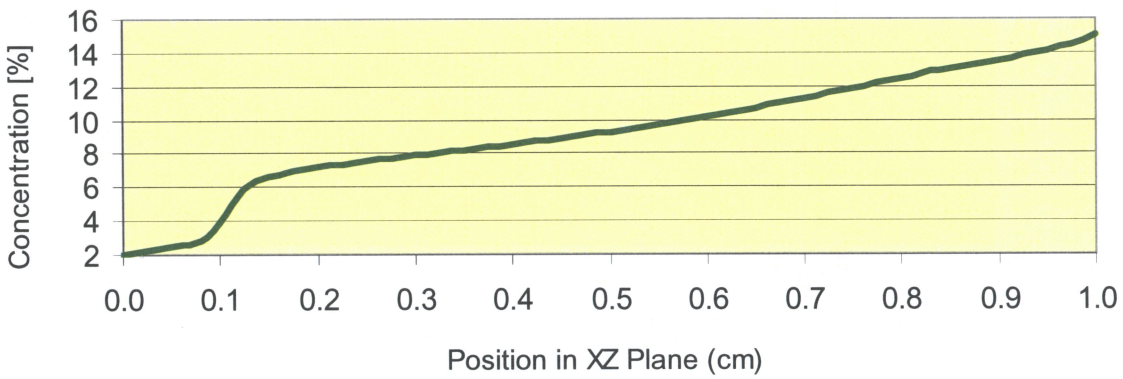

(d)

Figure 33 Silicon Concentration under magnetic force of **B**=20mT and rotation of **Ω** = 6 rpm, in terrestrial condition

a)- Concentration in Vertical cross section

b)- Concentration in Horizontal cross section

c)- Concentration plot at z=0.1cm above Growth Interface

d)- Concentration along the vertical axis of the entire model

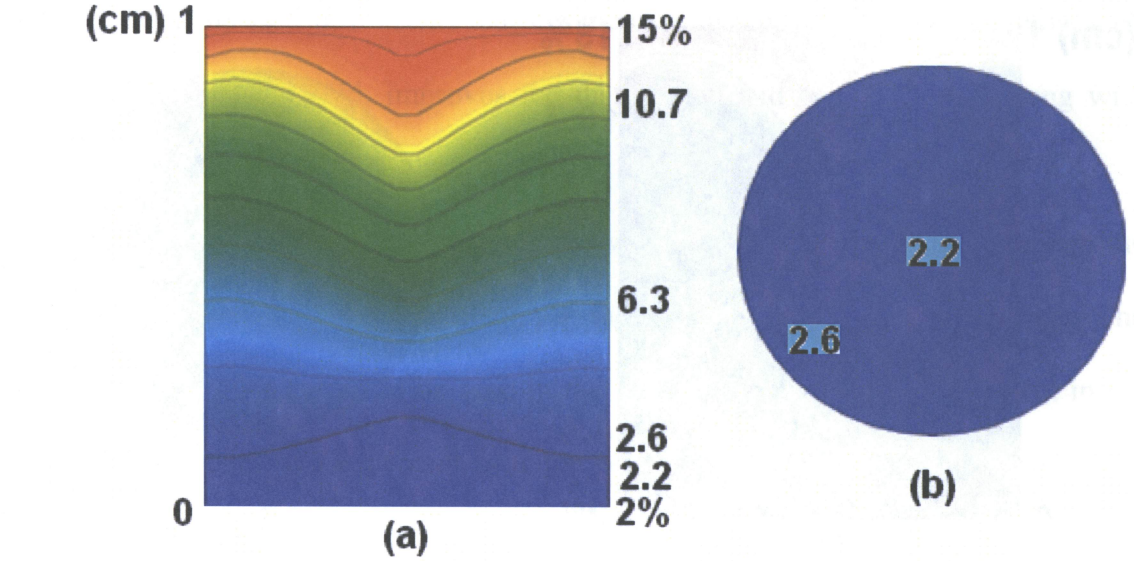

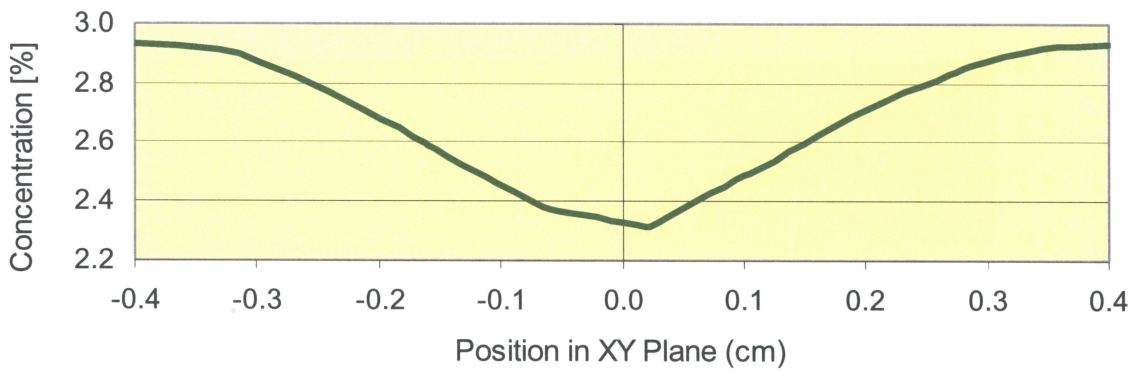

(c)

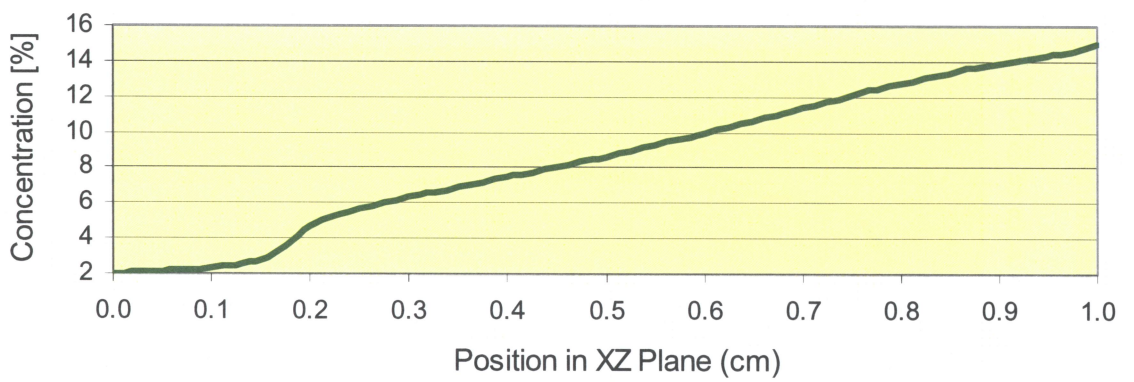

(d)

Figure 34 Silicon Concentration under magnetic force of **B**=20mT and rotation of **Ω** = 8 rpm, in Terrestrial Condition
a)- Concentration in Vertical cross section
b)- Concentration in Horizontal cross section
c)- Concentration plot at z=0.1cm above Growth Interface
d)- Concentration along the vertical axis of the entire model

Among the three sets of the applied magnetic forces of 10, 15 and 20mT, the two settings of the 15 and 20mT had a better result however with contrary results. To more elaborate on them, from the Figure 35, we can conclude that the lower rpm ($\Omega = 2$) with 15mT of magnetic force generate the same result as higher rpm ($\Omega = 8$) and 20mT of external magnetic force.

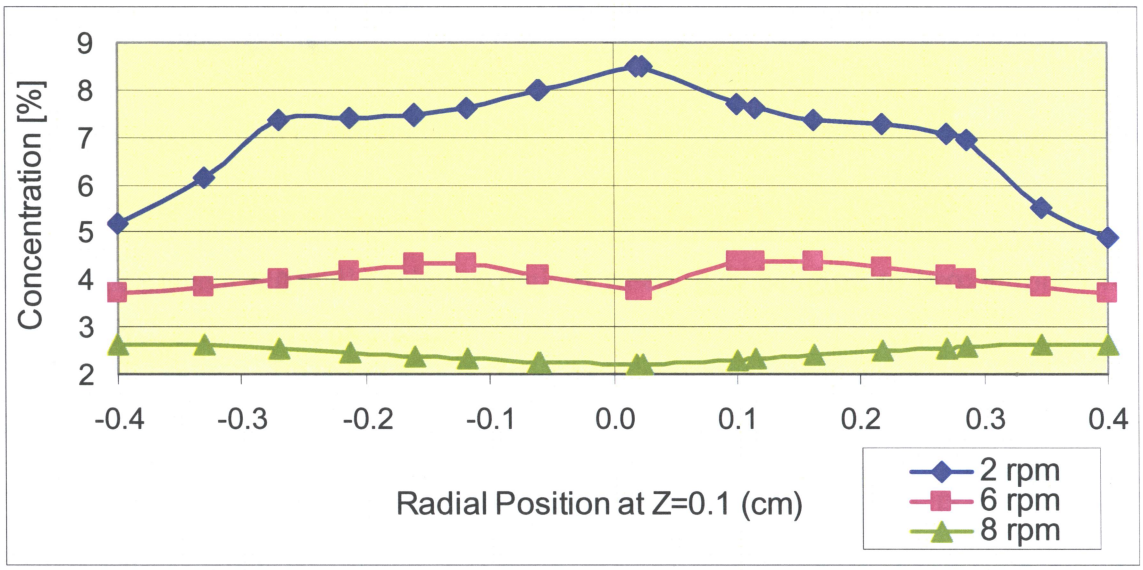

Figure 35 Terrestrial Condition, 20mT Magnetic Field Applied with 2, 6, and 8 rpm

This led the study to explore another set of simulation in order to see how the lower rotation would affect on the results. By reducing the number of revolution to 1/12 of one revolution per minute which is almost next to zero rotation and testing higher magnetic field force ranges from 50 to 150mT, Figure 36. The higher magnetic field force has been tested before [51] and [52], it can easily be seen that only 50mT, as it can be seen in Figure 37, creates a uniform concentration in the range of 2 percent (as low as 2.3 to 2.9 percent). This result is comparable to those of the 2 rpm with 15mT and 8 rpm with 20mT of magnetic field force which have been discussed earlier in this chapter. From the

practical point of view and the fact that the higher magnet literally is hard to be built and employed, one can appreciate and compromise with smaller magnetic field with minimal rotation under the terrestrial gravitational force and condition.

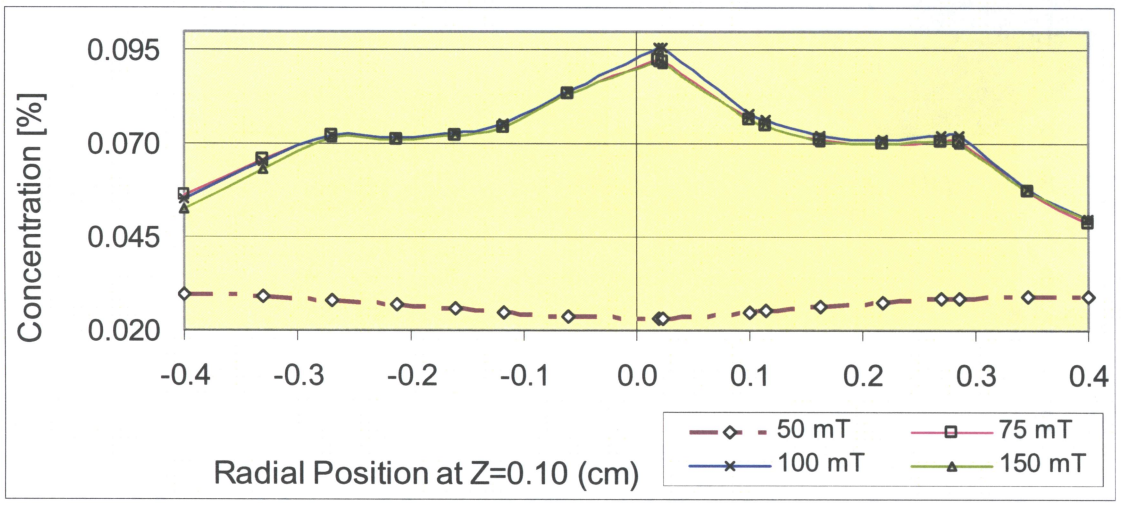

Figure 36 Terrestrial Condition, 50, 75, 100 & 150mT Magnetic Field with 1/12 rpm

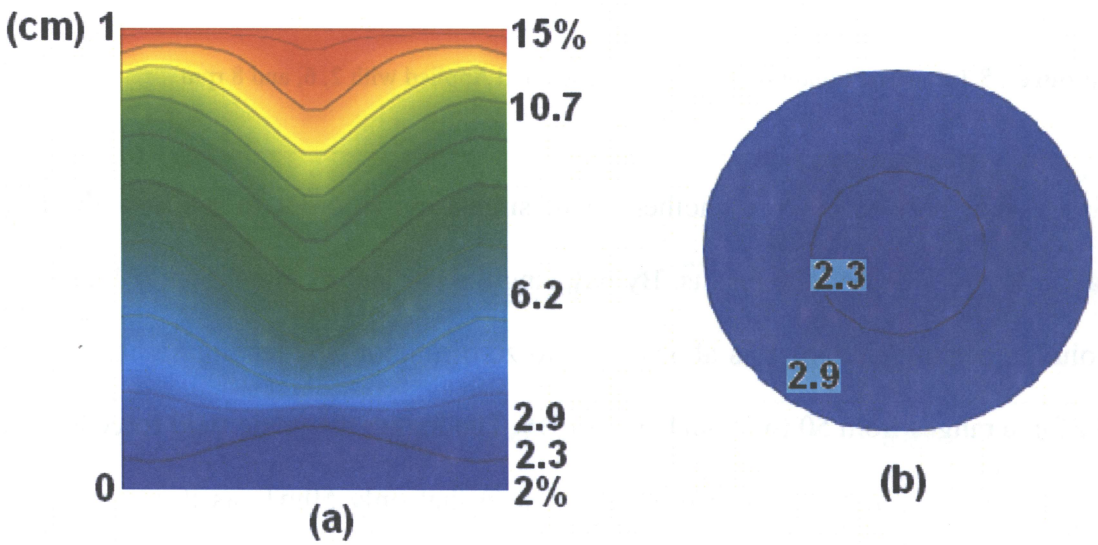

Figure 37 Silicon Concentration under magnetic force of **B**=50mT and rotation of **Ω** = 1/12 rpm, in Terrestrial Condition
a)- Concentration in Vertical cross section
b)- Concentration in Horizontal cross section

4.3 Microgravity Condition

As reported by many experiments conducted either on the board of International Space Station or on the board of the European space orbiter "FOTON-12", the microgravity condition is referred to the gravity in space, where "g" is in the range of 10^{-4} to 10^{-6} of that of the earthbound gravity. In this study, it will suffice to incorporate 10^{-5} in all calculations and simulations for steady state or $g = g_0 \times 10^{-5}$ m/s^2. The idea behind the application of microgravity lies on the fact that the buoyant convection is very weak and this would help the research to focus and understand the flow phenomenon within the solvent (crystal's solution region) where it is believed to be controlled by a pure diffusion.

Figure 38-a, shows silicon concentration in a vertical cross section passing through the "z" axis in the centre of the model which verifies that the contours are perfectly flat and horizontally parallel; this shows that the buoyancy is diminished. As it can be seen in Figure 38-b, there is no co-center contour and there is only one color from the color spectrum at z=1mm above growth interface.

Figure 38-c, illustrates that the distribution of silicon concentration is uniform and it is averaged out as 3.3 percent in the "XY" plane at z=0.1 cm above the growth interface. Figure 38.1-d-e show the speed of the silicon distribution both in vertical and horizontal plane and how the contours are becoming concentric and with less variation in the speed at z=1mm above growth interface. Figure 38.1-f shows that how concentration along the entire model follows a linear distribution.

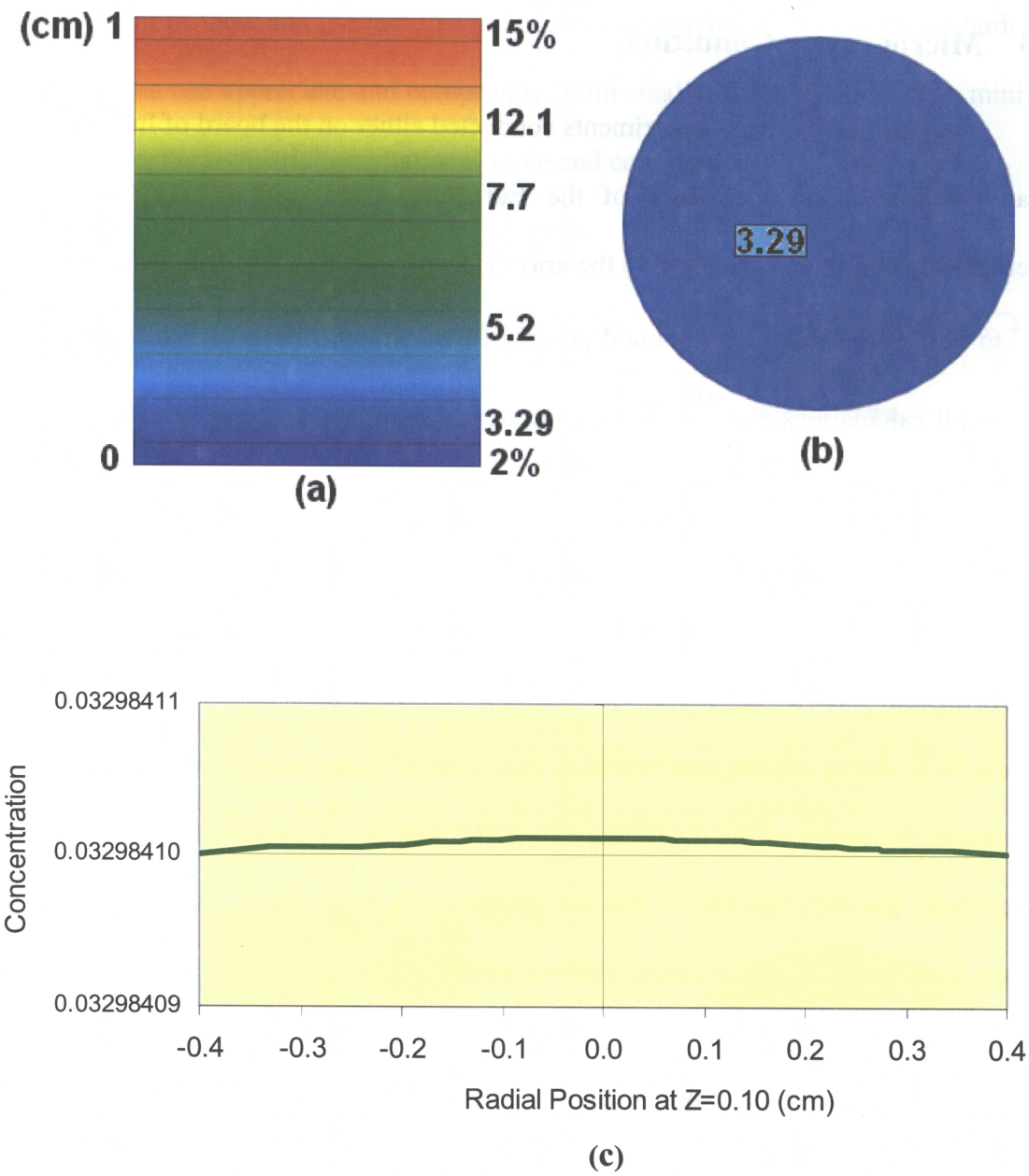

Figure 38 Silicon Concentration and Speed distribution, in Microgravity Condition
a)- Concentration in Vertical cross section
b)- Concentration in Horizontal cross section
c)- Concentration plot at z=0.1cm

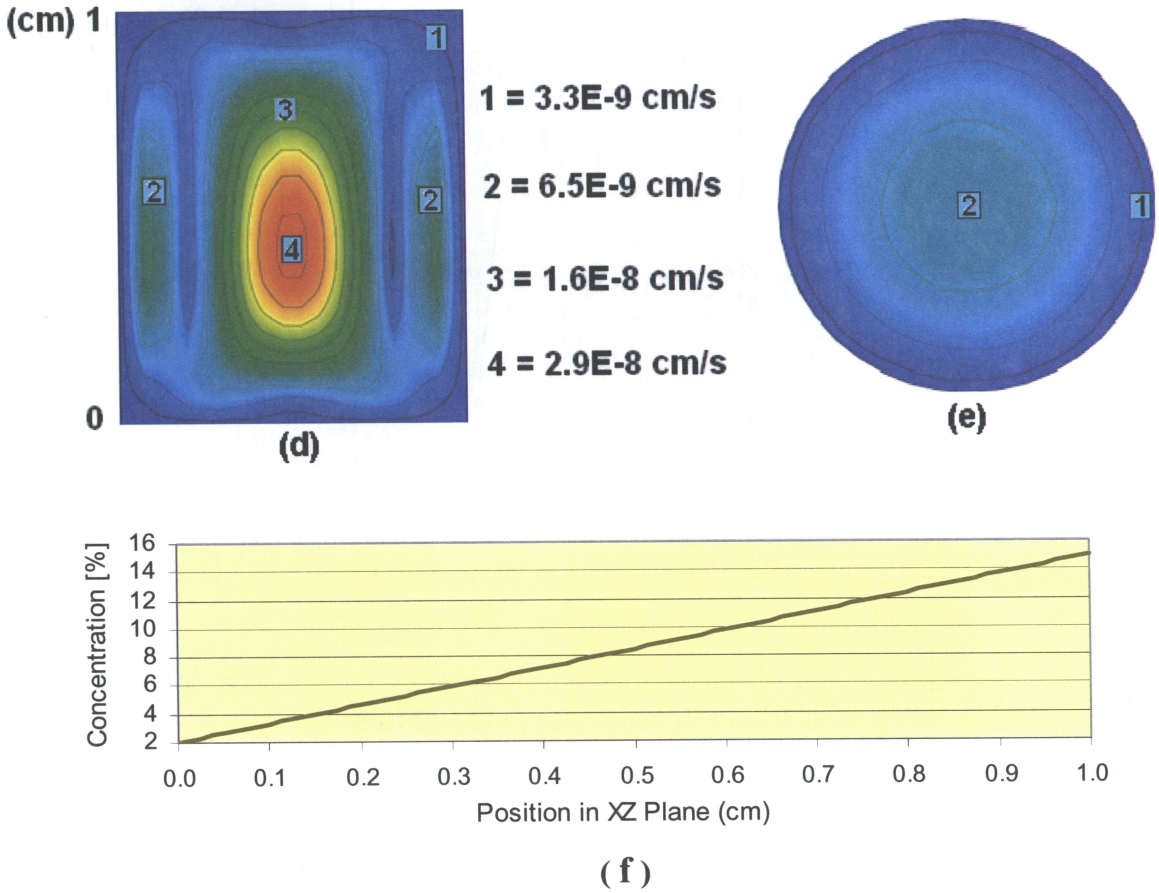

Figure 38.1 Silicon Concentration and Speed distribution, in Microgravity Condition
d)- Speed in Vertical cross section
e)- Speed in Horizontal cross section
f)- Concentration along the vertical axis of entire model

By examining the vector velocity of the flow as shown in the Figure 39, it is clear that in spite of the radial uniformity of the distribution as described in the above, the flow has a downward movement in the middle or in the center of the model and upward flow near the crucible wall. This is more noticeable in the upper level of the model where dissolution interface is located. As it is expected that not to have any convection, this infinitesimal flow which is in the order of 9.2×10^{-7} cm/s can be associated with the residual gravity and has to be taken care of and dealt with.

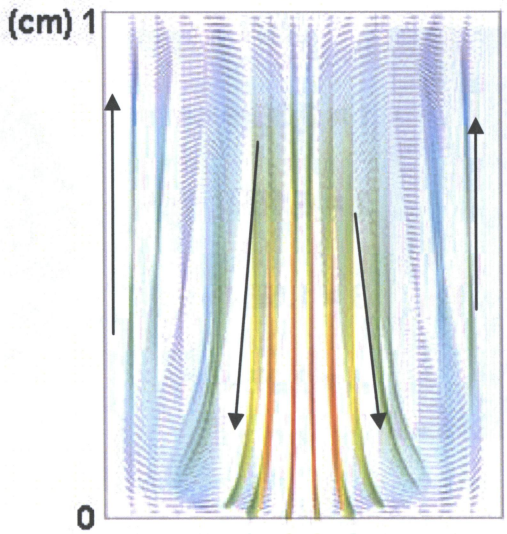

Figure 39 Vector Velocities, in Microgravity Condition

4.3.1 Effects of Applied Rotating Magnetic field in Microgravity Condition

The application of the rotating crucible and rotating magnetic field under microgravity condition, as described by other studies [37], [40], [49] show that not only these efforts do not improve the growth condition but also increases the movement in the center part of the model along the vertical axis even more than that of the movement shown in Figure 39. Therefore, this study would only consider a very small number of rotations such as 1/12 rpm which is next to zero and would study the higher intensity of magnetic field as external body force in the order of 50mT, 75mT and 100mT.

From Figure 40-b, it can be seen that the speed through out the model is in the range of 3.1×10^{-11} cm/s to 5.6×10^{-10} cm/s.

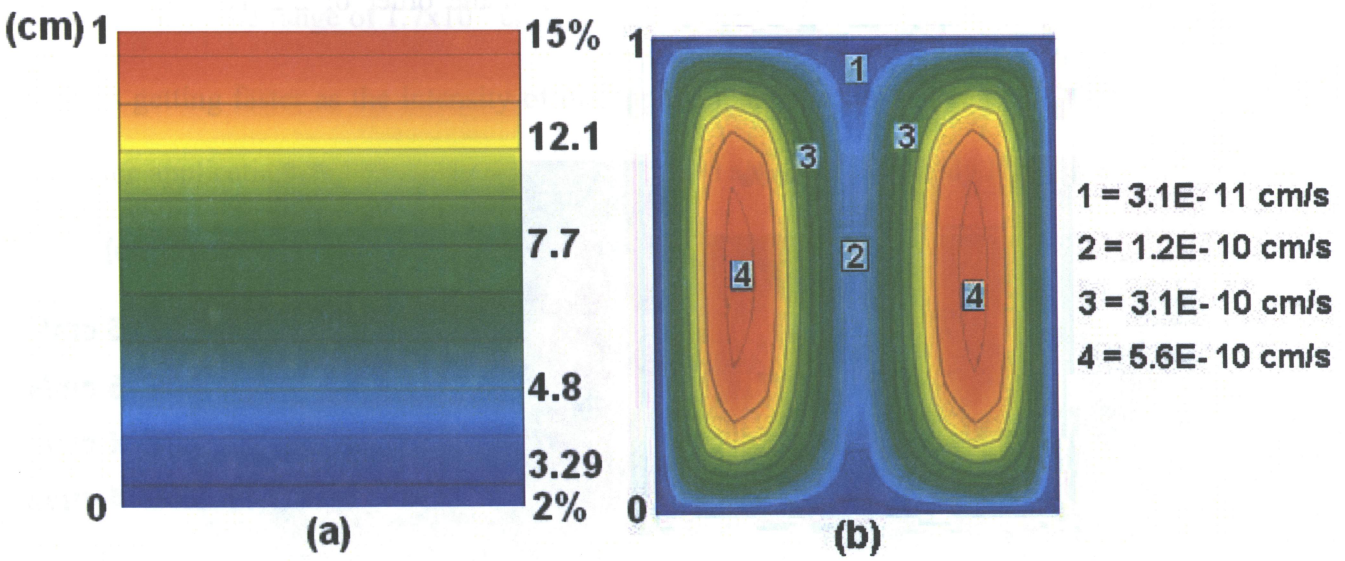

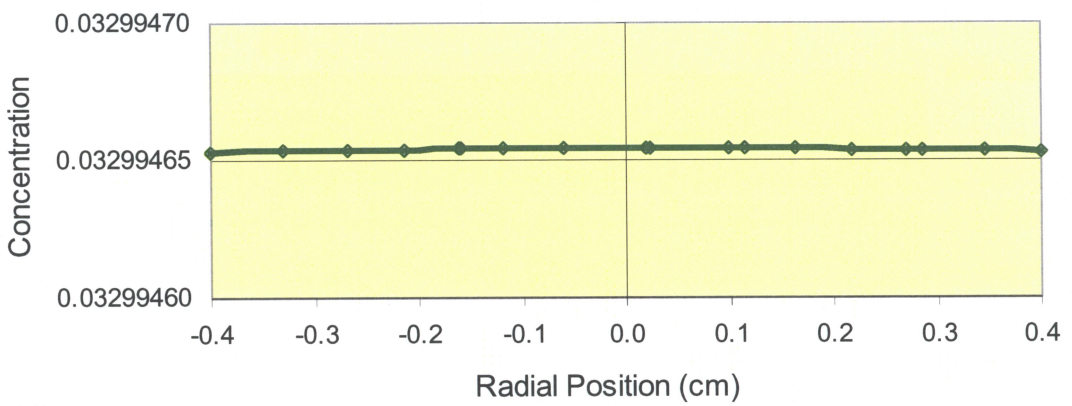

(c)

Figure 40 Silicon concentration and Speed with 50mT & 1/12 rpm in Microgravity Condition
a)- Concentration in Vertical cross section
b)- Speed in Vertical cross section
c)- Concentration plot at z=0.1cm above Growth Interface

Figure 41-a, which is a vertical cross sectional view of the model, reveals that the distribution of silicon concentration is almost the same as that of the condition where no magnetic field was applied, however Figure 41-b, illustrates the speed (velocity) of silicon distribution which is becoming faster and is in the order of $2.2x10^{-5}$ cm/s to $3.9x10^{-4}$ cm/s.

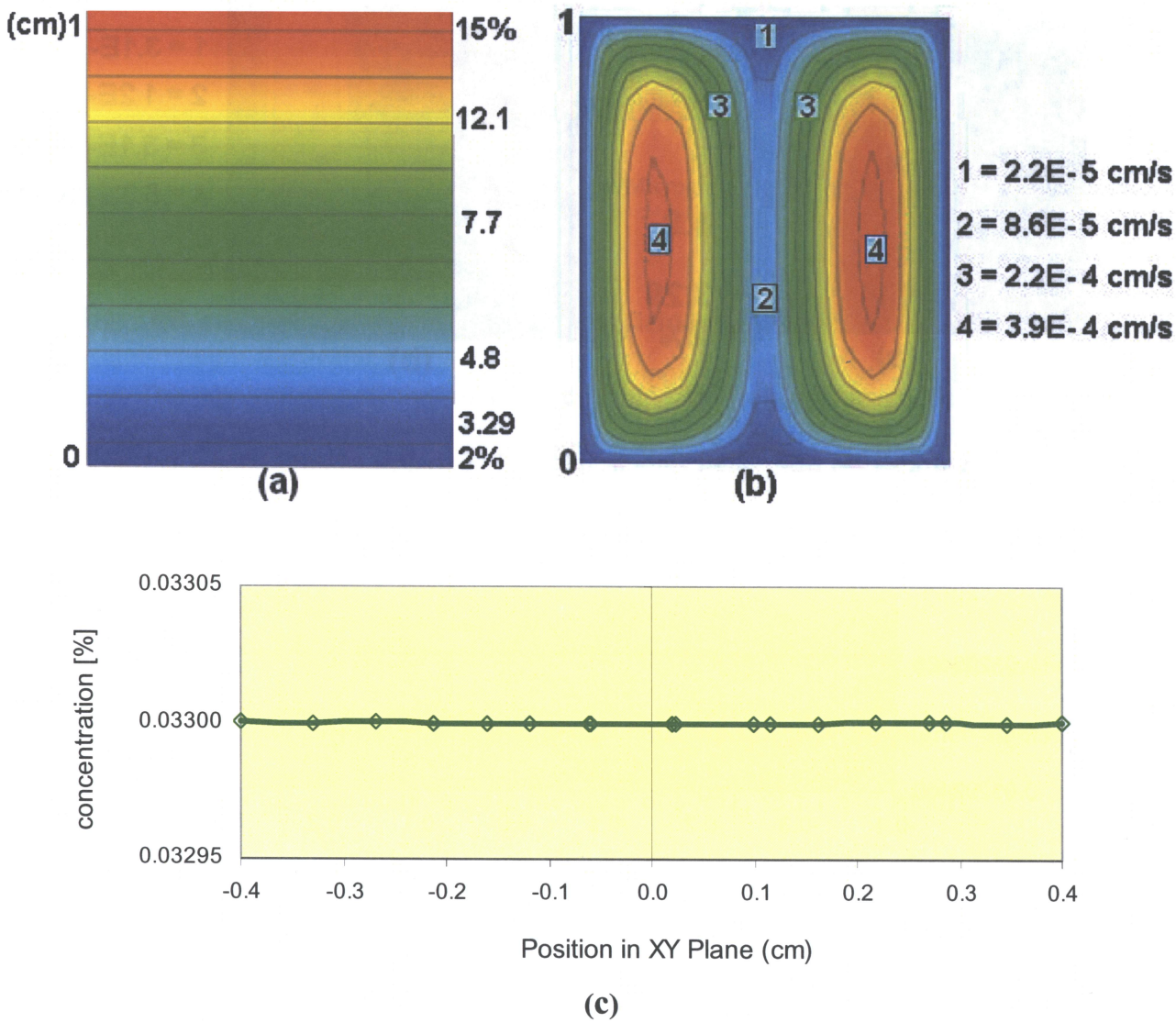

Figure 41 Silicon concentration and Speed with 75mT & 1/12 rpm in Microgravity Condition
a)- Concentration in Vertical cross section
b)- Speed in Vertical cross section
c)- Concentration plot at z=0.1cm above Growth Interface

Figure 42-a, which is a vertical cross section of the model along the "z" axis, is passing through the center of the model, depicts that silicon distribution remains uniform. But again as the Figure 42-b shows, the velocity of the distribution of the flow is increasing and is in the range of $1.7x10^{-4}$ cm/s to $3.1x10^{-3}$ cm/s. It is clear that the speed of the flow is getting faster as the intensity of the applied magnetic field increases. This proves that the application of higher order of magnetic filed as an external body force is not suitable

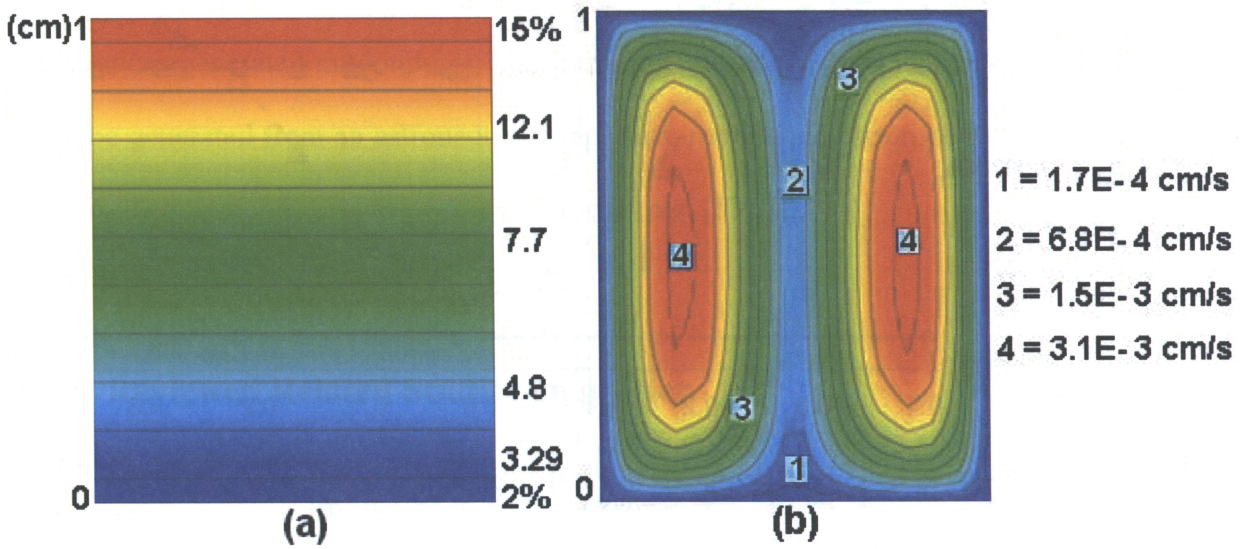

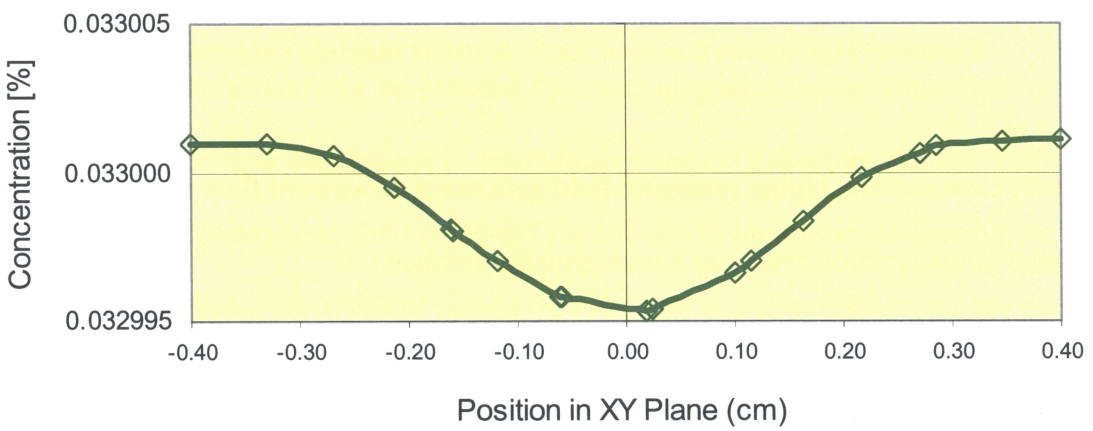

(c)

Figure 42 Silicon concentration and Speed with 100mT & 1/12 rpm in Microgravity Condition
a)- Concentration in Vertical cross section
b)- Speed in Vertical cross section
c)- Concentration plot at z=0.1cm above Growth Interface

for the purpose of growing bulk single crystal in the microgravity condition. Figure 43, represents a comparison of the silicon concentration for 50, 75 and 100mT respectively as external magnetic force which are in the 3.3 percent. Although they are very flat across the radial direction of the model but they are relatively away from the desired level of 0.02 percent.

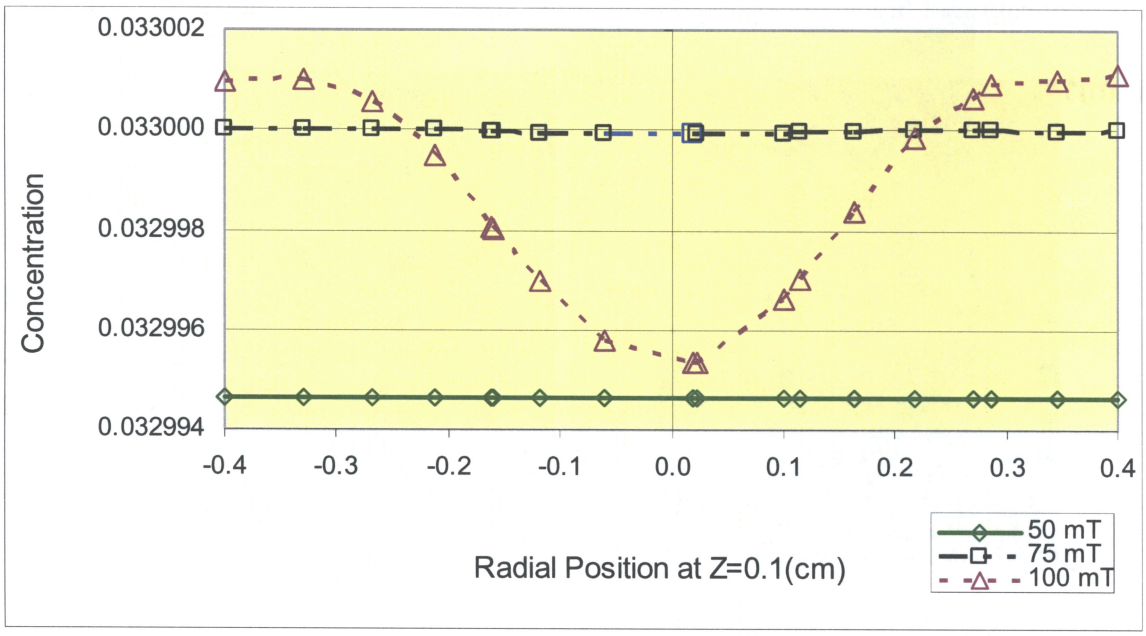

Figure 43 Microgravity Condition, 50, 75 & 100mT Magnetic Field with 1/12 rpm

It is quite clear that the higher magnetic field generate a downward flow in the middle of the model at the level of z=0.1 cm above growth interface.

CHAPTER 5

G-jitter effects in Microgravity Conditions

Results and discussions in Unsteady State (Transient) Condition

5.0 INTRODUCTION

The term g-jitter, also known as residual acceleration, means that the experiment which will be conducted in the space environment is subjected to low frequency disturbances generated randomly on board the International Space Station. Disturbances could be generated from an astronaut moving, fans, running an experiment with different motorized equipments, orbiter positioning rocket etc. [53].

5.1 Reviewed Related Studies on g-jitter

Muller et al, utilized a magnetic field to damp the action of gravity fluctuations (g-jitter) during crystal growth under microgravity. It was shown that melt flow oscillations caused by residual accelerations (g-jitter) in crystal growth experiments under microgravity, can effectively be reduced by static magnetic fields. The reduction of the amplitudes of the flow oscillations is depending on the excitation frequency. Strength and orientation of the magnetic field (~ 50 mT) are found to be important parameters. It was also stated that Since the (Prandtl number) Pr <<1 for metal or semiconductor melts, the influence of g-jitter flows on the temperature field can be neglected for practical purposes, on the contrary the effect on solutal fields (Schmitt number) Sc>>1 can be very noticeable. Thus g-jitter can cause the formation of compositional fluctuations (striations). The flow amplitude induced by $Dg_{0.1}$ are of order of 1 nm/s and are thus

sufficiently small not to be harmful to a growing crystal, whereas higher g-jitter amplitude like Dg_{100} can result in flow fluctuations that can provide an additional transport mechanism for solute species which is in general undesirable under mg conditions [54].

Ben Q. Li conducted an analytical analysis on g-jitter induced flow in the microgravity under the influence of a transverse magnetic field. It was shown that the g-jitter frequency, applied magnetic field and temperature gradients all contribute to affect convective flow. Also it was found that amplitude of velocity decreases at a rate inversely proportional to the g-jitter frequency. Magnetic field can suppress the oscillating flows associated with the g-jitter and act as a damper. It is more effective for low frequency oscillation and has moderate effect on high frequency oscillation as a result of g-jitter. Temperature gradient has a profound effect on the g-jitter induced flow. A residual gravity of 10^{-5} and 10^{-6} is found to be sufficient to cause unacceptable fluid motion in the liquid. For a time harmonic g-jitter with a frequency w, $g(t)=g_0e^{jwt}$, the flow field and the induced electric field should have a similar time varying behavior [55].

Yeckel et al, studied the transient accelerations in both axial and transverse directions in a simple prototype of a vertical Bridgman crystal growth technique. The residual acceleration was set to 10^{-6} and the jitter amplitude to 10^{-4} (used in US space shuttle). The effect of jitter on flow response over a wide range of frequencies and magnetic field has been studied. The effect of a steady magnetic field is to suppress flow in the low-frequency regime. For the conditions studied here, a transverse jitter of 10 Hz had essentially no impact on the flow, where as jitter below 10^{-3} Hz induced a quasi-steady (semi-steady) flow response. It was also stated that while a typical growth

experiment occurs in hours scale, the g-jitter occurs on sub-second scale. Axial magnetic field has more and stronger effect on reducing axial flow regardless of the expected g-jitter pattern. It was noted that rather than simply attempting to suppress flow altogether, the ability to selectively filter one of the flow components suggests an alternate approach to manipulating mass convection [56].

5.2 Calculating "g" for Momentum Equations

As described in chapter 3, the "g" in the last term of the Navier-Stokes equations 3.2 to 3.4, which is "ρg" should be described under the influence of g-jitter. This chapter studies a model of crystal growth under microgravity environments using measured g-jitter data on board the International Space Station (ISS) and Foton-12 [57].

$$g = g_{st} + g_{vib} \tag{5.1}$$

Where;

$$g_{st} = a_i^0 \tag{5.2}$$

$$g_{vib} = \sum a_i^1 \sin(2\pi f_i t) + b_i^1 \cos(2\pi f_i t) \tag{5.3}$$

Table 4 below shows those data and by applying the above equations, and of course after turning them in the non dimensional format, the values were utilized in the program (Appendix "E") for simulations. Figure 44 shows the magnitude of "g" in 3 different directions in (m/s^2) for the first one hour, among those the dt = 520 second of "Y" direction which had the smallest time difference was chosen to be used in the model under this study.

Table 4, G-jitter data on board FOTON-12 (TRAMP) [57]:

Direction	j	a_0 $(10^{-6} m/s^2)$	a_j $(10^{-6} m/s^2)$	b_j $(10^{-6} m/s^2)$	f_j $(10^{-3} Hz)$
X	1	-3.6615	-24.896	30.786	1.645209
Y	1	-116.65	1.5392	0.42332	1.157556
	2	-----	3.3976	-7.5033	2.51535
	3	-----	4.1744	1.4193	1.872925
	4	-----	-4.7073	-2.6550	2.237846
	5	-----	-0.96563	-1.4247	3.281500
Z	1	16.508	5.5583	2.8422	1.643534
	2	-----	-0.45562	-0.70390	1.870828
	3	-----	-1.5791	-0.094072	2.073682
	4	-----	-2.8356	1.0229	3.290399
	5	-----	-0.91597	-0.27967	4.149568

By applying the data from the Table 4 into the equations 5.3, 5.2, and 5.1 respectively, the plots in Figure 44 were generated in order to define the minimum time steps needed for the input file to analyze the effect of residual acceleration in unsteady state (transient) condition. It was found that the "y" direction has the smallest time interval; therefore, it should be the base for calculating the time steps for the finite element analysis file used in the FIDAP.

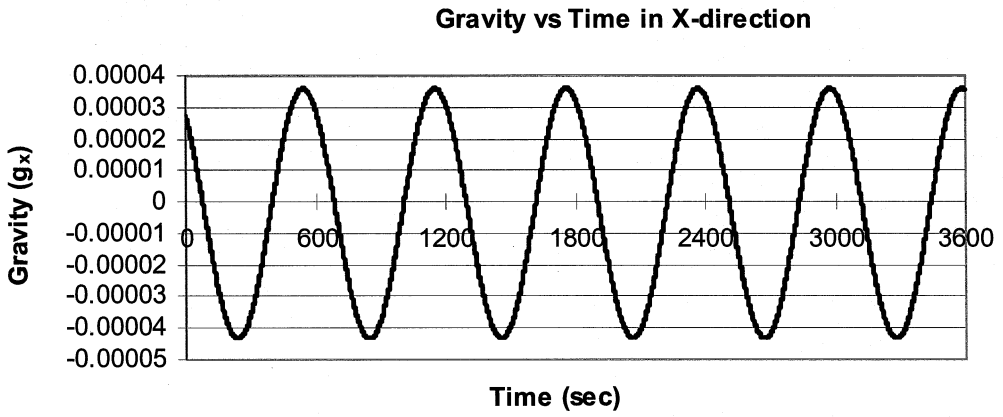

(a)

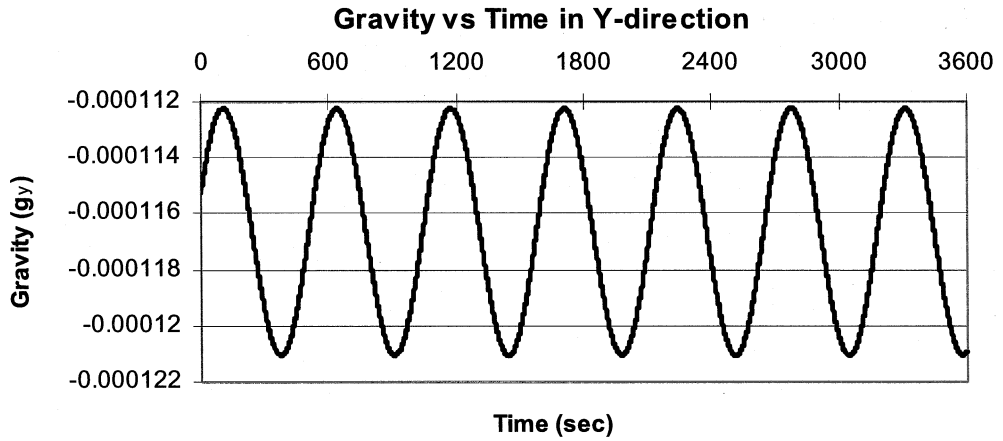

(b)

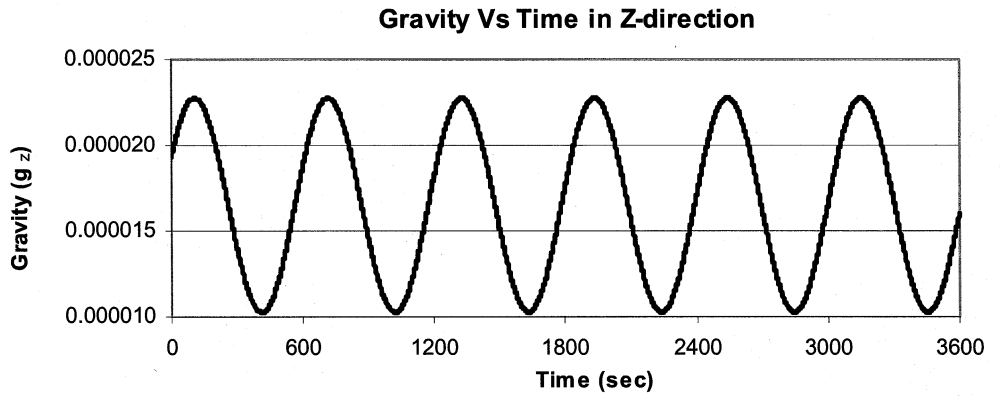

(c)

Figure 44 Plots of g-jitter magnitude in 3 different directions
a) in "X" direction with dt=600
b) in "Y" direction with dt=520
c) in "Z" direction with dt=608

5.3 Effects of g-jitter on fluid flow

First the fluid flow conditions under the presence of the g-jitter are analyzed and then the effects of applied rotating magnetic field are discussed in the following segments. The intention is to see if the residual accelerations can cause any convection in the melt region in the process of crystal growth.

5.3.1 No Magnetic no Rotations applied

The effect of velocity is being investigated and as it can be seen in the Figure 45, neither the silicon distribution figure 45-a, nor the temperature figure 45-b, are affected by the presence of g-jitter in microgravity and the contours remain the same as the case where no g-jitter was applied as discussed in chapter 4. This shows that since the speed, as shown in figure 46, is too weak or too small to have any impact on the temperature or silicon concentration. The multiplier for the legend of the concentration is 100, so the legend reads from 2% to15% and the multiplier for the temperature legend is [(T^* x 100) + 971 ^{0}C], where T^* is the dimensionless value of the temperature, therefore, temperature reads from Min. 1007.19 ^{0}C to Max. 1029.41 ^{0}C .

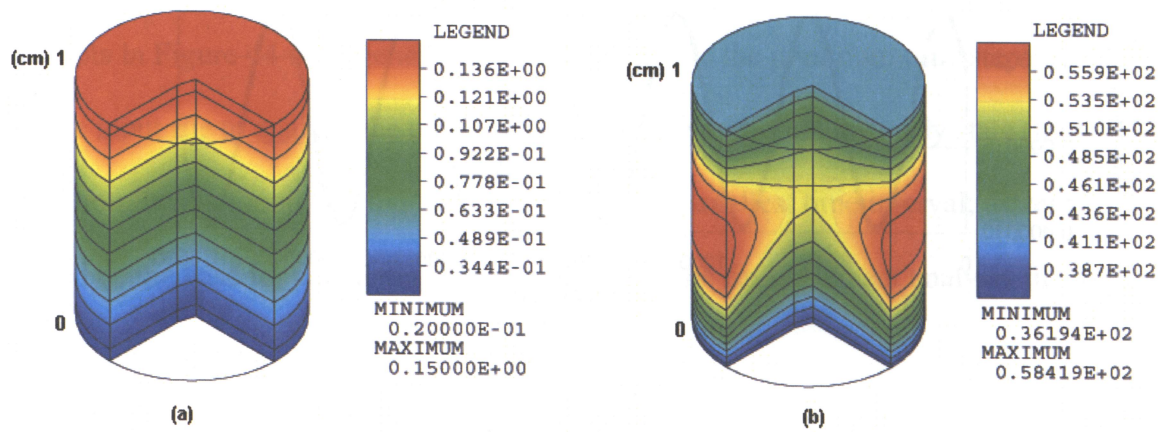

Figure 45 Silicon Concentration and Solvent Temperature contours under the effect of g-jitter
a) Silicon Concentration
b) Temperature Distribution

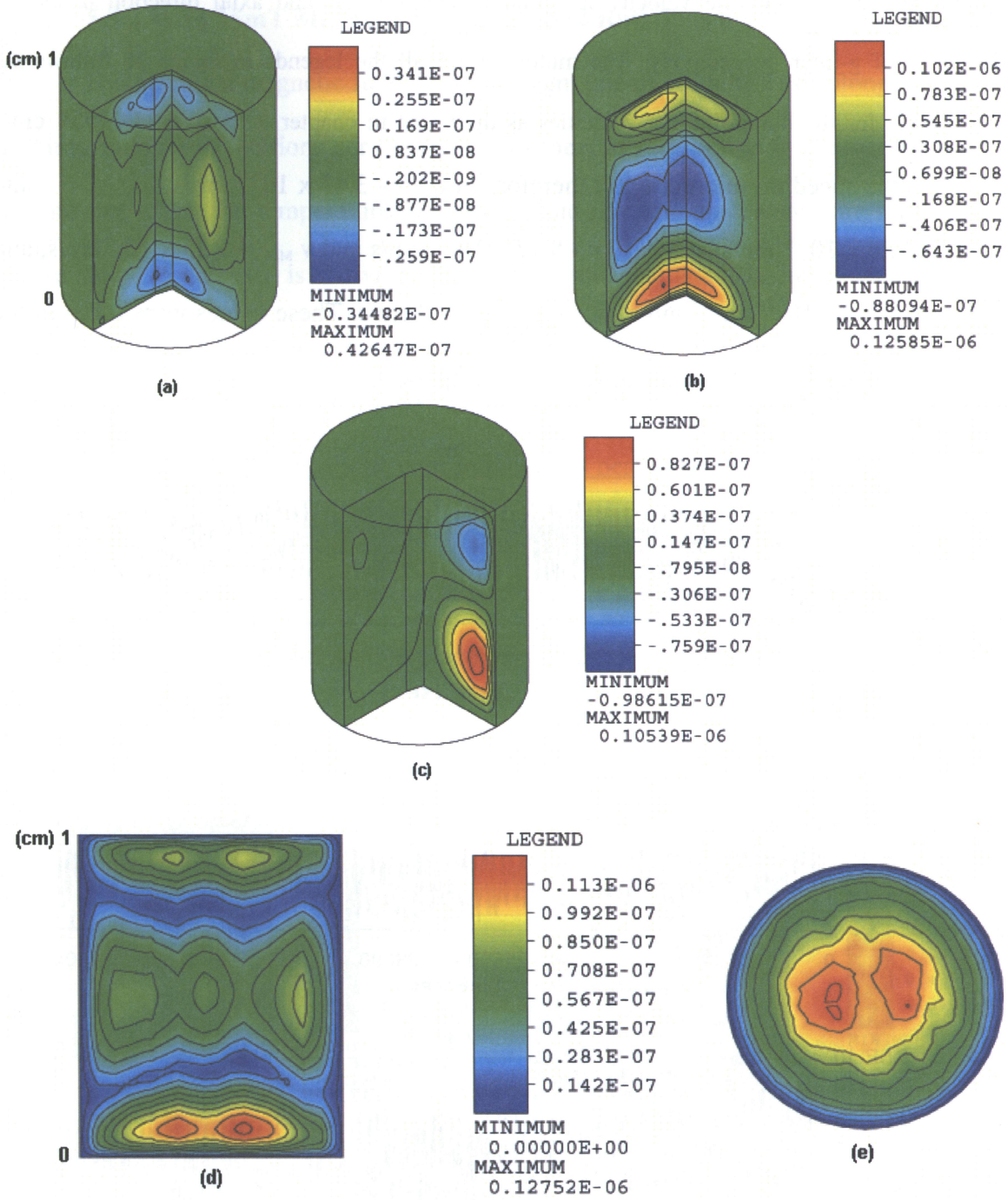

Figure 46 Speed Contour Plot under the effect of g-jitter
a) in radial direction
b) in circumferential direction
c) in axial direction
d) Speed in Vertical plane passing through the center of the Model
e) Speed in Horizontal plane at z=0.1 cm above growth interface

Figure 46-a-b-c, shows the velocity in radial, circumferential and axial direction under the influence of g-jitter, respectively. The multiplier for all the legends in figure 46 follows the description for the dimensionless velocities as discussed in chapter 3, is $\mathbf{u}_0$ =0.009954 cm/s which is the speed in microgravity; therefore, $\mathbf{u}_{Min.} = -3.43 \times 10^{-10}$ cm/s, and $\mathbf{u}_{Max.} = 4.24 \times 10^{-10}$ cm/s, and $\mathbf{v}_{Min.} = -8.77 \times 10^{-10}$ cm/s and $\mathbf{v}_{Max.} = 1.25 \times 10^{-9}$ cm/s, and $\mathbf{w}_{Min.} = -9.82 \times 10^{-10}$ cm/s and $\mathbf{w}_{Max.} = 1.05 \times 10^{-9}$ cm/s. These values were taken in the first 14 hours of the process and also plotted in figure 47.

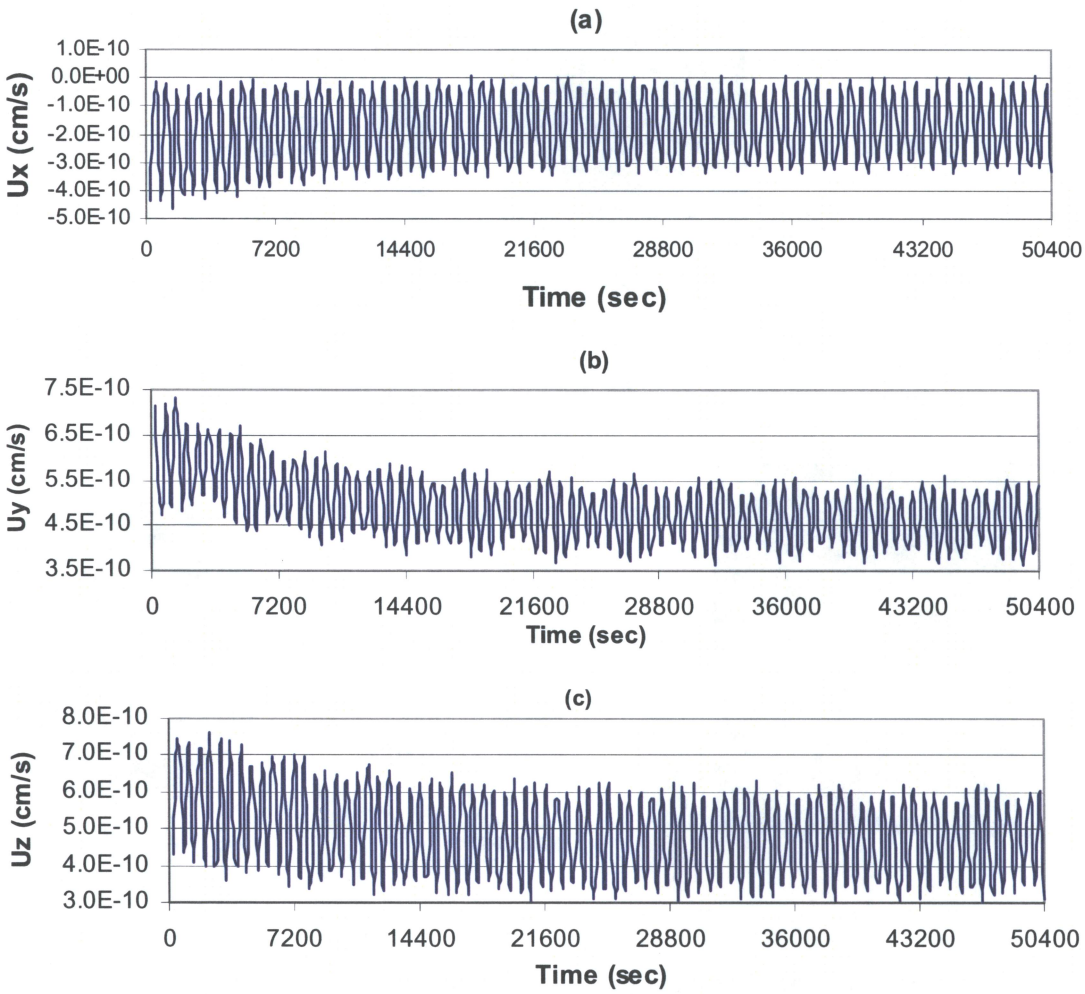

Figure 47 Velocity Plots under the effect of g-jitter for the first 14 hours of the process
a) in radial direction
b) in circumferential direction
c) in axial direction

5.3.2 With 15mT Magnetic Force and 1/12 Rotations per minute applied

By creating a magnetic field with the magnitude of 15 milli-Tesla along with a minimal number of rotations per minute, almost next to zero, it was found that the g-jitter has no impact on the temperature distribution and the contours remain the same as the entire study so far, as it is shown in figure 48-a, and that again is due to the extremely low speed (i.e., in the range of 2.4×10^{-6} cm/s) of the flow and the same as the steady state conditions which was found that the magnetic field had no effect on the temperature. But as for the silicon concentration, as per figure 48-b, the contour lines are starting to deviate from perfectly flat arrangement to a slightly inclined parallel lines which indicates that the distribution is becoming a non-uniform pattern of depositing throughout the vertical cross section plane passing along "Z" axis.

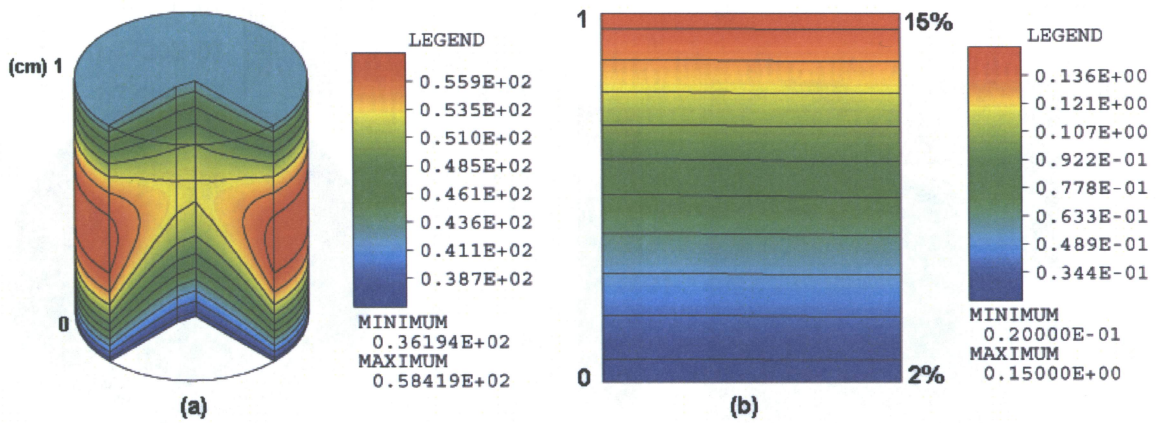

Figure 48 Solvent Temperature and Silicon Concentration Contour contours, under the effect of g-jitter with B=15mT and Ω = 1/12 rpm
a) Temperature Distribution
b) Silicon Concentration

Again the temperature reads the same from Min. 1007.19 ^{0}C to Max. 1029.41 ^{0}C and silicon concentration is ranged from 2% to 15%.

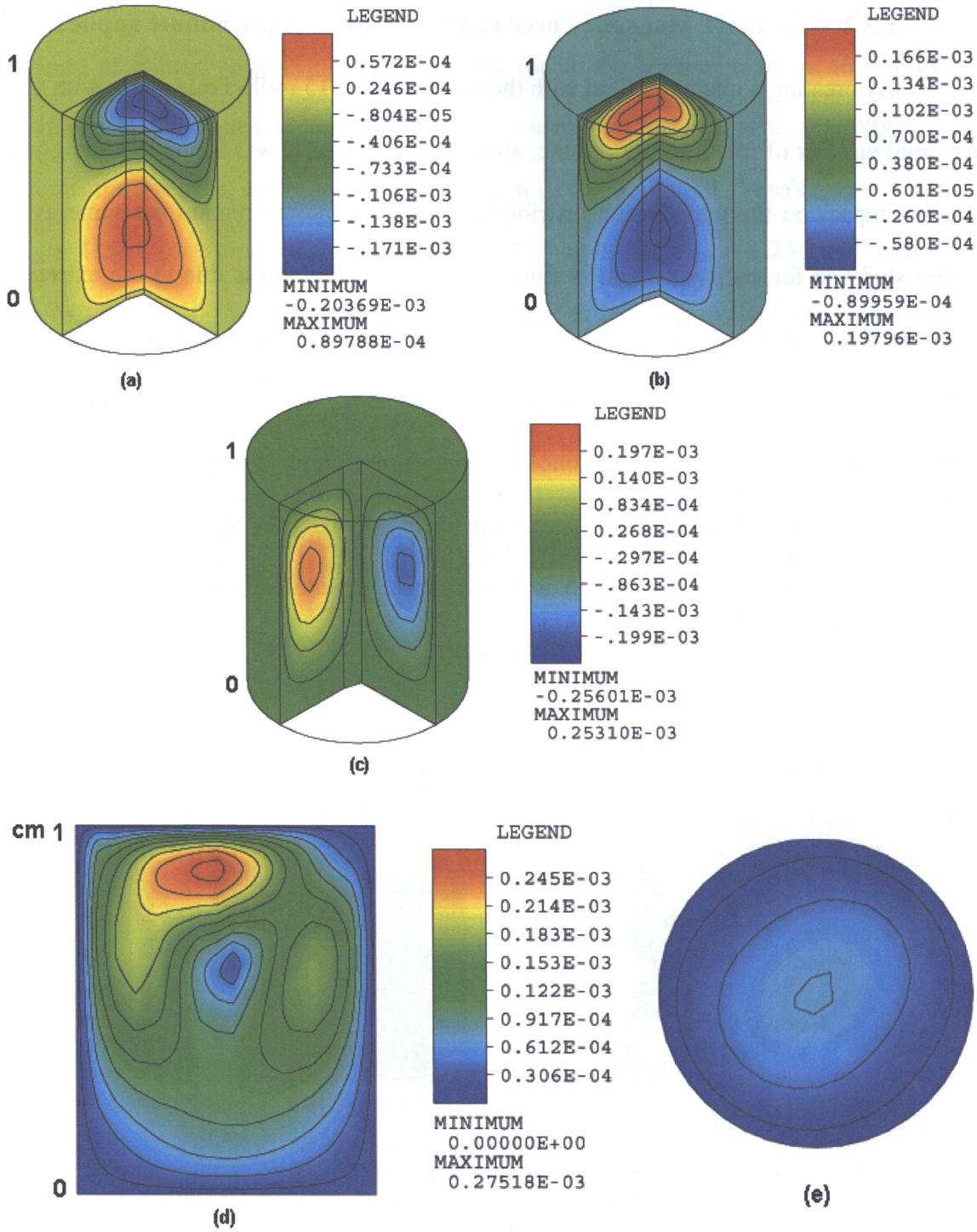

Figure 49 Speed Contours under the effect of g-jitter with B=15mT and Ω = 1/12 rpm
a) in radial direction
b) in circumferential direction
c) in axial direction
d) Speed in Vertical plane passing through the center of the Model
e) Speed in Horizontal plane at z=0.1 cm above growth interface

By utilizing the multiplier for the velocity which is the reference velocity of 0.009954 cm/s, for this case we would have velocity range from the minimum of -8.9 x 10^{-7} cm/s in circumferential direction to a maximum of 2.5 x 10^{-6} cm/s in the axial direction. As Figure 50 presents, the velocity in this case is varying from as low as -1 x 10^{-10} cm/s in the axial direction to as high as 1.81 x 10^{-7} cm/s in the radial direction.

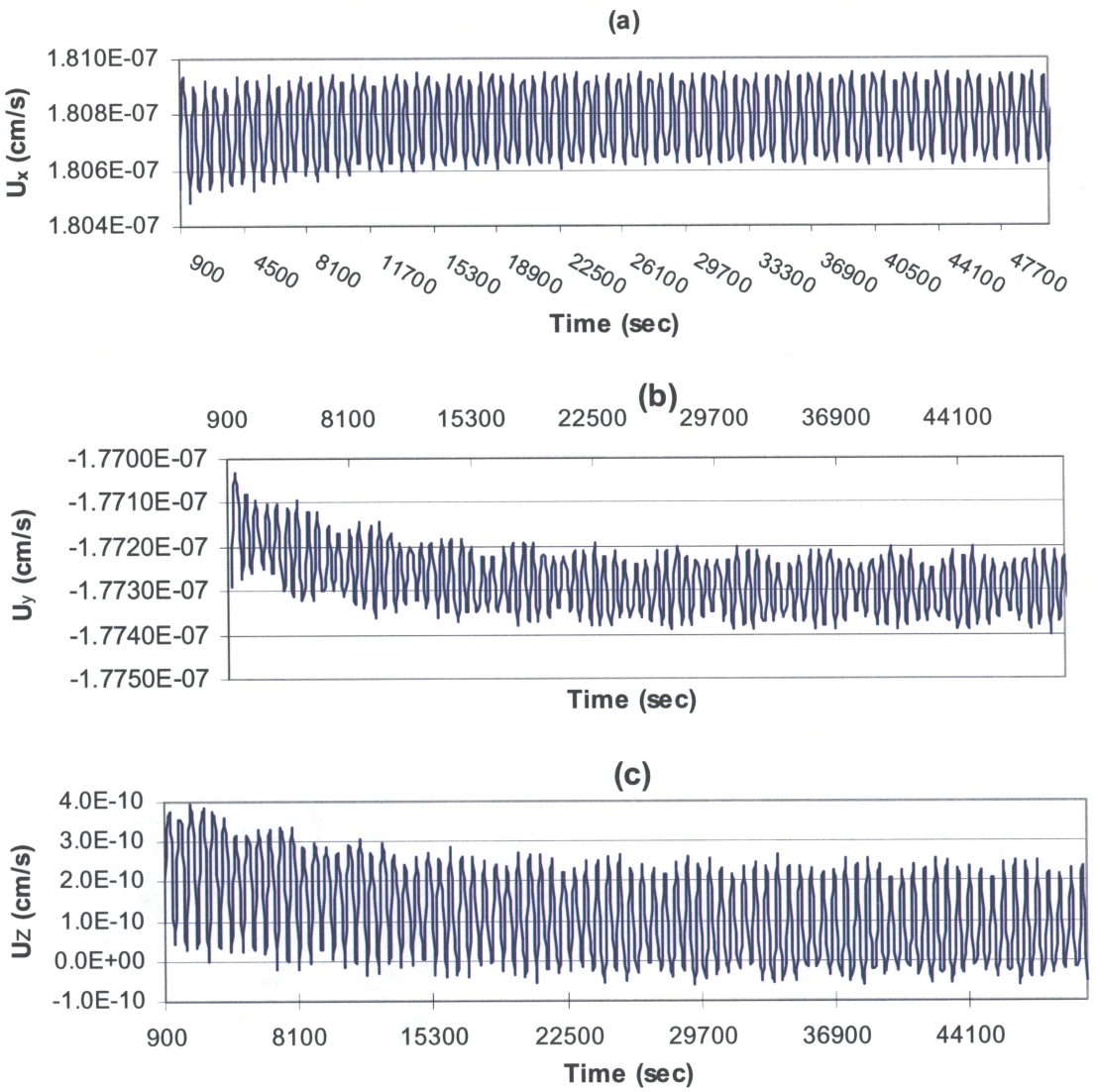

Figure 50 Velocity Plots under the effect of g-jitter with B=15mT and Ω = 1/12 rpm for the first 14 hours of the process.
a) in radial direction
b) in circumferential direction
c) in axial direction

These values indicate that the effect of the g-jitter in the presence of the magnetic field has been intensified by about two thousands times.

5.3.3 Magnetic Force of 15mT and 2 Rotations per Minute applied

In the previous case, it was found that the magnetic field had an impact on the flow velocity and started to destabilize the concentration pattern. In order to explore the effect of the rotation, therefore in the next case, 2 rotations per minute are applied. As mentioned in chapter 4, the combination of 15mT of magnetic field force along with 2 revolutions per minute in the terrestrial (earthbound) condition reduced the convection in the solvent region substantially. However, Figure 51-a reveals that the concentration of silicon is completely destabilized as a result of the application of $\Omega = 2$ rpm along with the B=15mT and clearly can be seen that the smooth parallel contour pattern in microgravity steady state condition changing to a non uniform pattern which is not desirable for crystal growth process. Temperature contours, however as seen in figure 51-b, are remaining the same as previous cases.

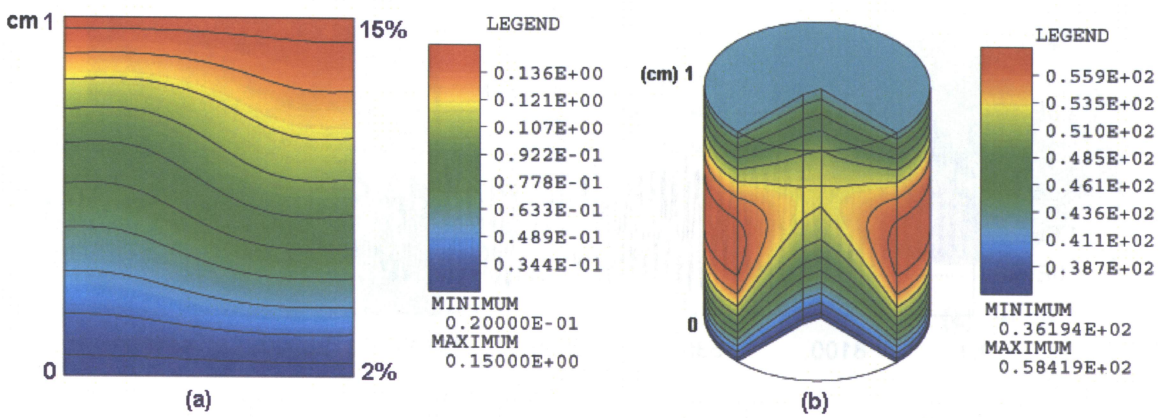

Figure 51 Silicon Concentration and Solvent Temperature Contour, under the effect of g-jitter with B=15mT and $\Omega = 2$ rpm
a) Silicon Concentration
b) Temperature Distribution

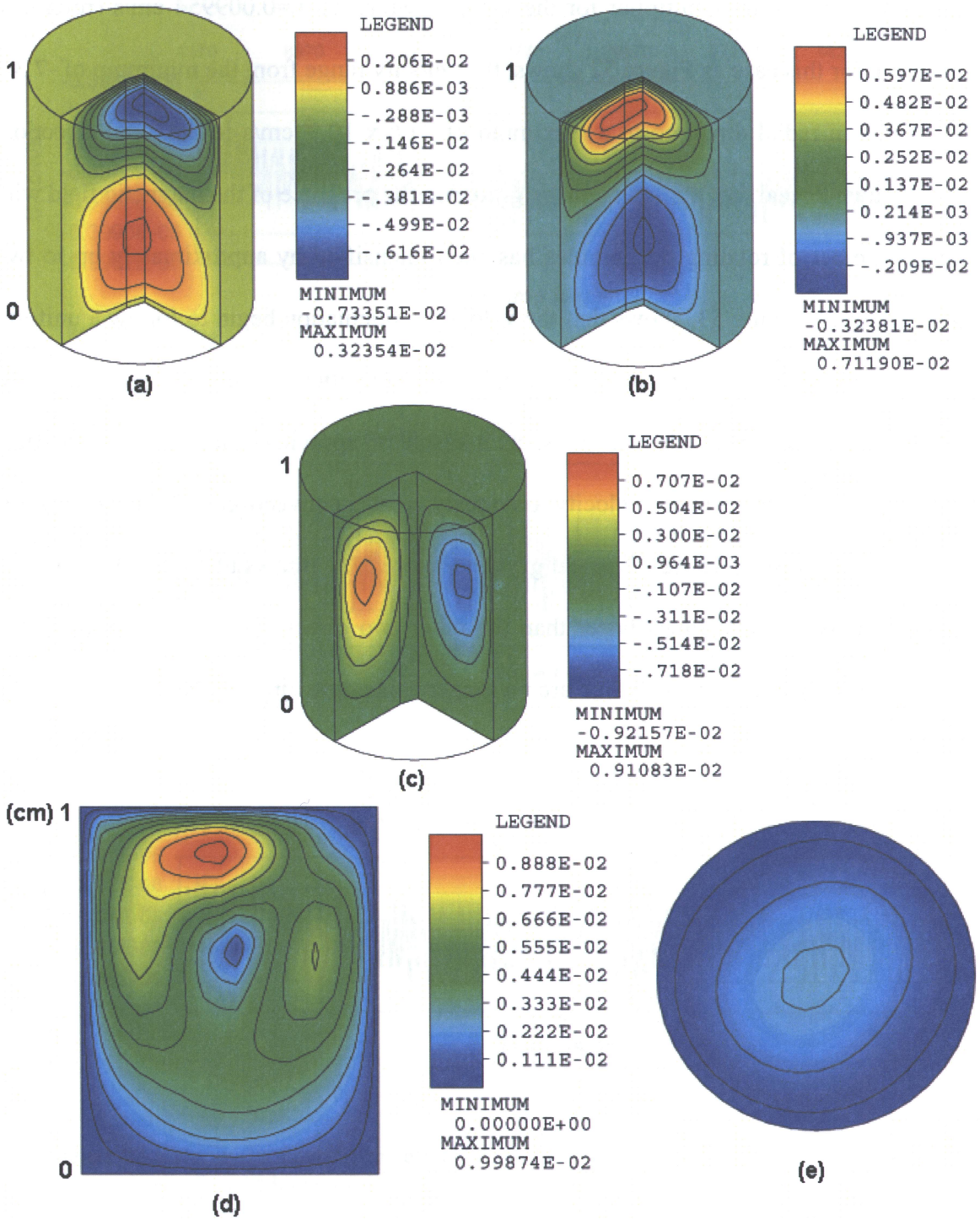

Figure 52 Speed Contours under the effect of g-jitter with B=15mT and Ω = 2 rpm
a) in radial direction
b) in circumferential direction
c) in axial direction
d) Speed in Vertical plane passing through the center of the Model
e) Speed in Horizontal plane at z=0.1 cm above growth interface

Again by utilizing the multiplier for the velocity which is u_0=0.009954 cm/s (reference velocity), for this case as Figure 52 shows, the velocity range from the minimum of -7.3 x 10^{-5} cm/s in radial direction to a maximum of 9.06 x 10^{-5} cm/s in the axial direction. These values reveal that the effect of the g-jitter in the presence of the magnetic field with higher number of rotating per minutes has been intensified by approximately up to two hundred times. Figure 53, shows that the velocity's fluctuation begin to follow a uniform pattern after about 4 hours. It also reveals that velocities are almost becoming two hundred times faster, in all directions, as a result of applying rotating magnetic field (RMF). These increase in the velocity, obviously creates convection in the flow which is not desirable for the purpose of crystal growth. Figure 53-a, shows that the radial speed is approximately hundred times faster than the other two directions and this validates the contour shape of Figure 52-e, which are no longer concentric circular shape contours.

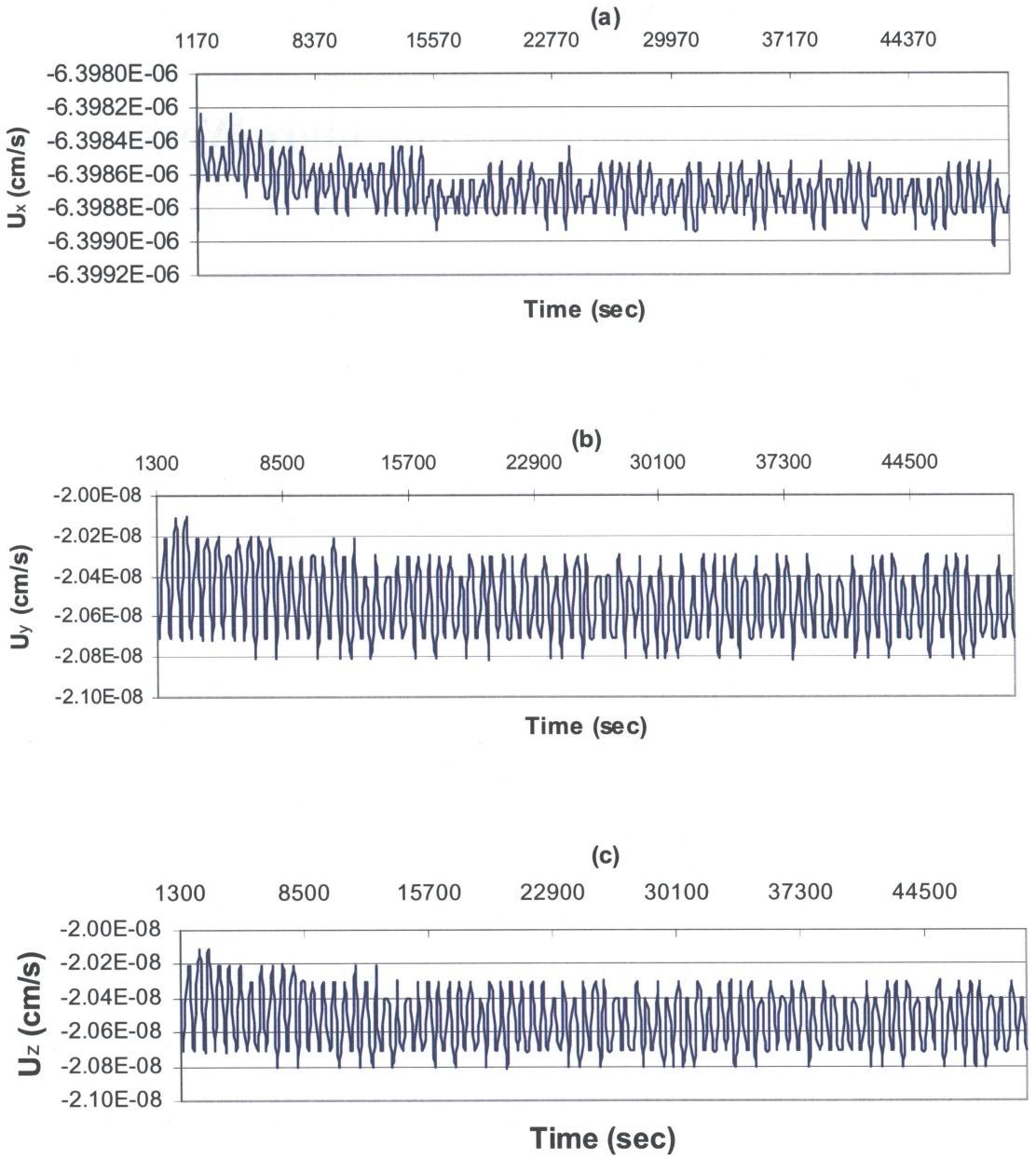

Figure 53 Velocity Plots under the effect of g-jitter with B=15mT and Ω = 1/12 rpm for the first 14 hours of the process.
a) in radial direction
b) in circumferential direction
c) in axial direction

CHAPTER 6

Summary, Conclusion and Future Works

6.1 Summary

Even now a single crystal alloy of SiGe with high quality of composition remains difficult to grow, but all the attempts and studies have been made, at least for the past 2 decades, to achieve this goal. All those relevant and related published papers in the academically approved journals, which have been reviewed and excerpted, show that different circumstances, such as the terrestrial (earthbound) condition, microgravity condition, rotating magnetic field condition, static axial magnetic field, individually or collectively, to some extent, affect and influence how to reduce the buoyancy induced convective flow in crystal growth processes. It should be mentioned that the influence of the g-jitter (residual accelerations) has also been taken into the consideration when the microgravity condition is being studied. Among all the methods and techniques practiced in the past century, it seems that the traveling solvent method (TSM), which is also known as traveling heater method (THM), is very promising for the purpose of growing the SiGe bulk single crystal (and semiconductor alloys in general) since it is works with the relatively lower temperature as compared to the other techniques.

A three-dimensional numerical simulation to study the effect of a magnetic field on the fluid flow, heat transfer and mass transfer in the presence of rotating magnetic field and g-jitter is investigated. The term g-jitter means that the experiment which will be conducted in a space environment is subjected to low frequency disturbances generated

randomly on board the International Space Station or European Space Orbiter, FOTON-12. Disturbances could be generated from an astronaut moving, fans, running an experiment, positioning rocket etc. At first, the study was conducted by applying the Rotating Magnetic Field (RMF) when the gravity vector was constant and equal to 9.8 m/s^2. The presence of the RMF suppressed the buoyancy convection in the $Ge_{0.98}Si_{0.02}$ solution zone in order to get homogeneity with a flat growth interface. It was found that the intensity of the flow at the centre of the crucible decreased at a faster rate compared to the flow near the walls when increasing magnetic field intensity is combined with a certain number of rotations. This behavior created a stable and uniform silicon distribution in the horizontal plane near the growth interface. Different magnetic field intensities for different rotational speeds (2, 6 and 8 rpm) were examined. The results showed that the RMF has a marked effect on the silicon concentration, changing it from convex to nearly flat when the magnetic field intensity increased. It was also revealed that, in the terrestrial condition, a 15 milli-Tesla magnetic intensity, along with two revolutions per minute, results in an acceptable flat silicon deposition near the growth interface. In the presence of low frequency g-jitter, the rotating magnetic field was found to be not so effective. Different cases were studied and presented for different magnetic field intensity and rotating speed. The full Navier Stokes equations combined with the energy and mass transfer equations were solved numerically using the finite element technique. Mesh sensitivity analysis was conducted on the three dimensional model generated by GAMBIT. Fluid flow behavior was also studied by utilizing the computational fluid dynamics (CFD) software known as FIDAP.

6.2 Conclusions

- The Traveling Solvent method (TSM) is a reliable technique to be used for the purpose of growing a bulk single crystal of $Ge_{0.98}Si_{0.02}$ in both terrestrial and microgravity conditions, since it operates near the melt temperature which does not have the high temperature complications.
- Although it might seem to be a disadvantage, the speed of the crystal growth in this technique is slow (about 4 mm per day), but this in turn reduces the risk of contaminations (i.e. striation).
- Even though crystal growth in a space (microgravity) condition provides a uniform, flat silicon concentration near the growth interface, at the same time, it is an expensive operation.
- The rotating magnetic field (i.e. B=15mT and Ω = 2 rpm) in the terrestrial condition can also be considered a reliable, controllable and cost effective alternative.

6.3 Future work

- To study the gravity orientation based on the position of the spacecraft (orbiter) in the space.

Also based on the newly installed furnace in the space station;

- Study on convective flow for a Bridgman technique.
- Study on convective flow for a Float Zone technique.
- Evaluate the optimum technique to be utilized in Micro-Gravity.

REFERENCES

[1] International Union of Pure and Applied Chemistry Report, Internet edition on Semiconductors

[2] W.L. Bond, Crystal Technology, 1976

[3] www.siliconfareast.com

[4] www.en.wikipedia.org

[5] B.G. Streetman, S. Banerjee, " Solid state Electronic Devices", fifth edition, 2000, ch.1, pp.1-12

[6] G. Muller, A. Ostrogorsky. "Convection in the melt" Handbook of crystal Growth, 1994 Elsevier Science pp. 711-819

[7] www.Imass.uah.edu

[8] www.chemicalelements.com

[9] www.efunda.com

[10] M.Z. Saghir, "A Study of the Marangoni Convection on the Germanium Float Zone", American Astronautical Society, 67 (1987), pp. 77-100

[11] "Czochralski Crystal Growth Technique" Internet www.physics.aamu.edu

[12] J. Schilz, V.N. Romanenko. "Review, Bulk growth of Silicon-Germanium Solid Solutions" Journal of Material Science, Materials in Electronics, Vol.6 (1995) pp. 265-279

[13] R. Graham, "A report on Crystal Growth Techniques", 2006, Aleghery Technologies

[14] I. Yonenaga. "Growth and Fundamental Properties of SiGe bulk crystals". Journal of Crystal Growth. 275 (2005) pp. 91-98

[15] I.Yonenaga, M. Nonaka. " Czochralski growth of bulk crystals of Si_xGe_{1-x} II. Si-rich alloys". Journal of Crystal Growth. 191 (1998) pp. 393-398

[16] N.V. Abrosimov, S.N. Rossolenko, W. Thieme, A. Gerhardt, W. Schroder "Czochralski growth of Si and Ge-rich SiGe single crystals". Journal of Crystal Growth. 174 (1997) pp. 182-186

[17] I. Yonenaga. "Czochralski growth of SiGe bulk alloy crystals". Journal of Crystal Growth. 198/199 (1999) pp. 404-408

[18] K. Kakimoto. "Modeling of fluid dynamics in the Czochralski Growth of Smiconductor Crystals" Research Institute for Applied Mechanics, Japan,Published by Elsevier, 2004, pp.169-182

[19] Y.Rosenstein, P.Z. Bar-Yoseph. " Three-dimensional instabilities in Czochralski process of crystal growth from silicon melt". Journal of Crystal Growth. 305 (2007) pp. 185-191

[20] M. Sage. "Crystal Growth by Floating Zone Technique" Rijksuniversiteit Groningen, Solid state Chemistry laboratory, Nijegborgh 4, 9747AG Groningen, The Netherlands. Internet PDF released. pp. 1-30

[21] N. Usami, M. Kitamura, K. Obara, Y. Nose, T. Shishido, K Nakajima. "Floating sone growth of Si-rich SiGe bulk crystal using pre-synthesized SiGe feed rod with uniform composition". Journal of Crystal Growth. 284 (2005) pp. 57-64

[22] A. Barz, U. Kerat, P. Dold, K. W. Benz. "Growth of Si_xGe_{1-x} (x=0 to 0.5) single crystals by a Zone melting Method". Cryst. Res. Technol. 33 (1998), 6, pp. 849-855

[23] K. Lin, P. Dold, K.W. Benz. "Optimization of thermal conditions during crystal growth in a multi-zone resistance furnace".Cryst. Res. Technol. 38 No. 6, (2003), pp. 419-428

[24] A. I. Feonychev, N. V. Bondareva. " Effect of A Rotating magnetic Field on Convection Stability and Crystal Growth in Zero Gravity and on the Ground" Journal of Engineering Physics and Thermodynamics. Vol. 77, N0.4, 2004, pp. 731-742

[25] M. Z. Saghir, M. R. Islam, N. Maffei, D. H. H. Quon. „ Three Dimensional Modeling of $Bi_{12}GeO_{20}$ using the Float Zone Technique". Journal of Crystal Growth, 193 (1998) pp. 623-635

[26] P. Dold, M. Schweizer, A. Croll, K. W. Benz. "Measurement of microscopic growth rates in float zone silicon crystals". Journal of Crystal Growth, 237-239 (2002) pp. 1671-1677

[27] "*Crystal Growth Descriptions and Definitions*". www.science.nasa.gov

[28] L. Helmers, J. Schilz, G. Bahr, W. A. Kaysser. "Macrosegregation during Bridgman growth of Si_xGe_{1-x} mixed crystals". Journal of Crystal Growth, 154(1995) pp. 60-67

[29] P. Dold, A. Barz, S. Recha, K. Pressel, M.Franz, K. W. Benz. "Growth and charachterization of Si_xGe_{1-x} (x <= 10 at%) single crystals". Journal of Crystal Growth, 192 (1998) pp. 125-135

[30] J. S. Walker, "Bridgman crystal growth with a strong, low-frequency, rotating magnetic field". Journal of Crystal Growth, 192 (1998) pp. 318-327

[31] S. Oishi, "Crystal Growth Journal" online pdf released.

[32] "Crystal Growth techniques", www.me.uvic.ca

[33] Y. Okano, S. Nishino, S. Ohkubo, S. Dost, "Numerical Study of Transport phenomena in the THM growth of compound semiconductor crystal". Journal of Crystal Growth, 237-239 (2002) pp. 1779-1784

[34] M.C. Martinez-Tomas, V. Munoz-Sanjose, C. Reig " A Numerical Study Thermal Conditions in the THM Growth of HgTe" Journal of Crystal Growth, 243 (2002) pp. 463-475

[35] D. Labrie, A. E. george, M. Jamieson, S. Obruchkov, J. P. Healey and B. E. Paton, "Homogeneity of Si_xGe_{1-x} alloys (x <=0.30) grown by the traveling solvent method". International Journal of Materials and Product Technology, Vol.22, No.1/2/3, 2005, pp. 105-121

[36] D. Labrie, A. E. george, M. Jamieson, S. Obruchkov, J. P. Healey and B. E. Paton, M. Z. Saghir. "Single Crystal of Si_xGe_{1-x} alloys using the traveling solvent method". Jor. Vac. Sci. Technol. A 22(3), May/Jun 2004, 962-965

[37] T. J. Makriyannis, M. Z. Saghir. "Three Dimensional Modeling of $Si_{1-x}Ge_x$ by the TSM in the presence of the coriolis and centrifugal forces" International Journal of Materials and Product Technology, Vol.22, No 1/2/3, 2005, pp. 135-150

[38] M. Z. Saghir, T. J. Makriyannis, D. Labrie. "Buoyancy Convection During the Growth of Si_xGe_{1-x} by the TSM, Journal of Fluid Engineering, Vol.126, March 2004, pp 223-228

[39] C. W. Lan, D. T. Yang. " A computer simulation of crystal growth by the traveling solvent method; pseudo-steady-state calculations" Modeling Simul. Mater. Sci. Eng. Vol. 3 (1995), pp. 71-92

[40] M. Z. Saghir, T. J. Jaber, D. Labrie. "Si_xGe_{1-x} crystal Grown by the THM using axial magnetic field and rotating crucible". International Journal of Materials and Product Technology, pp. 1-15

[41] M. Z. Saghir, T. J. Jaber, "The effect of rotating magnetic field on the Growth of SiGe using the Traveling Solvent Method". Tech. Science press paper, CMES, vol. 1, no. 1, pp. 11-26

[42] FIDAP User manual, vol. 8.7.2, 1999

[43] Fluent User manual, 2004

[44] R.W. Olesinski, G.J. Abbaschian, " Bulletin of Alloy Phase Diagram" fifth edition (1984)

[45] C.W. Lan, I.F. Lee, B.C. Yeh, "Three Dimensional analysis of flow and segregation in vertical Bridgman crystal growth under axial and transversal magnetic fields", Journal of crystal growth 254 (2003) pp. 503-515

[46] R.V. Giles, Fluid mechanics and Hydraulics, third edition, 1995. Chap. 6, p82

[47] F.M. White, Fluid Mechanics, Sixth edition, 2008. Chap. 5, p287

[48] C.K. Ghaddar, C.K. Lee, S. Motakef, D.C. Gillies, "Numerical simulation of THM growth of CdTe in presence of rotating magnetic fields (RMF), Journal of crystal growth 250 (1999) pp. 99-111

[49] T.A. Campbell et al, "Float Zone Growth and Characterization of $Si_{1-x}Ge_x$ (x<10%) Single Crystal" Journal of Crystal Growth 226 (2001) pp. 231-239

[50] Y. Liu, S. Dost, B. Lent, R. F. Redden, "A Three Dimensional Numerical Model for the Growth of CdTe Single Crystal by Traveling Heater Method under Magnetic Field " Journal of Crystal Growth 254 (2003) pp.285-297

[51] Y. Y. Khine, R. M. Banish, J. J. D. Alexander, " Convective Contamination in self-diffusivity experiments with an applied magnetic field " Journal of Crystal Growth 250 (2003) pp. 274 – 278

[52] Y. Y. Khine, R. M. Banish, " 3 D mass diffusivity model of liquid metals in the presence of a magnetic field "Journal of Crystal Growth 287 (2006) pp. 287 – 290 Newly added, JAN 27/08

[53] S. Lehoczky, F. R. Szofran, D. C. Gillies,„"Growth of solid solution single crystals" Second United States Microgravity Payload. Six Month Sciences Report. NASA MSC (1994).

[54] G. Muller, J. Baumgartl, "The use magnetic fields for damping the action of gravity fluctuations (g-jitter) during crystal growth under microgravity" Journal of Crystal Growth, 169, (1996), pp. 582-586

[55] B. Q. Li, "g-jitter induced free convection in a transverse magnetic field".Int'l. Jour. Heat/mass transfer, Vol. 39, No. 14, pp.2853-2860, 1996

[56] A.Yeckel, J.J. Derby, "Dynamics of 3-dimensional convection in microgravity crystal growth: g-jitter with steady magnetic fields" Journal of Crystal Growth, 263 (2004) pp. 40-52

[57] Y. Yan, S. Pan, K. Jules, M.Z. Saghir, " Vibrational effect on thermal diffusion under different microgravity environment" Z-Tech Publishing, Bremen Microgravity sci. technol. XIX-2 (2007)

APPENDIX "A"
Non-Dimensionalization

Navier-Stokes Equations

r-Component:

Dimensional form of the r-component of the Navier-Stokes equation reads as;

$$\rho\left(\frac{\partial u}{\partial t}+u\frac{\partial u}{\partial r}+\frac{v}{r}\frac{\partial u}{\partial \varphi}+w\frac{\partial u}{\partial z}-\frac{v^2}{r}\right)= \\ -\frac{\partial p}{\partial r}+\mu\left(\nabla^2 u-\frac{u}{r^2}-\frac{2}{r^2}\frac{\partial v}{\partial \varphi}\right)+F_r^M+\rho g_r\left[\beta_T(T-T_0)-\beta_C(c-c_0)\right] \tag{a.1}$$

When the dimensionless variables, as discussed in chapter 3, are introduced into the above equation:

For L-Side, we get;

$$\rho\left(\frac{\partial Uu_0}{\partial\frac{\tau L}{u_0}}+Uu_0\frac{\partial Uu_0}{\partial RL}+\frac{Vu_0}{RL}\frac{\partial Uu_0}{\partial \varphi}+Wu_0\frac{\partial Uu_0}{\partial ZL}-\frac{(Vu_0)^2}{RL}\right)= \tag{a.2}$$

And for R-side, we get;

$$-\frac{\partial\frac{P\mu u_0}{L}}{\partial RL}+\mu\left(\frac{1}{RL}\frac{\partial}{\partial RL}\left[RL\frac{\partial Uu_0}{\partial RL}\right]+\frac{1}{(RL)^2}\frac{\partial^2 Uu_0}{\partial\varphi^2}+\frac{\partial^2 Uu_0}{\partial(ZL)^2}-\frac{Uu_0}{(RL)^2}-\frac{2}{(RL)^2}\frac{\partial Uu_0}{\partial\varphi}\right) \\ -\frac{1}{2}\sigma\omega B_1^2+\rho g_r\left[\beta_T(T-T_0)-\beta_C(c-c_0)\right] \tag{a.3}$$

Multiplying both sides by $\left(\frac{L^2}{\mu u_0}\right)$, and simplifying further and by equating common factors to a known dimensionless number (Table-2, Chapter-3) such as Reynolds number, we get;

$$\mathrm{Re}\left(\frac{\partial U}{\partial\tau}+U\frac{\partial U}{\partial R}+\frac{V}{R}\frac{\partial U}{\partial\varphi}+W\frac{\partial U}{\partial Z}-\frac{V^2}{R}\right)= \\ -\frac{\partial P}{\partial R}+\left(\frac{\partial^2 U}{\partial R^2}+\frac{1}{R^2}\frac{\partial^2 U}{\partial\varphi^2}+\frac{\partial^2 U}{\partial Z^2}-\frac{U}{R^2}-\frac{2}{R^2}\frac{\partial V}{\partial\varphi}\right)-\frac{1}{2}Ha^2\omega^* B_1^2+\frac{(Gr_T)_r}{\mathrm{Re}}\theta-\frac{(Gr_C)_r}{\mathrm{Re}}C \tag{a.4}$$

φ-Component:

Dimensional form of the φ-component of the Navier-Stokes equation reads as;

$$\rho\left(\frac{\partial v}{\partial t}+u\frac{\partial v}{\partial r}+\frac{v}{r}\frac{\partial v}{\partial \varphi}+w\frac{\partial v}{\partial z}+\frac{uv}{r}\right)= \\ -\frac{1}{r}\frac{\partial p}{\partial \varphi}+\mu\left(\nabla^2 v+\frac{2}{r^2}\frac{\partial v}{\partial \varphi}-\frac{v}{r^2}\right)+F_\varphi^M+\rho g_\varphi\left[\beta_T\left(T-T_0\right)-\beta_C\left(c-c_0\right)\right] \tag{a.5}$$

When the dimensionless variables, as discussed in chapter 3, are introduced into the above equation:

For L-Side, we get;

$$\rho\left(\frac{\partial Vu_0}{\partial\frac{\tau L}{u_0}}+Uu_0\frac{\partial Vu_0}{\partial RL}+\frac{Vu_0}{RL}\frac{\partial Vu_0}{\partial \varphi}+Wu_0\frac{\partial Vu_0}{\partial ZL}+\frac{Uu_0Vu_0}{(RL)^2}\right)= \tag{a.6}$$

And for R-side, we get;

$$-\frac{1}{RL}\frac{\partial\frac{P\mu u_0}{L}}{\partial \varphi}+\mu\left(\frac{1}{RL}\frac{\partial}{\partial RL}(RL\frac{\partial Vu_0}{\partial RL})+\frac{\partial^2 Vu_0}{\partial \varphi^2}+\frac{\partial^2 Vu_0}{\partial (ZL)^2}+\frac{2}{r^2}\frac{\partial v}{\partial \varphi}-\frac{v}{r^2}\right) \\ +\frac{1}{2}\sigma\omega^* B_2^2+\rho g_\varphi\left[\beta_T\left(T-T_0\right)-\beta_C\left(c-c_0\right)\right] \tag{a.7}$$

Again, Multiplying both sides by $\left(\frac{L^2}{\mu u_0}\right)$, and simplifying further and by equating common factors to a known dimensionless number (Table-2, Chapter-3) such as Hartman number, we get;

$$\mathrm{Re}\left(\frac{\partial V}{\partial \tau}+U\frac{\partial V}{\partial R}+\frac{V}{R}\frac{\partial V}{\partial \varphi}+W\frac{\partial V}{\partial Z}+\frac{UV}{R}\right)= \\ -\frac{1}{R}\frac{\partial P}{\partial \varphi}+\left(\frac{\partial^2 V}{\partial R^2}+\frac{1}{R^2}\frac{\partial^2 V}{\partial \varphi^2}+\frac{\partial^2 V}{\partial Z^2}-\frac{V}{R^2}+\frac{2}{R^2}\frac{\partial U}{\partial \varphi}\right)+\frac{1}{2}Ha^2\omega^* B_2^2+\frac{(Gr_T)_\varphi}{\mathrm{Re}}\theta-\frac{(Gr_C)_\varphi}{\mathrm{Re}}C \tag{a.8}$$

z-Component:

Dimensional form of the z-component of the Navier-Stokes equation reads as;

$$\rho\left(\frac{\partial w}{\partial t}+u\frac{\partial w}{\partial r}+\frac{v}{r}\frac{\partial w}{\partial \varphi}+w\frac{\partial w}{\partial z}\right)=$$
$$-\frac{\partial p}{\partial z}+\mu\left(\nabla^2 w\right)+F_z^M+\rho g_z[\beta_T(T-T_0)-\beta_C(c-c_o)] \qquad \text{(a.9)}$$

When the dimensionless variables, as discussed in chapter 3, are introduced into the above equation:

For L-Side, we get;

$$\rho\left(\frac{\partial Wu_0}{\partial\frac{\tau L}{u_0}}+Uu_0\frac{\partial Wu_0}{\partial RL}+\frac{Vu_0}{RL}\frac{\partial Wu_0}{\partial\varphi}+Wu_0\frac{\partial Wu_0}{\partial ZL}\right)= \qquad \text{(a.10)}$$

And for R-side, we get;

$$-\frac{\partial\frac{P\mu u_0}{L}}{\partial ZL}+\mu\left(\frac{1}{RL}\frac{\partial}{\partial RL}\left(RL\frac{\partial Wu_0}{\partial RL}\right)+\frac{1}{(RL)^2}\frac{\partial^2 Wu_0}{\partial\varphi^2}+\frac{\partial^2 Wu_0}{\partial(ZL)^2}\right) \qquad \text{(a.11)}$$
$$+0+\frac{(Gr_T)_z}{\mathrm{Re}}\theta-\frac{(Gr_C)_z}{\mathrm{Re}}C$$

Again, by Multiplying both sides with $\left(\frac{L^2}{\mu u_0}\right)$, and simplifying further and by equating common factors to a known dimensionless number (Table-2, Chapter-3) such as Grashof number, we get;

$$\mathrm{Re}\left(\frac{\partial W}{\partial\tau}+U\frac{\partial W}{\partial R}+\frac{V}{R}\frac{\partial W}{\partial\varphi}+W\frac{\partial W}{\partial Z}\right)= \qquad \text{(a.12)}$$
$$-\frac{\partial P}{\partial Z}+\left(\frac{\partial^2 W}{\partial R^2}+\frac{1}{R^2}\frac{\partial^2 W}{\partial\varphi^2}+\frac{\partial^2 W}{\partial Z^2}\right)+0+\frac{(Gr_T)_z}{\mathrm{Re}}\theta-\frac{(Gr_C)_z}{\mathrm{Re}}C$$

Energy Equation:

Dimensional form of energy equation for the solvent region is presented as:

$$\rho c_p\left(\frac{\partial T}{\partial t}+u\frac{\partial T}{\partial r}+\frac{v}{r}\frac{\partial T}{\partial\varphi}+w\frac{\partial T}{\partial z}\right)=\kappa\left(\frac{1}{r}\frac{\partial}{\partial r}\left(r\frac{\partial T}{\partial r}\right)+\frac{1}{r^2}\frac{\partial^2 T}{\partial\varphi^2}+\frac{\partial^2 T}{\partial z^2}\right) \qquad \text{(a.13)}$$

When the dimensionless variables, as discussed in chapter 3, are introduced into the above equation, we get;

$$\left(\frac{\partial\theta}{\partial\tau}+U\frac{\partial\theta}{\partial R}+\frac{V}{R}\frac{\partial\theta}{\partial\varphi}+W\frac{\partial\theta}{\partial Z}\right)=\frac{1}{Re.Pr}\left(\frac{\partial^2\theta}{\partial R}+\frac{1}{R^2}\frac{\partial^2\theta}{\partial\varphi^2}+\frac{\partial^2\theta}{\partial Z^2}\right) \tag{a.14}$$

Continuity Equation:

The dimensional form of continuity equation is expressed as:

$$\frac{\partial\rho}{\partial t}+\frac{1}{r}\frac{\partial}{\partial r}(ru)+\frac{1}{r}\frac{\partial v}{\partial\varphi}+\frac{\partial w}{\partial z}=0 \tag{a.15}$$

When the dimensionless variables, as discussed in chapter 3, are introduced into the above equation, we get;

$$\frac{\partial\rho}{\partial\tau}+\frac{1}{R}\frac{\partial}{\partial R}(RU)+\frac{1}{R}\frac{\partial V}{\partial\varphi}+\frac{\partial W}{\partial Z}=0 \tag{a.16}$$

Mass Transport Equation

The dimensional form of Mass transport equation reads as:

$$\frac{\partial c}{\partial t}+u\frac{\partial c}{\partial r}+\frac{v}{r}\frac{\partial c}{\partial\varphi}+w\frac{\partial c}{\partial z}=\alpha_c\left(\frac{1}{r}\frac{\partial}{\partial r}\left(r\frac{\partial c}{\partial r}\right)+\frac{1}{r^2}\frac{\partial^2 c}{\partial\varphi^2}+\frac{\partial^2 c}{\partial z^2}\right) \tag{a.17}$$

When the dimensionless variables, as discussed in chapter 3, are introduced into the above equation, we get;

$$\frac{\partial C}{\partial\tau}+U\frac{\partial C}{\partial R}+\frac{V}{R}\frac{\partial C}{\partial\varphi}+W\frac{\partial C}{\partial Z}=\frac{1}{Re.Sc}\left(\frac{\partial^2 C}{\partial R^2}+\frac{1}{R^2}\frac{\partial^2 C}{\partial\varphi^2}+\frac{\partial^2 C}{\partial Z^2}\right) \tag{a.18}$$

APPENDIX "B"

Dimensionless Rotational Speed

The rotational speed is used in all input files in FIDAP as angular velocity. The dimensionless angular velocity used in this study should be solved and defined. Dimensionless angular velocity can be defined as:

$$v^* = \omega^* r^* \qquad \text{(b.1)}$$

Where;

$$v^* = \frac{v}{u_0} = \frac{\omega r}{u_0} \qquad \text{(b.2)}$$

and

$$\omega^* r^* = \omega^* \frac{r}{L} \qquad \text{(b.3)}$$

Applying (b.2) and (b.3) into the (b.1), we get;

$$\frac{\omega r}{u_0} = \omega^* \frac{r}{L} \qquad \text{(b.4)}$$

And by simplifying (b.4), we arrive to definition;

$$\omega^* = \frac{\omega L}{u_0} \qquad \text{(b.5)}$$

Where;

ω^* is the dimensionless angular velocity

ω is the angular velocity, L is the characteristic length and u_0 reference speed. It should be noted that the "rpm" is related to angular velocity by the following expression;

$$N_{rpm} = N \cdot \frac{2\pi}{60} = N \cdot 0.1047 \text{ rad/s} \qquad \text{(b.6)}$$

Table b.1 shows a list of the applied "rpm" and the associated dimensionless angular velocities in this study.

Table b.1 Dimensionless Value for Angular Velocity

RPM	Dimensionless Angular Velocity
1	0.3233
2	0.6647
3	0.9971
4	1.3295
5	1.6619
6	1.9942
7	2.3267
8	2.6590

APPENDIX "C"

Table c.1 Temperature Profile data

Dimensionless Temperature	"Z" value of the Model	Dimensionless Temperature	"Z" value of the Model	Dimensionless Temperature	"Z" value of the Model
36.22801	0.000	56.53806	0.340	55.71061	0.690
36.25120	0.000	56.78632	0.350	55.44217	0.699
37.10698	0.010	57.01584	0.360	55.16223	0.709
37.92077	0.020	57.22692	0.370	54.87093	0.719
38.75225	0.030	57.41985	0.380	54.56841	0.729
39.57938	0.040	57.59493	0.390	54.25479	0.739
40.40031	0.050	57.75243	0.400	53.93019	0.749
41.21311	0.060	57.89263	0.410	53.59474	0.759
42.01594	0.070	58.01580	0.420	53.24854	0.769
42.80699	0.080	58.12220	0.430	52.89170	0.779
43.58463	0.090	58.21208	0.440	52.52430	0.789
44.34732	0.100	58.28568	0.450	52.14645	0.799
45.09371	0.110	58.34324	0.460	51.75822	0.809
45.82260	0.120	58.38500	0.470	51.35968	0.819
46.53293	0.130	58.41117	0.480	50.95090	0.829
47.22381	0.140	58.42197	0.490	50.53192	0.839
47.89449	0.150	58.41763	0.500	50.10281	0.849
48.54435	0.160	58.39834	0.510	49.66359	0.859
49.17289	0.170	58.36431	0.520	49.21430	0.869
49.77976	0.180	58.31574	0.530	48.75498	0.879
50.36468	0.190	58.25282	0.540	48.28566	0.889
50.92749	0.200	58.17576	0.550	47.80636	0.899
51.46811	0.210	58.08472	0.560	47.31712	0.909
51.98652	0.220	57.97991	0.570	46.81800	0.919
52.48279	0.230	57.86149	0.580	46.30904	0.929
52.95704	0.240	57.72966	0.590	45.79032	0.939
53.40941	0.250	57.58458	0.600	45.26194	0.949
53.84013	0.260	57.42644	0.610	44.72402	0.959
54.24942	0.270	57.25539	0.620	44.17671	0.969
54.63753	0.280	57.07161	0.630	43.62017	0.979
55.00476	0.290	56.87526	0.640	43.06848	0.989
55.35139	0.300	56.66651	0.650	42.48007	0.999
55.67772	0.310	56.44552	0.660	42.43300	1.000
55.98407	0.320	56.21243	0.670		
56.27074	0.330	55.96742	0.680		

APPENDIX "D"

Table d.1 Different Hartmann Numbers

Mag.filed (B) [Tesla]	Ch.Length (L) [meter]	Elec.Conductivity(σ) [Siemens/centimeter]	Dynamic Viscosity(μ) [kg/centimeter.second]		Hartmann #
0.010	0.01	25000	8.3496E-06		5.4718876
0.015	0.01	25000	8.3496E-06		8.2078314
0.020	0.01	25000	8.3496E-06		10.943775
0.025	0.01	25000	8.3496E-06		13.679719
0.038	0.01	25000	8.3496E-06		20.793173
0.050	0.01	25000	8.3496E-06		27.359438
0.075	0.01	25000	8.3496E-06		41.039157
0.100	0.01	25000	8.3496E-06		54.718876
0.150	0.01	25000	8.3496E-06		82.078314

Reference speed is defined as $u_0 = \sqrt{g\beta_T \Delta TL}$ (d.1)

Therefore;

For Terrestrial condition is considered as:

$u_0 = 0.315$ (cm/s), and

For Microgravity condition is considered as:

$u_0 = 0.009954$ (cm/s)

Table d.2 Dimensionless Parameters

Item	Parameter Name (Dimensionless)	Symbol	Terrestrial Condition	Microgravity Condition
1	Reynolds Number	(Re)	206	0.65
2	Schmidt //	(Sc)	29	29
3	Prandtl //	(Pr)	13 E-4	13 E-4
4	Grashof //	$(Gr)_T$	42 E+3	42 E-2
5	Grashof //	$(Gr)_C$	2 E+6	21
6	Peclet // (Thermal Diffusion)	$(Pe)_T$	27 E-2	8.5 E-3
7	Peclet // (Mass Diffusion)	$(Pe)_m$	6 E+3	19
8	Solutal Diffusivity of the Species	α_C^*	1.674 E-4	5.22 E-2
9	Thermal Expansion of the Species	β_T^*	1	1
10	Volume Expansion of the Species	β_C^*	49	49.5

APPENDIX "E"

The following input files are some samples used in different cases in this study.

E.1 Terrestrial Condition, Steady State

```
/CONVERSION OF NEUTRAL FILE TO FIDAP Database
/
FICONV( NEUTRAL )
INPUT( FILE="J31-4080-G1.FDNEUT" )
OUTPUT( DELETE )
END
/
TITLE
J31-4080-G1
/
FIPREP
/
/           PROBLEM SETUP
/
PROBLEM (3-D, LAMINAR, NONLINEAR, BUOYANCY, BUOYANCY = 1)
EXECUTION( NEWJOB )
PRINTOUT( NONE )
DATAPRINT( CONTROL )
/
/           CONTINUUM ENTITIES
/
RENUMBER(PROFILE)
ENTITY ( NAME = "solvent", FLUID, PROPERTY = "solvent",
        SPECIES = 1, MDIFF = 3, MEXP = 3 )
/
/           BOUNDARY ENTITIES
/
ENTITY ( NAME = "dissolution", PLOT, ATTACH = "solvent")
ENTITY ( NAME = "growth", PLOT, ATTACH = "solvent" )
ENTITY ( NAME = "shell", PLOT )
/
/           SOLUTION PARAMETERS
/
SOLUTION( SEGREGATED = 250)
PRESSURE( MIXED = 1.E-8, DISCONTINUOUS )
OPTIONS( UPWINDING)
UPWIND(1STO)
/
/           MATERIAL PROPERTIES
/
/ Partial list of Material Properties data
/
DENSITY( SET = "solvent", CONSTANT = 206, TYP2, TEMPERATURE,
        SPECIES = 1 )
VISCOSITY( SET = "solvent", CONSTANT = 1 )
CONDUCTIVITY( SET = "solvent", CONSTANT = 1 )
SPECIFICHEAT( SET = "solvent", CONSTANT = 1E-3 )
VOLUMEXPANSION( SET = "solvent", CONSTANT = 1, TEMPERATURE )
```

```
GRAVITY(MAGNITUDE = 1)
/
VOLUMEXPANSION( SET = 3, CONSTANT = 49, SPECIES = 1)
DIFFUSIVITY( SET = 3, CONSTANT = 1.674E-4, SPECIES = 1)
/
/          INITIAL AND BOUNDARY CONDITIONS
/
/ICNODE( , CONSTANT = 0, ALL )
/
BCNODE( SPECIES = 1, CONSTANT = 0.15, ENTITY = "dissolution" )
BCNODE( SPECIES = 1, CONSTANT = 0.02, ENTITY = "growth" )
/BCNODE( , CONSTANT = 0, ENTITY = "shell" )
/
BCNODE( VELOCITY, CONSTANT = 0, ENTITY = "dissolution" )
BCNODE( VELOCITY, CONSTANT = 0, ENTITY = "growth" )
BCNODE( VELOCITY, CONSTANT = 0, ENTITY = "shell" )
/
BCNODE( TEMPERATURE, CONSTANT = 42.433, ENTITY = "dissolution" )
BCNODE( TEMPERATURE, CONSTANT = 36.228, ENTITY = "growth" )
BCNODE( TEMPERATURE, POLYNOMIAL = 6, ENTITY = "shell" )
36.1937 86.1424 0 0 1 -19.0372 0 0 2 -314.1486 0 0 3 548.1576
0 0 4 -414.598 0 0 5 119.7495 0 0 6
END
/
CREATE( FIPREP,DELETE )
PARAMETER( LIST )
CREATE( FISOLV )
/RUN( FISOLV, FOREGROUND )
```

E.2 Terrestrial Condition, with Applied RMF, Steady State

```
/CONVERSION OF NEUTRAL FILE TO FIDAP Database
/
FICONV( NEUTRAL )
INPUT( FILE="AUG10-4080-G1.FDNEUT" )
OUTPUT( DELETE )
END
/
TITLE
AUG10-4080-G1
/
FIPREP
/
/          PROBLEM SETUP
/
PROBLEM (3-D, LAMINAR, NONLINEAR, BUOYANCY, BUOYANCY = 1)
EXECUTION( NEWJOB )
PRINTOUT( NONE )
DATAPRINT( CONTROL )
/
/          CONTINUUM ENTITIES
/
RENUMBER(PROFILE)
ENTITY ( NAME = "solvent", FLUID, PROPERTY = "solvent",
        SPECIES = 1, MDIFF = 3, MEXP = 3 )
```

```
/
/          BOUNDARY ENTITIES
/
ENTITY ( NAME = "dissolution", PLOT, ATTACH = "solvent")
ENTITY ( NAME = "growth", PLOT, ATTACH = "solvent" )
ENTITY ( NAME = "shell", PLOT )
/
/          SOLUTION PARAMETERS
/
SOLUTION( SEGREGATED = 250)
PRESSURE( MIXED = 1.E-8, DISCONTINUOUS )
OPTIONS( UPWINDING)
UPWIND(1STO)
/
/          MATERIAL PROPERTIES
/
/ Partial list of Material Properties data
/
DENSITY( SET = "solvent", CONSTANT = 206, TYP2, TEMPERATURE,
        SPECIES = 1 )
VISCOSITY( SET = "solvent", CONSTANT = 1 )
CONDUCTIVITY( SET = "solvent", CONSTANT = 1 )
SPECIFICHEAT( SET = "solvent", CONSTANT = 1E-3 )
VOLUMEXPANSION( SET = "solvent", CONSTANT = 1, TEMPERATURE )
GRAVITY(MAGNITUDE = 1)
/
VOLUMEXPANSION( SET = 3, CONSTANT = 49, SPECIES = 1)
DIFFUSIVITY( SET = 3, CONSTANT = 1.674E-4, SPECIES = 1)
/
/          INITIAL AND BOUNDARY CONDITIONS
/
/ICNODE( , CONSTANT = 0, ALL )
/
BODYFORCE(ENTITY = "solvent", SUBROUTINE)
/
BCNODE( SPECIES = 1, CONSTANT = 0.15, ENTITY = "dissolution" )
BCNODE( SPECIES = 1, CONSTANT = 0.02, ENTITY = "growth" )
/BCNODE( , CONSTANT = 0, ENTITY = "shell" )
/
BCNODE( VELOCITY, CONSTANT = 0, ENTITY = "dissolution" )
BCNODE( VELOCITY, CONSTANT = 0, ENTITY = "growth" )
BCNODE( VELOCITY, CONSTANT = 0, ENTITY = "shell" )
/
BCNODE( TEMPERATURE, CONSTANT = 42.433, ENTITY = "dissolution" )
BCNODE( TEMPERATURE, CONSTANT = 36.228, ENTITY = "growth" )
BCNODE( TEMPERATURE, POLYNOMIAL = 6, ENTITY = "shell" )
36.1937 86.1424 0 0 1 -19.0372 0 0 2 -314.1486 0 0 3 548.1576
0 0 4 -414.598 0 0 5 119.7495 0 0 6
END
/
CREATE( FIPREP,DELETE )
PARAMETER( LIST )
CREATE( FISOLV )
/RUN( FISOLV, FOREGROUND )
```

E.3 Sub-routine used for Terrestrial with RMG

```
C       SUBROUTINE USRBDY (NELT,NE,NG,BDYF,VARI,DVARI,NDFCD,LDOFU,SHP,
     1                     DSDX,XYZL,PROP,TIME,NPTS,ndp,MNDP,IERR,IOPT)
C
C      USER DEFINED BODY FORCES
C
C      NELT   = GLOBAL ELEMENT NUMBER
C      NE     = LOCAL ELEMENT NUMBER
C      NG     = GROUP NUMBER
C      BDYF   = BODY FORCES
C      VARI   = ARRAY OF SOLUTION VARIBLES AT INTEGRATION POINTS
C      DVARI  = GRADIENTS OF SOLUTION VARIABLES AT INTEGRATION POINTS
C      NDFCD  = 2(3) COORDINATES DIMENSION, ACCORDING TO THE
                DEFINITION IN
C      LDOFU  = pointer array for accessing vari and dvari information
C      XYZL   = X,Y,Z COORDINATES
C      SHP    = ELEMENT SHAPE FUNCTIONS
C      DSDX   = SHAPE FUNCTION DERIVATIVES IN THE X,Y,Z DIRECTION
C      PROP   = USER DEFINED PARAMETERS
C      MNDP   = FIRST DIMENSION OF SHAPE FUNCTION MATRICES
C      TIME   = TIME
C      NPTS   = NUMBER OF POINTS
C      IOPT   = 0 - BODY FORCE
C      IOPT   = 1 - LORENTZ FORCE
C
#include "IMPLCT.COM"
#include "PARUSR.COM"
       DIMENSION BDYF(3,NPTS)
       DIMENSION SHP(NPTS,MNDP),DSDX(NPTS,NDFCD,MNDP),XYZL(NPTS,NDFCD)
       DIMENSION PROP(*),VARI(NPTS,*),DVARI(NPTS,NDFCD,*),LDOFU(*)
       ZRO = 0.D0
       Ha=8.2078
       W=0.6647
       IERR=0
       Do 100 N=1,NPTS
       x=XYZL(N,1)
       y=XYZL(N,2)
       BDYF(1,N)=-1*0.5*Ha*Ha*W*B*B*y
       BDYF(2,N)=1*0.5*Ha*Ha*W*B*B*x
       BDYF(3,N)=0
C
       IP1 = IOPT + 1
C       GO TO (10,20) IP1
C    10 CALL ERMSGS (7101, 0, 3,
C      1              0,0,0,0,0,ZRO,ZRO,ZRO,' ',' ',' ')
C       RETURN
C    20 CALL ERMSGS (7102, 0, 3,
C      1              0,0,0,0,0,ZRO,ZRO,ZRO,' ',' ',' ')
  100  CONTINUE
       RETURN
       END
C
```

E.4 Terrestrial Condition, with Higher RMF applied, Steady State

```
/          CONVERSION OF NEUTRAL FILE TO FIDAP Database
/
FICONV( NEUTRAL )
INPUT( FILE="50mTW03.FDNEUT" )
OUTPUT( DELETE )
END
/
TITLE
50mTW03
/
FIPREP
/
/          PROBLEM SETUP
/
PROBLEM (3-D, LAMINAR, NONLINEAR, BUOYANCY, BUOYANCY = 1)
EXECUTION( NEWJOB )
PRINTOUT( NONE )
DATAPRINT( CONTROL )
/
/          CONTINUUM ENTITIES
/
RENUMBER(PROFILE)
ENTITY ( NAME = "solvent", FLUID, PROPERTY = "solvent",
        SPECIES = 1, MDIFF = 3, MEXP = 3 )
/
/          BOUNDARY ENTITIES
/
ENTITY ( NAME = "dissolution", PLOT, ATTACH = "solvent")
ENTITY ( NAME = "growth", PLOT, ATTACH = "solvent" )
ENTITY ( NAME = "shell", PLOT )
/
/          SOLUTION PARAMETERS
/
SOLUTION( SEGREGATED = 250)
PRESSURE( MIXED = 1.E-8, DISCONTINUOUS )
OPTIONS( UPWINDING)
UPWIND(1STO)
/
/          MATERIAL PROPERTIES
/
/ Partial list of Material Properties data
/
DENSITY( SET = "solvent", CONSTANT = 206, TYP2,
        TEMPERATURE, SPECIES = 1 )
VISCOSITY( SET = "solvent", CONSTANT = 1 )
CONDUCTIVITY( SET = "solvent", CONSTANT = 1 )
SPECIFICHEAT( SET = "solvent", CONSTANT = 1E-3 )
VOLUMEXPANSION( SET = "solvent", CONSTANT = 1, TEMPERATURE )
GRAVITY(MAGNITUDE = 1)
/
VOLUMEXPANSION( SET = 3, CONSTANT = 49, SPECIES = 1)
DIFFUSIVITY( SET = 3, CONSTANT = 1.674E-4, SPECIES = 1)
/
```

```
/          INITIAL AND BOUNDARY CONDITIONS
/
/ICNODE( , CONSTANT = 0, ALL )
/
BODYFORCE(ENTITY = "solvent", SUBROUTINE)
/
BCNODE( SPECIES = 1, CONSTANT = 0.15, ENTITY = "dissolution" )
BCNODE( SPECIES = 1, CONSTANT = 0.02, ENTITY = "growth" )
/BCNODE( , CONSTANT = 0, ENTITY = "shell" )
/
BCNODE( VELOCITY, CONSTANT = 0, ENTITY = "dissolution" )
BCNODE( VELOCITY, CONSTANT = 0, ENTITY = "growth" )
BCNODE( VELOCITY, CONSTANT = 0, ENTITY = "shell" )
/
BCNODE( TEMPERATURE, CONSTANT = 42.433, ENTITY = "dissolution" )
BCNODE( TEMPERATURE, CONSTANT = 36.228, ENTITY = "growth" )
BCNODE( TEMPERATURE, POLYNOMIAL = 6, ENTITY = "shell" )
36.1937 86.1424 0 0 1 -19.0372 0 0 2 -314.1486 0 0 3 548.1576
0 0 4 -414.598 0 0 5 119.7495 0 0 6
END
/
CREATE( FIPREP,DELETE )
PARAMETER( LIST )
CREATE( FISOLV )
/RUN( FISOLV, FOREGROUND )
```

E.5 Sub-routine for Higher RMF

```
C (Terrestrial condition, SS- with B=50mT and W=1/12rpm)
      SUBROUTINE USRBDY (NELT,NE,NG,BDYF,VARI,DVARI,NDFCD,LDOFU,SHP,
     1                   DSDX,XYZL,PROP,TIME,NPTS,ndp,MNDP,IERR,IOPT)
C
C     USER DEFINED BODY FORCES
C
C     NELT  = GLOBAL ELEMENT NUMBER
C     NE    = LOCAL ELEMENT NUMBER
C     NG    = GROUP NUMBER
C     BDYF  = BODY FORCES
C     VARI  = ARRAY OF SOLUTION VARIBLES AT INTEGRATION POINTS
C     DVARI = GRADIENTS OF SOLUTION VARIABLES AT INTEGRATION POINTS
C     NDFCD = 2(3) COORDINATES DIMENSION, ACCORDING TO
                THE DEFINITION IN
C     LDOFU = pointer array for accessing vari and dvari information
C     XYZL  = X,Y,Z COORDINATES
C     SHP   = ELEMENT SHAPE FUNCTIONS
C     DSDX  = SHAPE FUNCTION DERIVATIVES IN THE X,Y,Z DIRECTION
C     PROP  = USER DEFINED PARAMETERS
C     MNDP  = FIRST DIMENSION OF SHAPE FUNCTION MATRICES
C     TIME  = TIME
C     NPTS  = NUMBER OF POINTS
C     IOPT  = 0 - BODY FORCE
C     IOPT  = 1 - LORENTZ FORCE
C
#include "IMPLCT.COM"
#include "PARUSR.COM"
      DIMENSION BDYF(3,NPTS)
```

```
      DIMENSION SHP(NPTS,MNDP),DSDX(NPTS,NDFCD,MNDP),XYZL(NPTS,NDFCD)
      DIMENSION PROP(*),VARI(NPTS,*),DVARI(NPTS,NDFCD,*),LDOFU(*)
      ZRO = 0.D0
      Ha=27.359438
      W=0.02769167
      IERR=0
      Do 100 N=1,NPTS
      x=XYZL(N,1)
      y=XYZL(N,2)
      BDYF(1,N)=-1*0.5*Ha*Ha*W*B*B*y
      BDYF(2,N)=1*0.5*Ha*Ha*W*B*B*x
      BDYF(3,N)=0
C
      IP1 = IOPT + 1
C      GO TO (10,20) IP1
C   10 CALL ERMSGS (7101, 0, 3,
C     1             0,0,0,0,0,ZRO,ZRO,ZRO,' ',' ',' ')
C      RETURN
C   20 CALL ERMSGS (7102, 0, 3,
C     1             0,0,0,0,0,ZRO,ZRO,ZRO,' ',' ',' ')
 100  CONTINUE
      RETURN
      END
```

E.6 Microgravity Condition, Steady State

```
/          CONVERSION OF NEUTRAL FILE TO FIDAP Database
/
FICONV( NEUTRAL )
INPUT( FILE="A07-4080-microG.FDNEUT" )
OUTPUT( DELETE )
END
/
TITLE
A07-4080-microG
/
FIPREP
/
/          PROBLEM SETUP
/
PROBLEM (3-D, LAMINAR, NONLINEAR, BUOYANCY, BUOYANCY = 1)
EXECUTION( NEWJOB )
PRINTOUT( NONE )
DATAPRINT( CONTROL )
/
/          CONTINUUM ENTITIES
/
RENUMBER(PROFILE)
ENTITY ( NAME = "solvent", FLUID, PROPERTY = "solvent", SPECIES = 1,
MDIFF = 3, MEXP = 3 )
/
/          BOUNDARY ENTITIES
/
ENTITY ( NAME = "dissolution", PLOT, ATTACH = "solvent")
ENTITY ( NAME = "growth", PLOT, ATTACH = "solvent" )
ENTITY ( NAME = "shell", PLOT )
```

```
/
/          SOLUTION PARAMETERS
/
SOLUTION( SEGREGATED = 250)
PRESSURE( MIXED = 1.E-8, DISCONTINUOUS )
OPTIONS( UPWINDING)
UPWIND(1STO)
/
/          MATERIAL PROPERTIES
/
/ Partial list of Material Properties data
/
DENSITY( SET = "solvent", CONSTANT = 0.206, TYP2, TEMPERATURE, SPECIES
= 1 )
VISCOSITY( SET = "solvent", CONSTANT = 1 )
CONDUCTIVITY( SET = "solvent", CONSTANT = 1 )
SPECIFICHEAT( SET = "solvent", CONSTANT = 1E-3 )
VOLUMEXPANSION( SET = "solvent", CONSTANT = 1, TEMPERATURE )
GRAVITY(MAGNITUDE = 1E-6)
/
VOLUMEXPANSION( SET = 3, CONSTANT = 49.25, SPECIES = 1)
DIFFUSIVITY( SET = 3, CONSTANT = 1.674E-4, SPECIES = 1)
/
/          INITIAL AND BOUNDARY CONDITIONS
/
/ICNODE( , CONSTANT = 0, ALL )
/
BCNODE( SPECIES = 1, CONSTANT = 0.15, ENTITY = "dissolution" )
BCNODE( SPECIES = 1, CONSTANT = 0.02, ENTITY = "growth" )
/BCNODE( , CONSTANT = 0, ENTITY = "shell" )
/
BCNODE( VELOCITY, CONSTANT = 0, ENTITY = "dissolution" )
BCNODE( VELOCITY, CONSTANT = 0, ENTITY = "growth" )
BCNODE( VELOCITY, CONSTANT = 0, ENTITY = "shell" )
/
BCNODE( TEMPERATURE, CONSTANT = 42.433, ENTITY = "dissolution" )
BCNODE( TEMPERATURE, CONSTANT = 36.228, ENTITY = "growth" )
BCNODE( TEMPERATURE, POLYNOMIAL = 6, ENTITY = "shell" )
36.1937 86.1424 0 0 1 -19.0372 0 0 2 -314.1486 0 0 3 548.1576
0 0 4 -414.598 0 0 5 119.7495 0 0 6
END
/
CREATE( FIPREP,DELETE )
PARAMETER( LIST )
CREATE( FISOLV )
/RUN( FISOLV, FOREGROUND )
```

E.7 Microgravity Condition, with Higher RMF, Steady State

```
/          CONVERSION OF NEUTRAL FILE TO FIDAP Database
/
FICONV( NEUTRAL )
INPUT( FILE="mG-50mT-W03.FDNEUT" )
OUTPUT( DELETE )
END
/
TITLE
```

```
mG-50mT-W03
/
FIPREP
/
/          PROBLEM SETUP
/
PROBLEM (3-D, LAMINAR, NONLINEAR, BUOYANCY, BUOYANCY = 1)
EXECUTION( NEWJOB )
PRINTOUT( NONE )
DATAPRINT( CONTROL )
/
/          CONTINUUM ENTITIES
/
RENUMBER(PROFILE)
ENTITY ( NAME = "solvent", FLUID, PROPERTY = "solvent",
         SPECIES = 1, MDIFF = 3, MEXP = 3 )
/
/          BOUNDARY ENTITIES
/
ENTITY ( NAME = "dissolution", PLOT, ATTACH = "solvent")
ENTITY ( NAME = "growth", PLOT, ATTACH = "solvent" )
ENTITY ( NAME = "shell", PLOT )
/
/          SOLUTION PARAMETERS
/
SOLUTION( SEGREGATED = 250)
PRESSURE( MIXED = 1.E-8, DISCONTINUOUS )
OPTIONS( UPWINDING)
UPWIND(1STO)
/
/          MATERIAL PROPERTIES
/
/ Partial list of Material Properties data
/
DENSITY( SET = "solvent", CONSTANT = .65, TYP2,
        TEMPERATURE, SPECIES = 1 )
VISCOSITY( SET = "solvent", CONSTANT = 1 )
CONDUCTIVITY( SET = "solvent", CONSTANT = 1 )
SPECIFICHEAT( SET = "solvent", CONSTANT = 1E-3 )
VOLUMEXPANSION( SET = "solvent", CONSTANT = 1, TEMPERATURE )
GRAVITY(MAGNITUDE = 1E-5)
/
VOLUMEXPANSION( SET = 3, CONSTANT = 49, SPECIES = 1)
DIFFUSIVITY( SET = 3, CONSTANT = 1.674E-4, SPECIES = 1)
/
/          INITIAL AND BOUNDARY CONDITIONS
/
/ICNODE( , CONSTANT = 0, ALL )
/
BODYFORCE(ENTITY = "solvent", SUBROUTINE)
/
BCNODE( SPECIES = 1, CONSTANT = 0.15, ENTITY = "dissolution" )
BCNODE( SPECIES = 1, CONSTANT = 0.02, ENTITY = "growth" )
/BCNODE( , CONSTANT = 0, ENTITY = "shell" )
/
BCNODE( VELOCITY, CONSTANT = 0, ENTITY = "dissolution" )
BCNODE( VELOCITY, CONSTANT = 0, ENTITY = "growth" )
BCNODE( VELOCITY, CONSTANT = 0, ENTITY = "shell" )
/
BCNODE( TEMPERATURE, CONSTANT = 42.433, ENTITY = "dissolution" )
BCNODE( TEMPERATURE, CONSTANT = 36.228, ENTITY = "growth" )
BCNODE( TEMPERATURE, POLYNOMIAL = 6, ENTITY = "shell" )
36.1937 86.1424 0 0 1 -19.0372 0 0 2 -314.1486 0 0 3 548.1576
0 0 4 -414.598 0 0 5 119.7495 0 0 6
```

```
END
/
CREATE( FIPREP,DELETE )
PARAMETER( LIST )
CREATE( FISOLV )
/RUN( FISOLV, FOREGROUND )
```

E.8 Sub-routine for Micro-Gravity with Higher RMF

```
C (Micro-Gravity Condition, SS, with 50mT RMF and W=1/12 rpm)
      SUBROUTINE USRBCN (VAL,NODE,IDF,TIME,SOL,NUMEQA,NDOF,NUMNP,LDOFU,
     1                   CONSTR,NODEPR,XYZ,iflag)
C
C     USER DEFINED BOUNDARY CONDITIONS
C
C     VAL    = COMPUTED (SPECIFIED) BOUNDARY CONDITION
C     SOL    = GLOBAL SOLUTION VECTOR
C     NUMEQA = GLOBAL EQUATION NUMBER ARRAY
C     NDOF   = ACTIVE NUMBER OF DEGREES OF FREEDOM
C     NUMNP  = NUMBER OF NODAL POINTS
C     NODE   = NODE NUMBER OF B.C.
C     IDF    = DEGREE OF FREEDOM FOR NODE
C     TIME   = TIME
C     LDOFU  = ACTIVE DEGREE OF FREEDOM ARRAY
C     CONSTR = ARRAY OF SPECIFIED NONZERO BOUNDARY CONDITIONS
C     XYZ    = nodal coordinates
C     iflag  = flag for user to set (not equal to 0) if coordinates
C              are updated
C     NODEPR = reverse permutation array
C              node(external) = NODEPR(NODE) where NODE = internal node
no.
C
#include "IMPLCT.COM"
#include "PARUSR.COM"
      DIMENSION SOL(*),NUMEQA(NUMNP,NDOF),CONSTR(*),LDOFU(*)
      DIMENSION NODEPR(*),XYZ(NUMNP,*)
      F_DOUBLEPRECISION GETSOL
      F_DOUBLEPRECISION GETSOLP
      ZRO = 0.D0

      CALL ERMSGS (8901, 0, 3,
     1             0,0,0,0,0,ZRO,ZRO,ZRO,' ',' ',' ')
c
      RETURN
      END
C
      SUBROUTINE USRBDY (NELT,NE,NG,BDYF,VARI,DVARI,NDFCD,LDOFU,SHP,
     1                   DSDX,XYZL,PROP,TIME,NPTS,ndp,MNDP,IERR,IOPT)
C
C     USER DEFINED BODY FORCES
C(UNDER TERRESTRIAL CONDITION GRAVITY=1, AND MAGNETIC FIELD MAGNITUDE
OF 50 mT AND 1/12 RPM)
C     NELT   = GLOBAL ELEMENT NUMBER
C     NE     = LOCAL ELEMENT NUMBER
C     NG     = GROUP NUMBER
C     BDYF   = BODY FORCES
C     VARI   = ARRAY OF SOLUTION VARIBLES AT INTEGRATION POINTS
```

```
C     DVARI = GRADIENTS OF SOLUTION VARIABLES AT INTEGRATION POINTS
C     NDFCD = 2(3) COORDINATES DIMENSION, ACCORDING TO
                THE DEFINITION IN
C     LDOFU = pointer array for accessing vari and dvari information
C     XYZL  = X,Y,Z COORDINATES
C     SHP   = ELEMENT SHAPE FUNCTIONS
C     DSDX  = SHAPE FUNCTION DERIVATIVES IN THE X,Y,Z DIRECTION
C     PROP  = USER DEFINED PARAMETERS
C     MNDP  = FIRST DIMENSION OF SHAPE FUNCTION MATRICES
C     TIME  = TIME
C     NPTS  = NUMBER OF POINTS
C     IOPT  = 0 - BODY FORCE
C     IOPT  = 1 - LORENTZ FORCE
C
#include "IMPLCT.COM"
#include "PARUSR.COM"
      DIMENSION BDYF(3,NPTS)
      DIMENSION SHP(NPTS,MNDP),DSDX(NPTS,NDFCD,MNDP),XYZL(NPTS,NDFCD)
      DIMENSION PROP(*),VARI(NPTS,*),DVARI(NPTS,NDFCD,*),LDOFU(*)
      ZRO = 0.D0
      Ha=27.359438
      W=0.02769167
      IERR=0
      Do 100 N=1,NPTS
      x=XYZL(N,1)
      y=XYZL(N,2)
      BDYF(1,N)=-1*0.5*Ha*Ha*W*B*B*y
      BDYF(2,N)=1*0.5*Ha*Ha*W*B*B*x
      BDYF(3,N)=0
C
      IP1 = IOPT + 1
C      GO TO (10,20) IP1
C   10 CALL ERMSGS (7101, 0, 3,
C     1             0,0,0,0,0,ZRO,ZRO,ZRO,' ',' ',' ')
C      RETURN
C   20 CALL ERMSGS (7102, 0, 3,
C     1             0,0,0,0,0,ZRO,ZRO,ZRO,' ',' ',' ')
 100  CONTINUE
      RETURN
      END
C
```

E.9 Microgravity Condition by taking g-jitter, with Applied RMF, Unsteady State (Transient) into the Consideration, low rpm

```
/          CONVERSION OF NEUTRAL FILE TO FIDAP Database
/
FICONV( NEUTRAL )
INPUT( FILE="gj15B112w.FDNEUT" )
OUTPUT( DELETE )
END
/
/Jan-31-08
TITLE
gj15B112w
/
```

```
/G-jitter in the "XYZ" axis direction with B=15mT and w=1/12rpm for
 14 hrs)
FIPREP
/
/          PROBLEM SETUP
/
PROBLEM (3-D, LAMINAR, NONLINEAR, ENERGY, SPECIES = 1, TRANSIENT)
TIMEINT(back, dt=1.3, fixed, nsteps=390, tend=507)
EXECUTION( NEWJOB )
PRINTOUT( NONE )
DATAPRINT( CONTROL )
/
/          CONTINUUM ENTITIES
/
RENUMBER(PROFILE)
ENTITY ( NAME = "solvent", FLUID, PROPERTY = "solvent", SPECIES = 1,
MDIFF = 3)
/
/          BOUNDARY ENTITIES
/
ENTITY ( NAME = "dissolution", PLOT, ATTACH = "solvent")
ENTITY ( NAME = "growth", PLOT, ATTACH = "solvent" )
ENTITY ( NAME = "shell", PLOT )
/
/          SOLUTION PARAMETERS
/
SOLUTION( SEGREGATED = 250)
PRESSURE( MIXED = 1.E-8, DISCONTINUOUS )
OPTIONS( UPWINDING)
UPWIND(1STO)
/
/          MATERIAL PROPERTIES
/
/ Partial list of Material Properties data
/
DENSITY( SET = "solvent", CONSTANT = 0.206, TYP2, TEMPERATURE, SPECIES
= 1 )
VISCOSITY( SET = "solvent", CONSTANT = 1 )
CONDUCTIVITY( SET = "solvent", CONSTANT = 1 )
SPECIFICHEAT( SET = "solvent", CONSTANT = 1.65E-1 )
/VOLUMEXPANSION( SET = "solvent", CONSTANT = 1, TEMPERATURE )
/GRAVITY(MAGNITUDE = 1E-6)
/
VOLUMEXPANSION( SET = 3, CONSTANT = 49.25, SPECIES = 1)
DIFFUSIVITY( SET = 3, CONSTANT = 13.08E-4, SPECIES = 1)
/
/          INITIAL AND BOUNDARY CONDITIONS
/
/ICNODE( , CONSTANT = 0, ALL )
/
BODYFORCE(ENTITY = "solvent", SUBROUTINE)
/
BCNODE( SPECIES = 1, CONSTANT = 0.15, ENTITY = "dissolution" )
BCNODE( SPECIES = 1, CONSTANT = 0.02, ENTITY = "growth" )
/BCNODE( , CONSTANT = 0, ENTITY = "shell" )
/
BCNODE( VELOCITY, CONSTANT = 0, ENTITY = "dissolution" )
```

```
BCNODE( VELOCITY, CONSTANT = 0, ENTITY = "growth" )
BCNODE( VELOCITY, CONSTANT = 0, ENTITY = "shell" )
/
BCNODE( TEMPERATURE, CONSTANT = 42.433, ENTITY = "dissolution" )
BCNODE( TEMPERATURE, CONSTANT = 36.228, ENTITY = "growth" )
BCNODE( TEMPERATURE, POLYNOMIAL = 6, ENTITY = "shell" )
36.1937 86.1424 0 0 1 -19.0372 0 0 2 -314.1486 0 0 3 548.1576 0 0 4 -
414.598 0 0 5 119.7495 0 0 6
END
/
CREATE( FIPREP,DELETE )
PARAMETER( LIST )
CREATE( FISOLV )
/RUN( FISOLV, FOREGROUND )
```

E.10 Sub-routine used for Microgravity Condition by taking g-jitter, with Applied RMF, Unsteady State into the consideration, low rpm.

```
C  SUBROUTINE USRBDY (NELT,NE,NG,BDYF,VARI,DVARI,NDFCD,LDOFU,SHP,
       1              DSDX,XYZL,PROP,TIME,NPTS,ndp,MNDP,IERR,IOPT)
C
C(**UNDER mG-CONDITION (FOTON12TRAMP) and With 15mT and 1/12rpm
  direction**)
C     USER DEFINED BODY FORCES
C     NELT  = GLOBAL ELEMENT NUMBER
C     NE    = LOCAL ELEMENT NUMBER
C     NG    = GROUP NUMBER
C     BDYF  = BODY FORCES
C     VARI  = ARRAY OF SOLUTION VARIBLES AT INTEGRATION POINTS
C     DVARI = GRADIENTS OF SOLUTION VARIABLES AT INTEGRATION POINTS
C     NDFCD = 2(3) COORDINATES DIMENSION, ACCORDING TO
                THE DEFINITION IN
C     LDOFU = pointer array for accessing vari and dvari information
C     XYZL  = X,Y,Z COORDINATES
C     SHP   = ELEMENT SHAPE FUNCTIONS
C     DSDX  = SHAPE FUNCTION DERIVATIVES IN THE X,Y,Z DIRECTION
C     PROP  = USER DEFINED PARAMETERS
C     MNDP  = FIRST DIMENSION OF SHAPE FUNCTION MATRICES
C     TIME  = TIME
C     NPTS  = NUMBER OF POINTS
C     IOPT  = 0 - BODY FORCE
C     IOPT  = 1 - LORENTZ FORCE
C
#include "IMPLCT.COM"
#include "PARUSR.COM"
      DIMENSION BDYF(3,NPTS)
      DIMENSION SHP(NPTS,MNDP),DSDX(NPTS,NDFCD,MNDP),XYZL(NPTS,NDFCD)
      DIMENSION PROP(*),VARI(NPTS,*),DVARI(NPTS,NDFCD,*),LDOFU(*)
      ZRO = 0.D0
      IERR=0
C
            Tref=0.0
      BETAT=1.0
      Cref=0.0
```

```
      BETAC=49.25
C
      GRAVXS=-3.324E-7
      GRAVX1=-2.5378E-6
      GRAVX2=3.1382E-6
C
      GRAVYS=-1.189E-5
      GRAVY1=4.2552E-7
      GRAVY2=1.4468E-7
C
      GRAVZS=1.683E-6
      GRAVZ1=5.666E-7
      GRAVZ2=2.897E-7
C
      Fx=0.1653
      Fy=0.1881
      Fz=0.1651
      PI=4.0*ATAN(1.0)
C
  GRAVX=GRAVXS+GRAVX1*DCOS(2.0*PI*Fx*TIME)+GRAVX2*DSIN(2.0*PI*Fx*TIME)
C
  GRAVY=GRAVYS+GRAVY1*DCOS(2.0*PI*Fy*TIME)+GRAVY2*DSIN(2.0*PI*Fy*TIME)
C
  GRAVZ=GRAVZS+GRAVZ1*DCOS(2.0*PI*Fz*TIME)+GRAVZ2*DSIN(2.0*PI*Fz*TIME)
C
        Ha=8.2078314
        W=0.02769167
C
      DO I=1,NPTS
        x=XYZL(1,I)
        y=XYZL(2,I)
      z=XYZL(3,I)
      TEMP=VARI(I,LDOFU(KDT))
      Conc=VARI(I,LDOFU(KDS+1))
      BDYF(1,I)=GRAVX*(BETAT*(TEMP-Tref)-BETAC*(Conc-Cref))-
                1*0.5*Ha*Ha*W*B*B*y
      BDYF(2,I)=GRAVY*(BETAT*(TEMP-Tref)-BETAC*(Conc- Cref))+
                1*0.5*Ha*Ha*W*B*B*x
      BDYF(3,I)=GRAVZ*(BETAT*(TEMP-Tref)-BETAC*(Conc-Cref))+0
C
        IP1 = IOPT + 1
      ENDDO
      RETURN
      END
C
```

E.11 Microgravity Condition by taking g-jitter, with Applied RMF, Unsteady State (Transient) into the Consideration with w=2rpm

```
/          CONVERSION OF NEUTRAL FILE TO FIDAP Database
/
FICONV( NEUTRAL )
INPUT( FILE="gj15B2w.FDNEUT" )
OUTPUT( DELETE )
END
/
```

```
/Feb-06-08
TITLE
gj15B2w
/
/(G-jitter in the "XYZ" axis direction with B=15mT and w=12rpm for
 14 hrs)
FIPREP
/
/          PROBLEM SETUP
/
PROBLEM (3-D, LAMINAR, NONLINEAR, ENERGY, SPECIES = 1, TRANSIENT)
TIMEINT(back, dt=1.3, fixed, nsteps=390, tend=507)
EXECUTION( NEWJOB )
PRINTOUT( NONE )
DATAPRINT( CONTROL )
/
/          CONTINUUM ENTITIES
/
RENUMBER(PROFILE)
ENTITY ( NAME = "solvent", FLUID, PROPERTY = "solvent", SPECIES = 1,
MDIFF = 3)
/
/          BOUNDARY ENTITIES
/
ENTITY ( NAME = "dissolution", PLOT, ATTACH = "solvent")
ENTITY ( NAME = "growth", PLOT, ATTACH = "solvent" )
ENTITY ( NAME = "shell", PLOT )
/
/          SOLUTION PARAMETERS
/
SOLUTION( SEGREGATED = 250)
PRESSURE( MIXED = 1.E-8, DISCONTINUOUS )
OPTIONS( UPWINDING)
UPWIND(1STO)
/
/          MATERIAL PROPERTIES
/
/ Partial list of Material Properties data
/
DENSITY( SET = "solvent", CONSTANT = 0.206, TYP2, TEMPERATURE, SPECIES
= 1 )
VISCOSITY( SET = "solvent", CONSTANT = 1 )
CONDUCTIVITY( SET = "solvent", CONSTANT = 1 )
SPECIFICHEAT( SET = "solvent", CONSTANT = 1.65E-1 )
/VOLUMEXPANSION( SET = "solvent", CONSTANT = 1, TEMPERATURE )
/GRAVITY(MAGNITUDE = 1E-6)
/
VOLUMEXPANSION( SET = 3, CONSTANT = 49.25, SPECIES = 1)
DIFFUSIVITY( SET = 3, CONSTANT = 13.08E-4, SPECIES = 1)
/
/          INITIAL AND BOUNDARY CONDITIONS
/
/ICNODE( , CONSTANT = 0, ALL )
/
BODYFORCE(ENTITY = "solvent", SUBROUTINE)
/
BCNODE( SPECIES = 1, CONSTANT = 0.15, ENTITY = "dissolution" )
```

```
BCNODE( SPECIES = 1, CONSTANT = 0.02, ENTITY = "growth" )
/BCNODE( , CONSTANT = 0, ENTITY = "shell" )
/
BCNODE( VELOCITY, CONSTANT = 0, ENTITY = "dissolution" )
BCNODE( VELOCITY, CONSTANT = 0, ENTITY = "growth" )
BCNODE( VELOCITY, CONSTANT = 0, ENTITY = "shell" )
/
BCNODE( TEMPERATURE, CONSTANT = 42.433, ENTITY = "dissolution" )
BCNODE( TEMPERATURE, CONSTANT = 36.228, ENTITY = "growth" )
BCNODE( TEMPERATURE, POLYNOMIAL = 6, ENTITY = "shell" )
36.1937 86.1424 0 0 1 -19.0372 0 0 2 -314.1486 0 0 3 548.1576 0 0 4 -
414.598 0 0 5 119.7495 0 0 6
END
/
CREATE( FIPREP,DELETE )
PARAMETER( LIST )
CREATE( FISOLV )
/RUN( FISOLV, FOREGROUND )
```

E.12 Sub-routine used for Microgravity Condition by taking g-jitter, with Applied RMF, Unsteady State into the consideration, w=2rpm.

```
C       SUBROUTINE USRBDY (NELT,NE,NG,BDYF,VARI,DVARI,NDFCD,LDOFU,SHP,
        1            DSDX,XYZL,PROP,TIME,NPTS,ndp,MNDP,IERR,IOPT)
C
C(**UNDER mG-CONDITION (FOTON12TRAMP)and With B=15mT and w=2rpm in XYZ
direction**)
C      USER DEFINED BODY FORCES
C      NELT  = GLOBAL ELEMENT NUMBER
C      NE    = LOCAL ELEMENT NUMBER
C      NG    = GROUP NUMBER
C      BDYF  = BODY FORCES
C      VARI  = ARRAY OF SOLUTION VARIBLES AT INTEGRATION POINTS
C      DVARI = GRADIENTS OF SOLUTION VARIABLES AT INTEGRATION POINTS
C      NDFCD = 2(3) COORDINATES DIMENSION, ACCORDING TO
                THE DEFINITION IN
C      LDOFU = pointer array for accessing vari and dvari information
C      XYZL  = X,Y,Z COORDINATES
C      SHP   = ELEMENT SHAPE FUNCTIONS
C      DSDX  = SHAPE FUNCTION DERIVATIVES IN THE X,Y,Z DIRECTION
C      PROP  = USER DEFINED PARAMETERS
C      MNDP  = FIRST DIMENSION OF SHAPE FUNCTION MATRICES
C      TIME  = TIME
C      NPTS  = NUMBER OF POINTS
C      IOPT  = 0 - BODY FORCE
C      IOPT  = 1 - LORENTZ FORCE
C
#include "IMPLCT.COM"
#include "PARUSR.COM"
       DIMENSION BDYF(3,NPTS)
       DIMENSION SHP(NPTS,MNDP),DSDX(NPTS,NDFCD,MNDP),XYZL(NPTS,NDFCD)
       DIMENSION PROP(*),VARI(NPTS,*),DVARI(NPTS,NDFCD,*),LDOFU(*)
       ZRO = 0.D0
       IERR=0
```

```
C
            Tref=0.0
      BETAT=1.0
      Cref=0.0
      BETAC=49.25
C
      GRAVXS=-3.324E-7
      GRAVX1=-2.5378E-6
      GRAVX2=3.1382E-6
C
      GRAVYS=-1.189E-5
      GRAVY1=4.2552E-7
      GRAVY2=1.4468E-7
C
      GRAVZS=1.683E-6
      GRAVZ1=5.666E-7
      GRAVZ2=2.897E-7
C
      Fx=0.1653
      Fy=0.1881
      Fz=0.1651
      PI=4.0*ATAN(1.0)
C
      GRAVX=GRAVXS+GRAVX1*DCOS(2.0*PI*Fx*TIME)+GRAVX2*DSIN(2.0*PI*Fx*TI
ME)
C
      GRAVY=GRAVYS+GRAVY1*DCOS(2.0*PI*Fy*TIME)+GRAVY2*DSIN(2.0*PI*Fy*TI
ME)
C
      GRAVZ=GRAVZS+GRAVZ1*DCOS(2.0*PI*Fz*TIME)+GRAVZ2*DSIN(2.0*PI*Fz*TI
ME)
C
        Ha=8.2078314
        W=0.6647
C
      DO I=1,NPTS
        x=XYZL(1,I)
        y=XYZL(2,I)
      z=XYZL(3,I)
      TEMP=VARI(I,LDOFU(KDT))
      Conc=VARI(I,LDOFU(KDS+1))
      BDYF(1,I)=GRAVX*(BETAT*(TEMP-Tref)-BETAC*(Conc-Cref))-
1*0.5*Ha*Ha*W*B*B*y
      BDYF(2,I)=GRAVY*(BETAT*(TEMP-Tref)-BETAC*(Conc-
Cref))+1*0.5*Ha*Ha*W*B*B*x
      BDYF(3,I)=GRAVZ*(BETAT*(TEMP-Tref)-BETAC*(Conc-Cref))+0
        IP1 = IOPT + 1
      ENDDO
      RETURN
      END
```